UNIVERSITE D'OTTAWA
Ecole des Etudes Supérieures

UNIVERSITY OF OTTAWA
School of Graduate Studies

Title of thesis: INELASTIC INTERACTIONS OF INTERMEDIATE ENERGY POSITIVE PIONS WITH COMPLEX NUCLEI

Name of candidate: Subhas C. CHAKRAVARTTY

Degree: Ph.D.

Date: April 10, 1970

This thesis has been prepared under my supervision

....
(Thesis Supervisor)

April 10, 1970
(Date)

We, the undersigned, certify that we have approved this thesis, and that the candidate has defended it successfully.

1. .... Date: April 10, 1970
(Signature of examiners)

2. ... Date: April 10, 1970

3. .... Date: April 10, 1970

4. .... Date: April 10, 1970

5. .... Date: ....

6. .... Date: ....

7. .... Date: ....

....
(Dean of Graduate Studies)

SC

INELASTIC INTERACTIONS OF INTERMEDIATE ENERGY POSITIVE PIONS WITH COMPLEX NUCLEI

by

Subhas Chandra Chakravartty

Submitted in partial fulfillment of the requirements for the degree of Doctor of Philosophy.

Department of Physics,
Faculty of Pure and Applied Science,
University of Ottawa,
Ottawa, Canada.

January, 1970

ABSTRACT

This work deals with the study of interaction of pions in complex nuclei. The cross sections for inelastic interactions of positive pions with emulsion nuclei have been measured at various pion energies in the (3,3) resonance energy region. The results have been interpreted in terms of pion-nucleon interaction cross section through isobar formation, using the optical model formalism. Good agreements have been obtained between the experimental and calculated results.

The results indicate that the maximum in cross section occurs at about 160 MeV pion incident energy, which is less than the energy at which the (3,3) resonance occurs. This shift in the position of the maximum cross section is attributed to the optical model potential seen by the pion inside the nucleus. Other available experimental data of positive pion interaction cross sections with complex nuclei have been summarized and interpreted successfully by using our model.

This model has also been used to obtain the fraction of pions absorbed inside the nucleus in antiproton annihilation. When an antiproton annihilates on a nucleon

a number of pions are produced. If, however, the annihilation takes place inside the nucleus, a fraction of pions is absorbed before coming out of the nucleus. The available experimental data on pion multiplicities in $\bar{p}$ annihilation with hydrogen and emulsion nuclei are compared to obtain the absorption fraction. The results have good agreements with the calculated values in the (3,3) resonance region.

The pion-nucleus optical model potential used for our calculation has been obtained on the basis of the theory of Frank-Gammel and Watson in conjunction with the "effective-range" theory of Chew and Low. Many body effects have been taken into account by applying the Pauli exclusion principle to the intermediate state of the nucleon. It has been shown that in the nucleus the peak of the (3,3) resonance in pion-nucleon scattering is considerably reduced and its position shifts towards higher energy.

To investigate the mechanism of absorption of pions in complex nuclei, a detailed analysis of the energetic protons produced in the pion induced emulsion stars have been carried out. The stars were produced by
a) direct interaction of 70 MeV positive pions and

b) $\bar{p}$ annihilation in emulsion. In the latter case, $\bar{p}$ annihilates to produce pions which in turn interact with other nucleons in the nucleus. The absorption of a pion takes place on a pair of nucleons to emit two energetic nucleons. The distributions of energy and opening angles of the energetic proton pairs as well as the energy distribution of the individual energetic protons have been measured. The results are compared with the results obtained from Monte Carlo calculations.

ACKNOWLEDGEMENTS

The author wishes to express his sincere gratitude to Prof. J. Hébert for his guidance and encouragement during the entire course of this work.

The author would like to thank Prof. E. Ekspong (of the University of Stockholm) for supplying the 72 MeV pion irradiated emulsion plates and to Dr. N. Tanner and Dr. J. Domingo from CERN, for allowing us to use their electronics for the irradiation of our emulsion stacks (168, 224 and 254 MeV stacks). The author would also like to thank Dr. A. Herz and the staff of the emulsion laboratory, CERN, for extending the facilities for processing the emulsion stacks and to Dr. H. Mes for the Monte Carlo programme. Thanks are also due to Dr. J. Law, Dr. H. Mes, Dr. Joan Hébert, Mr. R. Molloy, Mr. A. Filion for valuable discussions on various occasions and to Mr. R. Banerjee for helping in computer programming.

It is a pleasure to express the author's appreciation to Prof. E. P. Hincks of Carleton University, from whose course (1965-1966) and stimulating discussions the author got the initial interest in high energy physics.

Finally, the author is indebted to the Physics Department of the University of Ottawa, for financial assistance in the form of teaching assistantship and to Prof. J. Hébert for financial support from his N. R. C. research grants. A travel grant to Canada from K.C.Mahindra Educational Trust,India is also gratefully acknowledged.

Statement of Originality

This project is the first accurate and systematic study of the inelastic interaction of positive pions with complex nuclei of emulsion in the low energy region extending up to the (3,3) resonance energy region. To the best of the author's knowledge, the following contributions are original:

Calculation of the pion-nucleus optical model potentials based on the Chew-Low theory, considering the effect of the (3,3) resonance as well as the Fermi motion of the nucleons.

A nearly monoenergetic and wide pion beam has been used to irradiate the emulsion plates; the incident beam being inclined at certain suitable angles (and at right angles) to the plane of the emulsion. The inclined beam has been shown to be very useful in cross section measurements.

Systematic and accurate measurement of the inelastic interaction cross sections of positive pions with the complex nuclei of emulsion in the energy region 10 to 60 MeV and at three higher energies.

The results have been interpreted on the basis of the pion-nucleon interaction through the isobar formation. The results tend to indicate the presence of the pion-nucleus interaction potential.

From the measured cross sections, the imaginary parts of the optical model potential, V_I, have been obtained.

Fractional loss of pions (pions being produced inside the nucleus due to the annihilation of antiproton), as a result of the absorption inside the nucleus, has been explained on the basis of the above model.

From about seven hundred pion induced stars (with pion energy 30 to 60 MeV) in nuclear emulsion, the following experimental distributions have been obtained:

1) Energy distribution of the fast protons emitted in pion absorption stars.

2) Energy distribution (sum of the energy of the two protons) of the fast proton pairs emitted in pion absorption stars.

3) Distribution of the opening angles between the two fast protons.

The results have been compared with the Monte Carlo calculations.

Similar distributions have also been obtained experimentally for about 450 $\bar{p}$ annihilation stars.

Table of Contents

List of Illustrations

List of Tables

List of Symbols and Abbreviations.

A	Atomic mass number
c	Velocity of light
f	Pion-nucleon coupling constant
f_α	Scattering amplitude
g^*	Normalized grain density
F	Fermi=10^{-13} cm.
F-G-W	Frank-Gammel and Watson
h	Planck's constant
$\hbar c$	197.3 MeV. Fermi
K	Absorption coefficient
K-N	Kimura and Nagashima
mb	Millibarn
MeV	Million electron volts
n	Neutron
N	Nucleon
N^*	Isobar
p	Proton
$\bar{p}$	Antiproton
P_α	Projection operator
r_o	Nuclear radius parameter

T_α	Scattering matrix
V	Optical model potential
V_R	Real part of the optical model potential
V_I	Imaginary part of the optical model potential
V_c	Coulomb potential
π^+	Pion with positive charge
ω	Total pion energy in the C. M.system
μ	Micron = 10^{-4} cm
μ^+	Muon with positive charge
δ_α	Pion-nucleon phase shifts
$\eta(\omega)$	Pauli exclusion factor
$\bar{\sigma}$	Average pion-nucleon interaction cross section

Chapter I

INTRODUCTION

I-1 Motivation for this Project

From the Yukawa's theory of nuclear forces, it is known that the pion is the main mediator of the nuclear forces, the range of which is determined by the pion-Compton wavelength $\sim$ 1.4 Fermi. Since the discovery of the pion in 1947, therefore, it has been used extensively as a nuclear probe. The pion is a strongly interacting boson of mass 139.6 MeV (positive and negative pion $\pi^{\pm}$) and 135 MeV (neutral pion π^{o}) having isospin 1 and spin 0. Because of its strong interaction with the nuclear nucleons, it is expected that these studies will give valuable informations regarding the behaviour of the nucleons inside the nucleus.

The advantage of the pion over the nucleon as a nuclear probe is due to the fact that the pion is a boson and consequently can be absorbed in nuclei provided the energy-momentum balance is satisfied. Thus pion can be used as a probe, like photon, which can disappear from the final products of the reactions. Moreover, the rest mass and the kinetic energy of the pion can be known accurately and hence the kinematics can be worked out without much difficulty. Since the pion has isotopic spin 1, it exists in three different charge states; π^+ (positive pion), π^- (negative pion) and π^0 (neutral pion) with the z component of the isotopic spin, T_z, equal to +1, -1 and 0, respectively. This makes the double charge exchange, $\pi^\pm \rightarrow \pi^\mp$ possible, with charged particles in both initial and final states. These reactions make it possible to study $\Delta T_z = \pm 2$ transitions in nuclei which are inaccessible by other means.

The pion, like other nuclear particles, can interact with the nucleus either elastically or inelastically. In an elastic process, the nucleus is left unexcited whereas in an inelastic process the incident particle transfers energy to the nucleus. A large number of theoretical and experimental studies have been carried out for the elastic scattering of pions (Rainwater 1956, Auerbach 1967). There is however a general lack of systematic study of inelastic interactions of pions. At the CERN conference (CERN 1963) the experimental knowledge of pion interactions with complex nuclei was , on the whole, characterized by a lack of quantitative information on the basic properties of the π-nuclear interaction. As a consequence much of the theoretical discussion was qualitative, tentative, even in part speculative. The need of a systematic study of pion nucleus interaction was, therefore, emphasized by Ericson (1965) and by Jean (1964). This group has, thus, undertaken a study of the inelastic interaction of pions (with special emphasis on low energy pions with energy less than 300 Mev) with complex nuclei. The particular interest of working with low energy pions, well below the (3,3) resonance energy, is due to the fact that the measurement of cross sections at these energies can yield valuable information regarding the pion nucleus potential. The results of Nikol'skii et al. (1957) (also Metropolis et al. (2); 1958 and Fuji; 1959) indicate that a nuclear potential, which is the real part of the optical model potential, is seen by the pion inside the nucleus. Any potential seen by the pion is expected to influence the interaction cross section. At low pion energies (i.e; the energy region of our interest), potentials of the order of 10 to 30 MeV (the magnitude of the potential which may be seen by the pion inside the nucleus) are expected to produce considerable changes in the interaction cross section. Thus a comparison of the experimental and the calculated results can give us the magnitude of the potential. The measurements near the resonance energy is expected to provide the effect of the (3,3) resonance inside the nucleus.

I-2 Inelastic Interaction of Pions

In an inelastic interaction, the pion can either get absorbed inside the nucleus or can come out of the nucleus with reduced energy. 'Inelastic events' include all the incoherent processes; i.e. absorption, inelastic scattering, single and double charge exchange and stops in flight. In absorption, the rest mass and its associated kinetic energy is transferred to the interacting nucleons. Experimentally, from a series of experiments on proton-proton (pp), proton-neutron (pn) and neutron-neutron (nn) pairs emitted in pion absorption (Ozaki 1960), it is well known that the absorption predominantly takes place on a pair of nucleons. This is also quite evident from the consideration of absorption kinematics. For, if all the available energy, which is the rest mass energy, 139 MeV or more, is given to one single nucleon, its momentum will be of the order of 500 MeV/c or more and this, by momentum conservation, must be the order of magnitude of its initial momentum. It is, however, unlikely to find inside a nucleus a nucleon with momentum higher than the Fermi momentum, 225 MeV/c, so that the emission of one nucleon must be strongly suppressed. On the other hand, if the available energy is shared about equally between a pair of nucleons, each nucleon carries with it only 70 MeV kinetic energy; i.e. a momentum of about 375 MeV/c. The angle between the two outgoing nucleons can be such that the resultant final momentum is equal to the resultant of the momenta of the two participating nucleons. Thus it is more likely that the absorption occurs predominantly on a pair of nucleons rather than on a single nucleon. The absorption on more than two nucleons is, however, permitted; but the cross sections are comparatively small.

If the pion is not absorbed, it can interact with one of the nucleons and can transfer a part of the kinetic energy to the nucleon. The pion can further interact or may come out with reduced energy. In any case, these nucleons can collide with other nucleons and start a cascade. During these collisions, the nucleus can become highly excited and evaporation may result emitting a few nucleons. In a charge sensitive medium; e.g. in emulsion, the charged particles are recorded and hence the event is manifested as a visible star. If no outgoing pion is visible, the star can be either due to absorption, or charge exchange if the incident pion is a charged one.

I-3 Models for Pion-Nucleus Interactions

On the basis that the absorption of pions takes place on a pair of nucleons, Brueckner et al. (Brueckner 1951) proposed a model in which the pion is absorbed on a pair of correlated nucleons. This model, known as Brueckner-Serber-Watson (B-S-W) model or 'quasi-deuteron model' of absorption, satisfactorily explained the pi-mesic X-rays. This model, however, fails to explain the correct ratio of n:n and n:p as observed by Ozaki et al. This model can only predict the pure absorption cross section, and cannot predict the total inelastic cross section which can be easily measured. According to this model, the absorption cross section is proportional to the pion-deuteron interaction cross section. This proportionality constant is a measure of the nuclear correlation inside the nucleus and is not a very well defined quantity.

Comparatively recently, Fraenkel (1963) has proposed a model in which the absorption takes place in two stages. According to this model, the incident pion interacts with one of the nucleons inside the nucleus to form an unstable resonance state or an isobar:

$$\pi + N_1 \rightarrow N^* \qquad \text{(a)}$$

where N and N* stand for a nucleon and an isobar, respectively.

The isobar may then either

i) interact with another nucleon and gets absorbed emitting two nucleons:

$$N^* + N_2 \rightarrow N_3 + N_4 \qquad \text{(b)}$$

or ii) the isobar may decay into a pion and a nucleon:

$$N^* \rightarrow \pi + N \qquad \text{(c)}$$

In this process, the pion can exchange its charge resulting in a charge exchange reaction. This process can occur twice and the result will be a double charge exchange. These outgoing nucleons and the pion (if present) can interact with other nucleons as described in the previous section. Generally, the two nucleons which are emitted due to the absorption will have high energy, since the rest mass energy of the incident pion is transferred as kinetic energy to these two primary nucleons. This model is also essentially a two-nucleon interaction model, but is much simpler than the B-S-W model. In this model the total interaction cross section is simply determined by the interaction given in stage 'a' which is precisely known over a wide energy range.

I-4 The Scope of the Work

In the present work the result of the experimental measurements of the cross section of inelastic interaction of positive pions with the complex nuclei in emulsion are presented for the (3,3) resonance energy region. More emphasis has been given in the lower energies up to about 70 MeV. The experimentally measured cross sections are compared with the predictions of the B-S-W model and the isobar model using the optical model potentials. The optical model potentials used for this purpose have been calculated in Chapter II on the basis of Chew-Low theory (Chew 1956). Other available data on $\pi^{\pm}$-nucleus interaction cross sections have also been compared with the isobar model calculations. In Chapter V, the absorption fraction of pions, emitted in the antiproton annihilation inside the nucleus have been interpreted with the same model. The spectra of the energy and the opening angles of the fast nucleon pairs (emitted in the primary interaction of pions) have been obtained experimentally and are analysed with the model by Monte-Carlo calculations.

I-5 Review of the Earlier Work.

Since 1950, a considerable number of experiments have been carried out to explain the mechanism of interaction of pions (both positive and negative) with complex nuclei. Due to the relative simplicity of obtaining a pure π^- beam, more experiments were done with π^- than with π^+ (Menon. et al. 1950; Adelman.1952). Bernardini (1951) measured the mean free path for the interaction of both π^+ and π^- in emulsion. They obtained the cross sections for star production by π^+ mesons at mean energies between 35 - 50 MeV, and 70 - 80 MeV, which were 380 and 670 mb, respectively. These results give the magnitude of the cross sections, but are not very useful for quantitative analysis due to the large energy width. Rankin and Bradner (Rankin 1952) also studied the interaction of 45.5 MeV π^+ with the emulsion nuclei. Blau, Oliver and Smith (Blau 1953) worked with a π^+ beam having an energy between 50 and 80 MeV. Using laminated emulsions they found that 24-30 percent of the emulsion stars originated in the light nuclei of the emulsion. Their result indicated that the absorption of pions occur chiefly on nucleon pairs. Byfield Kessler and Lederman (Byfield 1952) measured the elastic interaction cross section of 62 MeV π^+ and π^- with carbon nuclei.

The interaction of positive pions of energies 33, 46 and 68 MeV with beryllium, carbon, aluminum and copper was investigated by Stork (1954). These and earlier results were analyzed by means of the optical model, and a strong energy dependence was found for the pion interaction cross section in nuclear matter. The general features of the energy dependence were explained qualitatively by using optical model. A satisfactory representation of the energy dependence was given by:

$$\lambda_a/\gamma_o = [\ 2b\ (k\gamma_o)^4\ /\ w^2\ ]^{-1} \qquad 1.1$$

where

λ_a = mean free path of interaction

γ_o = pion Compton wavelength

k = pion wave number

= $p_\pi/\hbar$; p_π is the initial pion momentum and $\hbar$ is the Planck's constant.

w = total pion energy expressed in units of pion rest mass.

The quantity 'b' is a constant and was obtained by extrapolation. This analysis, however, does not give any physical interpretation of the interaction mechanism.

The sharp energy dependence of pion-nucleus interaction cross section was also observed by Tracy (1953) in his cloud chamber study of the interaction of π^+ meson with aluminum. He obtained the cross sections at average energies of 38, 57 and 82 MeV. These results are further discussed in section IV-6. Similar work was done by Saphir (1956) with lead at 50 ± 15 MeV. In most cases, however, the results can not be used for rigorous quantitative analysis either due to insufficient statistics or large pion beam energy or because of lack of exact knowledge of muon contamination. A comparatively more systematic study was carried out by Blinov et al. (Blinov 1958). They used a 17 liter bubble chamber to study the interaction of π^+ mesons with complex nuclei in freon. The cross sections for scattering, absorption, charge exchange and production of charged mesons were measured for the incident pion energy of 80 to 280 MeV.

From the theoretical point of view, the absorption mechanism was first given by Brueckner (1951), and the model (B-S-W model) has been explained in section I-3. In recent years, following the suggestion of Ericson and Jean many attempts have been made to investigate the pion interactions with nuclei. Kopaleishvili (1967) and his group have investigated the pion capture processes in

^{16}O and ^{12}C taking strictly into account the interaction between the emitted nucleons. The calculations were made with the independent pair model for target nuclei. The absorption of stopped negative pions on ^{6}Li and ^{12}C; accompanied by the emission of two nucleons, have been studied by Sakamoto (1966) in terms of the direct pion absorption by nucleon pairs. The absorption rates of pions were expressed as a function of the centre-of-mass and relative momenta of the nucleon pairs for investigating the momentum distributions of nucleons inside the nucleus.

Fraenkel (1963) proposed a model in which absorption takes place in two stages through isobar formation. This model has been discussed in section I-3. Recently, Le Tourneux (1966) has investigated the absorption of pions in a single nucleon inside the nucleus. In this case the absorption takes place by the Fermi motion of the nucleons. Since the nuclear Fermi momentum is small, this absorption mechanism is very weak. The absorption rate, through this channel, is 10^3 to 10^4 times smaller than the observed rate. This mechanism, therefore, does not play any significant role in the absorption of pions.

Chapter II

PION-NUCLEUS OPTICAL MODEL POTENTIAL

II-1 Introduction

"The Optical model" of a nucleus or the so-called 'cloudy crystal ball' model is one of the simplest nuclear models which can easily describe the interaction of a particle with a nucleus. The initial development of the model was due to Fernbach-Serber and Taylor (1949) following some earlier work of Serber (1947).

In the optical model, the nucleus is represented by a complex nuclear potential, V, which is a function of the space coordinate and incident energy of the particle. The imaginary part of the potential, V_I, describes inelastic processes permitted by the Pauli principle and by the law of conservation of energy. The real part, V_R, describes elastic processes and is manifested as the interaction energy of the incident particle with the nucleus.

In its simplest form, the optical model potential, V, can be represented by a square potential well

$$V = V_R + i\ V_I \qquad (2.1)$$

Many other complicated forms of V are available but in most cases a number of adjustable parameters are necessary. The real and the imaginary parts of the optical model potentials may be related to the propagation coefficient, k_1, and the absorption coefficient K, respectively:

$$V_R = \beta\ \hbar c k_1 \qquad (2.2)$$

$$V_I = \tfrac{1}{2}\beta\ \hbar c K \qquad (2.3a)$$

$$= \frac{\beta \hbar c}{2\lambda_t}\ ; \quad \frac{1}{\lambda_t} = \frac{1}{\lambda_s} + \frac{1}{\lambda_a} \qquad (2.3b)$$

Relativistically, V_I is given by

$$V_I = K\ \frac{\hbar c}{m}\ \frac{\sqrt{1 - \beta^2}}{\beta}\ E \qquad (2.4)$$

where β is the ratio of the velocity of the incident particle to the velocity of light c

m = mass of the incident particle in energy unit

E = kinetic energy of the incident particle.

$\hbar = \frac{h}{2\pi}$; h = Planck's constant.

λ_t = mean free path for either inelastic scattering or absorption of the incident particle.

λ_s and λ_a are the mean free paths for inelastic interaction and absorption, respectively.

The absorption coefficient, K, in nuclear matter is equal to the particle density times the cross section for scattering, $\bar{\sigma}$, of the incident particle by a nucleon in the nucleus:

$$K = \frac{3\ A\bar{\sigma}}{4\ \pi R^3} \tag{2.5}$$

Here A and R are the mass number and the radius of the nucleus, respectively. The propagation coefficient, k_1, is given by

$$k + k_1 + \tfrac{1}{2}iK = \frac{\left[2m\ (E + V)\right]^{\frac{1}{2}}}{\hbar c} \tag{2.6}$$

when the wave number k:

$$k = \frac{(2mE)^{\frac{1}{2}}}{\hbar c} \tag{2.7}$$

II-2 Theory of Frank-Gammel and Watson

The first systematic theory of pion-nucleus optical model potential was developed by Frank-Gammel and Watson (1955), hereafter referred to as F-G-W. According to F-G-W, $V(\omega_o)$ should have the form (excluding the term involving the meson absorption):

$$V(\omega_o) = V_R(\omega_o) + i\, V_I(\omega_o)$$
$$= - \frac{2\pi}{4\pi r_o{}^3} \frac{1}{E_\pi} \frac{W}{M} f_o(\omega_o) \qquad (2.8)$$

The meson absorption term is obtained by taking $1/\lambda_a$ to be proportional to the capture cross section, σ_d, of pions by deuterons

$$\frac{1}{\lambda_a} = \frac{m_\pi}{\hbar c} \left[\frac{0.107}{\eta_q} (0.14 + \eta_q^2) \right] \qquad (2.9)$$

The equation (2.9) is obtained by using the semiempirical formula for σ_d given by Gell-mann and Watson (1954). According to this, σ_d can be expressed as a function of the pion momentum:

$$\sigma_d = \left(\frac{4.45}{\eta_q}\right) \quad [0.14 + \eta_q^2]$$

where $\eta_q = qc/m_\pi$ is the C.M. pion momentum in units of pion rest mass. $f_o(\omega_o)$ is the pion-nucleon forward scattering amplitude in the C.M. system for a pion having C.M. energy ω_o. This is a complex quantity and consists of real and imaginary parts. M is the rest mass of nucleon, E_π is the total energy of the pion in the laboratory frame of reference, W is the total energy of the system in C.M. frame. F-G-W- used $r_o = 1.4F$.

Using Clebsh-Gordon coefficients, the forward scattering amplitude, $f_o(\omega_o)$, for positive pion in a nucleus having A nucleons and Z protons is

$$f_o(\omega_o) = \frac{2}{3}\left(\frac{Z}{A} + \frac{1}{2}\right) f_{03} + \frac{2}{3}\left(1 - \frac{Z}{A}\right) f_{01} \qquad (2.10)$$

where f_{03} and f_{01} are forward scattering amplitudes for isotopic spin 3/2 and ½, respectively; and are given by

$$\begin{aligned} f_{03} &= f_3 + f_{31} + 2f_{33} \\ f_{01} &= f_1 + f_{11} + 2f_{13} \end{aligned} \qquad (2.11)$$

where f_3 and f_1 are the S wave amplitudes and f_{31}, f_{33}, f_{11}, f_{13} are the P-wave partial wave amplitudes.

For a nucleus of equal number of protons and neutrons, equation (2.10) becomes identical for both positive and negative pions and is given by

$$f_o(\omega_o) = \frac{2}{3} f_{03} + \frac{1}{3} f_{01} \tag{2.12}$$

It is to be noted that the value of the energy, ω, at which $v(\omega_o)$ is to be evaluated is obtained from the relation

$$\omega = \omega_o - v(\omega) \tag{2.13}$$

where ω_o is the actual energy of the incoming meson. The scattering amplitude $f_o(\omega_o)$ is complex and the real part

$$\begin{aligned} \text{Re } f_o(\omega_o) &= \frac{1}{3} [2\text{Re } f_{03} + \text{Re } f_{01}] \\ &= \frac{1}{3q} [J_{03} + \tfrac{1}{2} J_{01}] \end{aligned} \tag{2.14}$$

with

$$\begin{aligned} J_{03} &= \sin 2\delta_3 + \sin 2\delta_{31} + 2\sin 2\delta_{33} \\ J_{01} &= \sin 2\delta_1 + \sin 2\delta_{11} + 2\sin 2\delta_{13} \end{aligned} \tag{2.15}$$

where δ's are the pion-nucleon phase shifts. Given the phase shifts, it is possible to evaluate the real part of the optical model potential, V_R, by using equations 2.15, 2.14 and 2.8. Similarly, the imaginary part of the forward scattering amplitude, Im $f_o(\omega_o)$, can be expressed in terms of α's to give V_I.

Frank-Gammel and Watson used the values of J_{03} and J_{01} directly determined from the pion-proton interaction studies by Anderson-Davidon and Kruse (1955). V_R and V_I obtained by F-G-W are shown in fig. 2.5 as a function of the pion kinetic energy outside the nucleus (dashed lines: V_R (F-G-W) and V_I (F-G-W)). A sharp energy dependence of the potentials are observed and V_R changes its sign at the free space resonance energy.

The F-G-W theory is based on the assumption that the two body forces within the nucleus are very nearly the same as between the free particles and that the many body forces are negligible. This assumption, however, is not quite justified, particularly near the (3,3) resonance energy for pion-nucleon scattering. The effect due to the many body forces can be taken into account through the Pauli exclusion principle. Instead of taking the phase shifts directly from the pion-nucleon interaction results, it is possible to calculate the scattering amplitude from the 'effective-range theory' of Chew and Low (1956). In its original form, the Chew-Low theory gives the pion-nucleon scattering amplitude in free space. Pauli exclusion principle can be applied to the intermediate state of the pion-nucleon system; i.e. to the isobar state, to account for the effect of the neighbouring nucleons. Preliminary attempts were made by Miyazawa (1964) and by Kimura and Nagashima (1965, hereafter referred to as K-N). In their calculations K-N assumed, for simplicity, that the nucleons are on the average at rest although a scattered nucleon must have energy greater than the Fermi energy to satisfy the Pauli exclusion principle. By neglecting the Fermi motion of the target nucleons, K-N have made the effect of the Pauli exclusion principle very severe. According to their calculations the resonance energy inside the nucleus shifts by about 200 MeV from the free state resonance value. It was shown by Mes et al (1967) that such a high resonance energy would cause much larger pion absorption than is observed experimentally.

In the following sections we will use the Chew-Low theory to obtain the (3,3) scattering amplitude inside the nucleus by taking into account the many body effect and the Fermi motion of the target nucleons. This amplitude will be used to obtain the optical model potential inside the nucleus.

II-3 Modified Theory for Pion-Nucleus Optical Model Potential

II-3.1 Scattering Amplitude

Let us consider the pion-nucleon scattering in free space. We start with the unitarity relationship between the scattering amplitudes as given by Chew and Low:

$$T^{+}_{pq}(\omega) - T_{qp}(\omega) = 2\pi i \sum_{n} \delta(\omega_n - \omega)\, T^{+}_{pn}(\omega)\, T_{qn}(\omega) \qquad (2.16)$$

where T's are the conventional T matrices of the scattering theory and are given by:

$$T_{pq}(\omega) = -v(q^2)\, v(p^2) \frac{4\pi}{\sqrt{4\omega_p \omega_q}} \sum_{\alpha=1}^{4} P_{\alpha}(p,q)\, h_{\alpha}(\omega) \qquad (2.17)$$

T^{+} is the conjugate transpose of T and $\omega_n = \sqrt{1 + n^2}$, where n includes the three components of the momentum.

$v(q^2)$ is related to the source function $\rho(x)$ by

$$v(q^2) = \int e^{-i\vec{q}\cdot\vec{x}}\, \rho(\vec{x})\, d^3x \qquad (2.18)$$

The scattering amplitude $f_{\alpha}(\omega)$ is obtained from $h_{\alpha}(\omega)$, from the relation

$$f_\alpha(\omega) = q^2 h_\alpha(\omega) \tag{2.19}$$

P's are the projection operators for the four states of the total angular momentum and the isotopic spin:

$$\begin{aligned}
P_{11} &= \tfrac{1}{3} t_p t_q (\vec{\sigma}\cdot\vec{p})(\vec{\sigma}\cdot\vec{q}) = \mathcal{T}_{1/2}(\vec{q},\vec{p})\, \jmath_{1/2}(\vec{q},\vec{p}) \\
P_{13} &= \tfrac{1}{3} t_p t_q \left[3\,\vec{p}\cdot\vec{q} - (\vec{\sigma}\cdot\vec{p})(\vec{\sigma}\cdot\vec{q})\right] = \mathcal{T}_{1/2}\, \jmath_{3/2} \\
P_{31} &= (\delta_{pq} - \tfrac{1}{3} t_p t_q)(\vec{\sigma}\cdot\vec{p})(\vec{\sigma}\cdot\vec{q}) = \mathcal{T}_{3/2}\, \jmath_{1/2} \\
P_{33} &= (\delta_{pq} - \tfrac{1}{3} t_p t_q)\left[3\,\vec{p}\cdot\vec{q} - (\vec{\sigma}\cdot\vec{p})(\vec{\sigma}\cdot\vec{q})\right] = \mathcal{T}_{3/2}\, \jmath_{3/2}
\end{aligned} \tag{2.20}$$

In the subscript $\alpha = (2I, 2J)$; I is the total isotopic spin and J is the total angular momentum. t_k is the kth component of the nucleon isotopic spin, $\bar{\sigma}$ is the nucleon spin vector, $\mathcal{T}_\alpha$ and $\jmath_\alpha$'s are the isospin and spin part of the projection operator, respectively. Substituting equation (2.17) in (2.16) one obtains

$$\sum_\alpha P_\alpha(q,p)\left\{ h_\alpha^\dagger(\omega) - h_\alpha(\omega) \right\}$$

$$= 2\pi i \sum_n \frac{4\pi}{\sqrt{4\omega_n^2}}\, v^2(n^2)\, \delta(\omega_n - \omega) \sum_{\alpha,\beta} P_\alpha^\dagger(p,n) P_\beta(q,n)\, h_\alpha^\dagger(\omega) h_\beta(\omega) \tag{2.21}$$

or

$$\sum_{\alpha} P_{\alpha}(q,p)\, \mathrm{Im}\, h_{\alpha}(\omega)$$

$$\doteq 2\pi^2 \sum_{n} \frac{v^2(n^2)}{\omega_n}\; \delta(\omega_n-\omega) \sum_{\alpha,\beta} P_{\alpha}(n,p)\, P_{\beta}(q,n)\, h_{\alpha}^{+} h_{\beta} \tag{2.22}$$

Now since

$$\sum_{n} \rightarrow \quad \frac{1}{(2\pi)^3} \sum_{spin} \int n^2\, dn\; d\Omega_n \tag{2.23}$$

$$d\Omega_n = \int d\phi \int d\cos\theta$$

and $\omega_n^2 = n^2 + 1$

equation (2.22) can be rewritten as

$$\sum_{\alpha} P_{\alpha}(q,p)\, \mathrm{Im}\, h_{\alpha}(\omega)$$

$$= \frac{2\pi^2}{(2\pi)^3} \sum_{spin} \int n\, d\omega_n\, v^2(n^2)\, \delta(\omega_n-\omega) \sum_{\alpha,\beta} \int d\Omega_n P_{\alpha}(n,p) P_{\beta}(q,n)\, h_{\alpha}^{+} h_{\beta} \tag{2.24}$$

But since P_{α}'s are projection operators, we can write

$$\sum_{\alpha,\beta}\sum_{spin}\int d\Omega_n P_\alpha(n,p)\, P_\beta(q;n)$$

$$=\sum_{\alpha,\beta}\delta_{\alpha\beta}\sum_{spin}\int d\Omega_n\, P_\alpha(n,p)\; P_\alpha(q,n) \tag{2.25}$$

Hence, to obtain Im $h_\alpha(\omega)$ we have to evaluate:

$$\sum_{spin}\int d\Omega_n P_\alpha(n,p)\, P_\alpha(q,n) \tag{2.26}$$

for (3,3) amplitude, in particular,we have to evaluate

$$\sum_{spin}\int d\Omega_n P_3(n,p)\; P_3(q,n) \tag{2.27}$$

$$=\sum_{spin}\int d\Omega_n\, \mathcal{T}_{3/2}(p,n)\,\mathcal{T}_{3/2}(n,q)\, J_{3/2}(p,n)\, J_{3/2}(n,q) \tag{2.28}$$

The isospin part yields (see Appendix 1):

$$\sum \mathcal{T}_{3/2}(p,n)\;\mathcal{T}_{3/2}(n,q) = \mathcal{T}_{3/2}(p,q) \tag{2.29}$$

The spin space part:

$$\sum\int d\Omega_n J_{3/2}(p,n)\, J_{3/2}(n,q)$$

$$=\sum\int d\Omega_n\left[3\,\vec{n}\cdot\vec{p}-(\vec{\sigma}\cdot\vec{n})(\vec{\sigma}\cdot\vec{p})\right]3\,\vec{q}\cdot\vec{n} \tag{2.30}$$

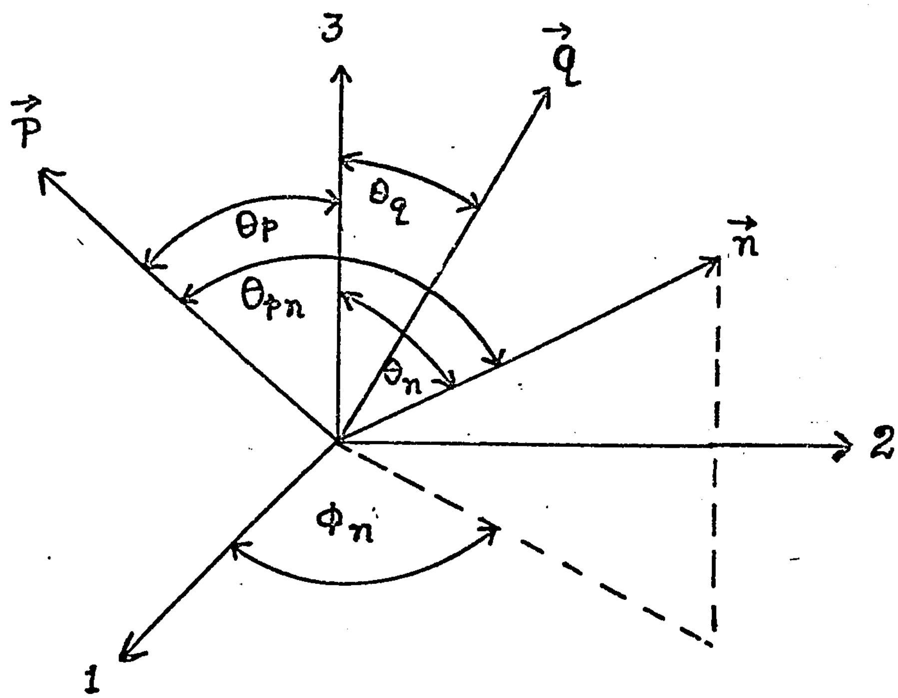

Fig. 2.1. Angle between two vectors

Referring to fig. 2.1, we write the first term of the R.H.S. of the equation 2.30;

$$\Sigma\, d\Omega_n (3\,\vec{n}\cdot\vec{p})(3\,\vec{q}\cdot\vec{n})$$

$$= q\int d\Omega_n\, n^2\, p\, q\, \cos\theta\, \cos\theta_{pn}$$

$$= q\, p\, q\, n^2 \int d\Omega_n \cos\theta \left[\cos\theta_p \cos\theta_n + \sin\theta_p \sin\theta_n \cos(\phi_p - \phi_n)\right]$$

(2.31a)

Here Cos θ_{pn} has been obtained by using spherical harmonic addition theorem (See Appendix 1). Now if we choose $\vec{q}$ to be our Z axis, then $\theta_q=0$, $\theta_p=\theta_{pq}$, $\theta_n=\theta$, $\Omega_n=\Omega$ and equation (2.31) takes the form:

$$\int d\Omega_n (3\vec{n}\cdot\vec{p})(3\vec{q}\cdot\vec{n})$$

$$= q p q n^2 \int d\Omega \cos\theta \left[\cos\theta_{pq}\cos\theta + \sin\theta_{pq}\sin\theta\cos(\phi_{pq}-\phi)\right] \tag{2.31b}$$

using $\vec{p}.\vec{q}$ = pq cos θ_{pq} and

$$\int_0^{2\pi} d\phi \cos(\phi_{pq}-\phi) = 0$$

the R.H.S. of equation (2.31b) becomes

$$3\,\vec{p}\cdot\vec{q}\; n^2 \int d\Omega\; 3\cos^2\theta \tag{2.32}$$

similarly, the second term of equation 2.30 can be written as:

$$-\int d\Omega_n\, \vec{\sigma}\cdot\vec{n}\;\; \vec{\sigma}\cdot\vec{p}\;\; 3\vec{q}\cdot\vec{n}$$

$$= -(\vec{\sigma}\cdot\vec{p})(\vec{\sigma}\cdot\vec{q})\int d\Omega\; 3\cos^2\theta\; n^2 \tag{2.33}$$

Using (2.32) and (2.33) in (2.30), we obtain

$$\sum \int d\Omega_n\, J_{3/2}(p,n)\, J_{3/2}(n,q)$$

$$= \left[3\,\vec{p}\cdot\vec{q} - (\vec{\sigma}\cdot\vec{q})(\vec{\sigma}\cdot\vec{p}) \right] n^2 \int d\Omega\ 3\cos^2\theta$$

$$= J_{3/2}(p,q)\, n^2 \int d\Omega\ 3\cos^2\theta \qquad (2.34)$$

Finally using (2.34) and(2.29) in (2.27) we obtain

$$\sum \int d\Omega_n P_3(n,p)\, P_3(q,n)$$

$$= \mathcal{J}_{3/2}(p,q)\ J_{3/2}(p,q)\, n^2 \int d\Omega\ 3\cos^2\theta$$

$$= P_3(q,p)\, n^2 \int d\Omega\ 3\cos^2\theta \qquad (2.35)$$

substituting (2.35) in (2.24) we have

$$\sum P_3(q,p) \operatorname{Im} h_3(\omega)$$

$$= \frac{2\pi^2}{(2\pi)^3} \sum_{spin} \int n\, d\omega_n\, v^2(n^2)\, \delta(\omega_n-\omega) P_3(q,p)\, n^2 \int d\Omega\ 3\cos^2\theta\, |h_\alpha|^2$$

or

$$\operatorname{Im} h_3(\omega)$$

$$= \frac{1}{4\pi} \int n^3\, d\omega_n\, v^2(n^2)\, \delta(\omega_n-\omega)\, |h_3(\omega)|^2 \int d\Omega\, 3\cos^2\theta$$

$$= \frac{1}{4\pi} q^3 v^2(q^2) | h_3(\omega)|^2 \int d\Omega \, 3\cos^2\theta$$

$$= \frac{1}{2} q^3 v^2(q^2) | h_3(\omega)|^2 \int_\theta 3\cos^2\theta (d\cos\theta) \tag{2.36}$$

In free state, there is no restriction due to the Pauli exclusion principle and θ varies from 0 to 180°. Hence for free space

$$\operatorname{Im} h_3(\omega) = q^3 v^2(q^2) | h_3(\omega)|^2 \tag{2.37}$$

Following Chew-Low, we also obtain, for free space

$$h_3(\omega) = \frac{\frac{\lambda_3}{\omega}}{1 - r_3\omega - i\lambda_3 q^3 v^2/\omega} \tag{2.38a}$$

and

$$\operatorname{Re} h_3(\omega) = \frac{\omega}{\lambda_3}(1 - r_3\omega) | h_3(\omega)|^2 \tag{2.38b}$$

with

$$r_3 f^2 = \frac{1}{(4\pi)^2} \int \frac{d\omega}{\omega q v^2} \left[\sigma_+(\omega) + \sigma_-(\omega) \right] \tag{2.39}$$

where $\lambda_3 = (\frac{4}{3}) f^2$, the pion-nucleon coupling constant $f^2 = 0.088$. r_3 is the reciprocal of the (3,3) resonance energy taken in units of pion mass, $\sigma_\pm(\omega)$'s are the pion-nucleon total cross sections.

However, for interaction inside the nucleus, θ in equation (2.36) is restricted and depends on the kinematics of the interaction. Thus the (3,3) amplitude inside the nucleus, Im $h_3^N(\omega)$, is given by

$$\mathrm{Im}\, h_3^N(\omega) = \frac{1}{2} q^3 v^2(q^2) \left| h_3^N(\omega) \right|^2 \int_{\cos\theta_{restricted}} 3\cos^2\theta \, (d\cos\theta)$$

$$= q^3 v^2(q^2) \left| h_3^N(\omega) \right|^2 \eta \tag{2.40}$$

where

$$\eta = \frac{\displaystyle\int_{\cos\theta_{restricted}} d\cos\theta\,(\cos^2\theta)}{\displaystyle\int_{\cos\theta=-1}^{+1} d\cos\theta\,(\cos^2\theta)} = \frac{3}{2} \int d\cos\theta\,(\cos^2\theta) \tag{2.41}$$

corresponding $h_3^N(\omega)$, Re $h_3^N(\omega)$ and r_3^N are given by

$$h_3^N(\omega) = \frac{\frac{\lambda_3}{\omega}}{1 - r_3^N \omega - i \lambda_3 q^3 v^2 \eta / \omega} \tag{2.42a}$$

$$\mathrm{Re}\, h_3^N(\omega) = \frac{\omega}{\lambda_3} \left(1 - r_3^N \omega\right) \left| h_3^N(\omega) \right|^2 \tag{2.42b}$$

with

$$r_3^N f^2 = \frac{1}{(4\pi)^3} \int \frac{d\omega\, \eta}{\omega q v^2} \left[\sigma_+^N(\omega) + \sigma_-^N(\omega) \right] \tag{2.43}$$

II-3.2 Application of the Pauli Exclusion Principle

Because of the exclusion principle, the momentum of the recoiled nucleon must be larger than the Fermi momentum P_F in the laboratory system. If P_L is the momentum of the target nucleon in the same system, then the Pauli exclusion principle requires:

$$E_\pi + \sqrt{P_L^2 + M^2} - E_\pi' \geqslant E_F = \sqrt{P_F^2 + M^2} \tag{2.44}$$

where E_π and E_π' are the laboratory energies of the incident and the scattered pion, respectively.

Now consider the pion-nucleon interaction in the C.M. system. Referring to fig. 2.2, the four-dimensional inner product of $(q-n)_\mu$ with P_μ, the energy momentum vector of the target nucleon, we get

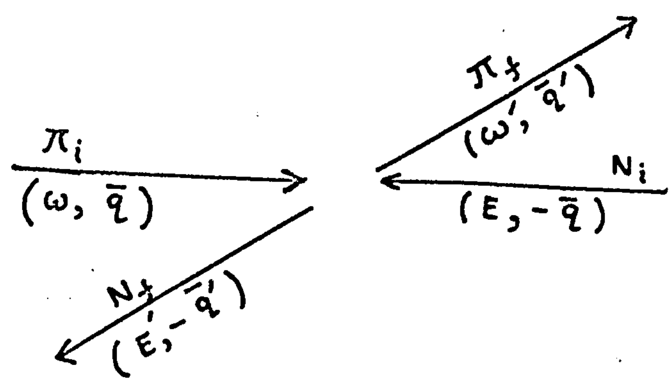

Fig. 2.2 Pion nucleon collision in the C.M. system

$$((q-n)_\mu \cdot p_\mu) = (\bar{q} - \bar{q}') \cdot \bar{q} + (q-q')_0 \cdot E$$

$$= q^2 (1 - \cos\theta)$$

in C.M. system

and

$$= (E_\pi - E_\pi')\sqrt{(P_L^2 + M^2)} - (\vec{P}_\pi - \vec{P}_\pi') \cdot \vec{P}_L$$

in Lab. system

(2.45)

i.e.

$$q^2(1-\cos\theta) + (\vec{P}_\pi - \vec{P}_\pi') \cdot \vec{P}_L = (E_\pi - E_\pi')\sqrt{(P_L^2 + M^2)}$$

But from (2.44)

$$(E_\pi - E_\pi')\sqrt{(P_L^2 + M^2)} \geqslant E_F\sqrt{(P_L^2 + M^2)} - (P_L^2 + M^2)$$

i.e.

$$q^2(1-\cos\theta) \geqslant \sqrt{(P_F^2 + M^2)}\sqrt{(P_L^2 + M^2)} - (\vec{P}_\pi - \vec{P}_\pi') \cdot \vec{P}_L - (P_L^2 + M^2) \tag{2.46}$$

Using binomial expansion and neglecting terms with orders higher than $(1/M)^2$ and the theta dependence of the second term in the right-hand-side of the above equation, we get

$$\left(2q\sin\frac{\theta}{2}\right) \geq \left(P_F^2 - P_L^2 + \frac{P_F^2 P_L^2}{2M^2}\right)^{1/2} = A \tag{2.47}$$

Using this limit of θ, we obtain from (2.41)

$$\eta(P_L, P_F, q)$$

$$= 1 - \frac{3}{4}\left(\frac{A}{q}\right)^2 + \frac{3}{8}\left(\frac{A}{q}\right)^4 - \frac{1}{16}\left(\frac{A}{q}\right)^6 \tag{2.48}$$

Since P_L can have any value from 0 to P_F, η is averaged over the whole Fermi sphere. The Fermi-averaged η is then given by

$$\bar{\eta}(P_F, q) = \frac{4\pi \int_0^{P_F} P_L^2\, \eta(P_L, P_F, q)\, dP_L}{4\pi \int_0^{P_F} P_L^2\, dP_L}$$

$$= \frac{3}{P_F^3}\int_0^{P_F} P_L^2\, \eta(P_L, P_F, q)\, dP_L$$

$$= 1 - \frac{3}{4q^2}\left(\frac{2P_F^2}{5} + \frac{3P_F^4}{10M^2}\right) + \frac{1}{8q^4}\left(\frac{8P_F^4}{105} + \frac{2P_F^6}{35M^2} + \frac{P_F^8}{28M^4}\right)$$

$$- \frac{1}{48q^6}\left(\frac{16P_F^6}{315} + \frac{53P_F^8}{210M^2} + \frac{P_F^{10}}{42M^4} + \frac{P_F^{12}}{72M^6}\right) \tag{2.49}$$

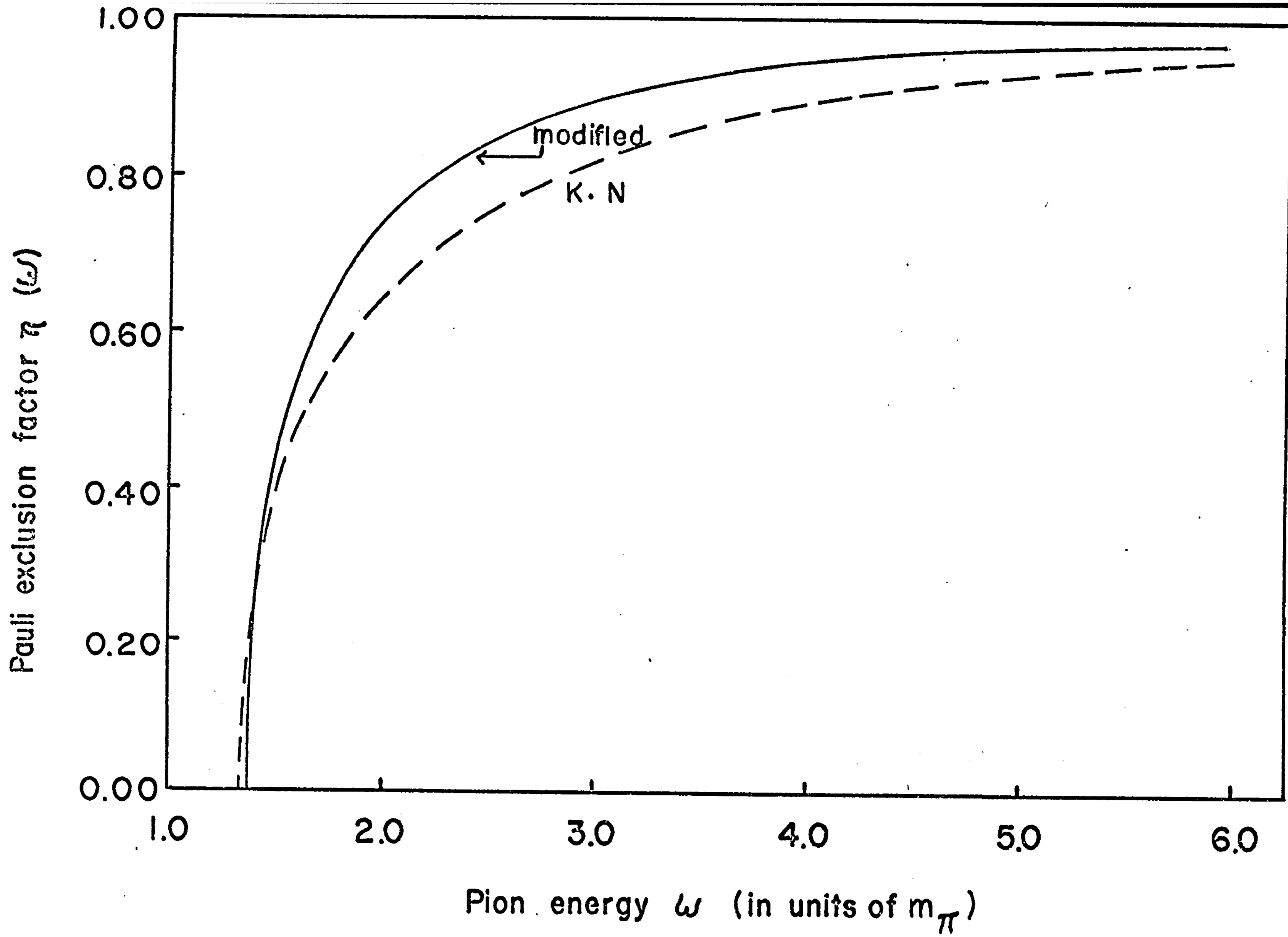

Fig. 2.3 The Pauli exclusion factor as a function of total pion energy. The modified curve is the result of our calculations and K-N is that of Kimura and Nagashima.

The energy dependence of η, for P_F=225 MeV is shown in fig. 2.3 by the solid curve (indicated as η modified). This is compared with η obtained by K-N (dashed curve, η(K-N)):

$$\eta(K\text{-}N) = 1 - \frac{1}{2}\left(\frac{P_F}{q}\right)^2 + \frac{3}{16}\left(\frac{P_F}{q}\right)^4 - \frac{1}{32}\left(\frac{P_F}{q}\right)^6 \qquad (2.50)$$

As mentioned earlier, their calculations are based under some simplifying assumptions and by considering the target nucleons to be, on the average at rest (P_L=0).

II-3.3 Calculation of h_3:

$|h_3|^2$ and the corresponding real and imaginary parts in free space were calculated from equations (2.37) and (2.38) and by using

$$r_3 = 1/\omega_r \qquad (2.51)$$

where ω_r is the (3,3) pion-nucleon resonance energy (total) in the C.M. system. Re $h_3(\omega)$ and Im $h_3(\omega)$ as functions of the total C.M. energy ω (ω expressed in units of pion mass) are plotted in figs. 2.4a and 2.4b (dashed curve), respectively.

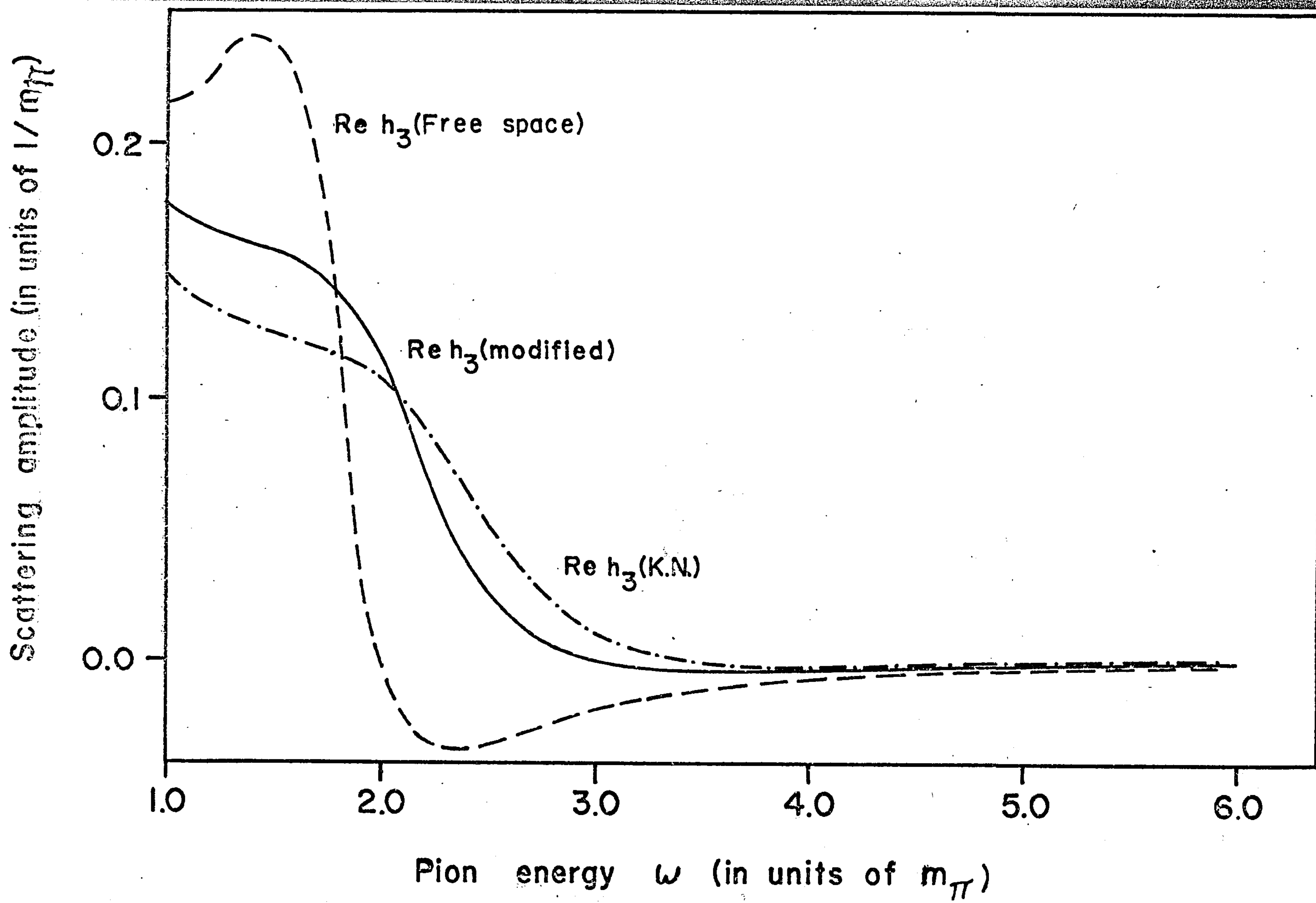

Fig. 2.4 (a) The real part of the (3,3) scattering amplitude, Re h_3, as a function of the total pion energy.

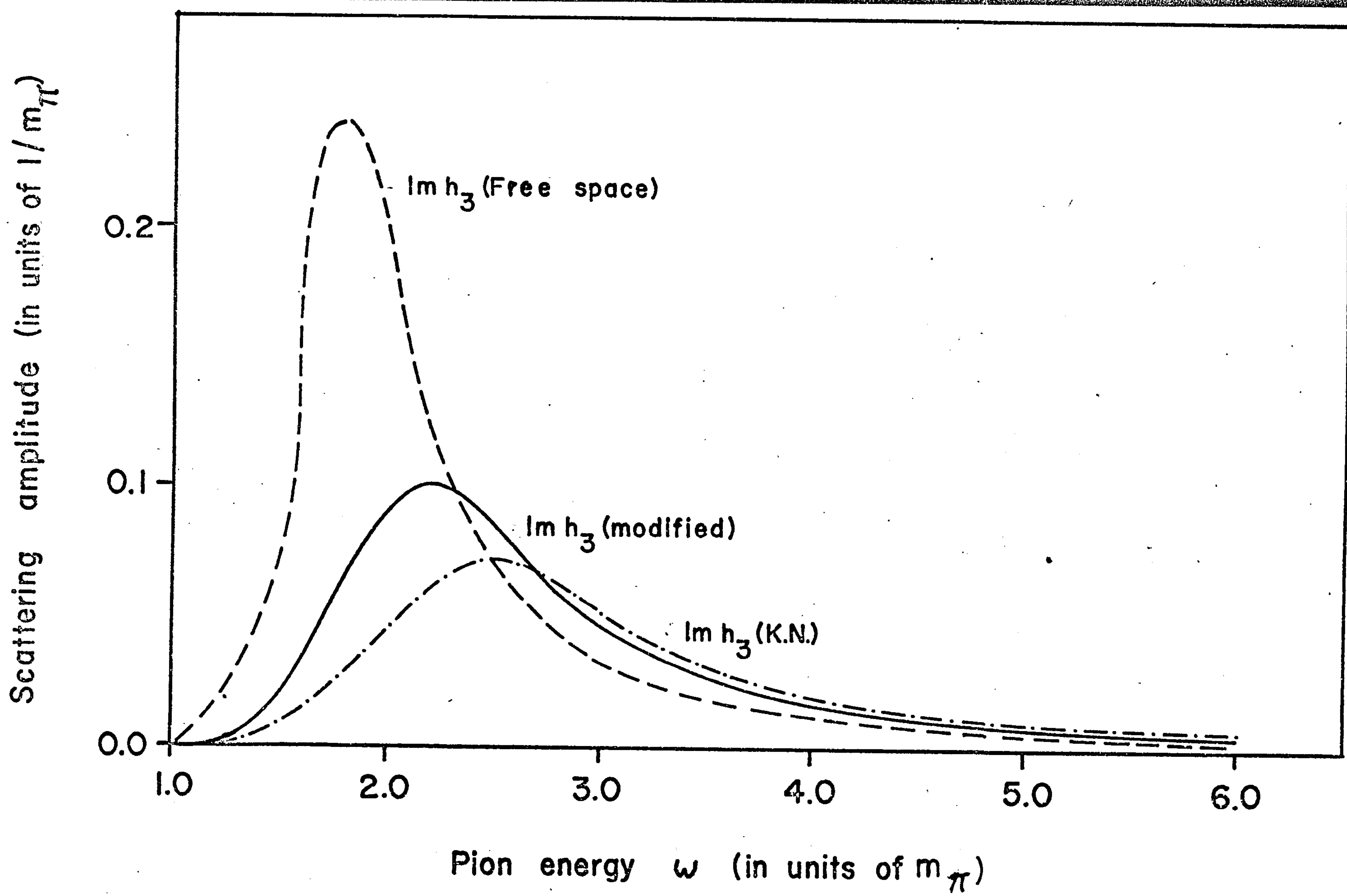

Fig. 2.4 (b) The imaginary part of the (3,3) scattering amplitude, Im h_3, as a function of the total pion energy.

h_3^N, however, cannot be obtained in a straight forward manner, since r_3^N is not known. To obtain r_3^N, following K-N, we separate the equation (2.43) in two parts; an integral part including h_3^N and a residual part containing all other contributions:

$$r_3^N f^2 = \frac{5}{6\pi} \int \frac{d\omega}{\omega} \operatorname{Im} h_3^N(\omega) + \text{residual part} \qquad (2.52)$$

similarly for free space

$$r_3 f^2 = \frac{5}{6\pi} \int \frac{d\omega}{\omega} \operatorname{Im} h_3(\omega) + \text{residual part} \qquad (2.53)$$

In each case, the residual part consists of small amplitudes other than the (3,3) amplitude and, hence, can be considered equal. Since $r_3 f^2$ and Im $h_3(\omega)$ are known, the two equations can be solved to obtain $r_3^N f^2$. The equations were numerically solved by Simpson's rule using the Ottawa University IBM 360 (model 65) digital computer. Solving these equations, r_3^N was found to be 0.34. This value was used in equation (2.42 a), (2.42 b) and (2.40) to obtain $|h_3^N(\omega)|^2$, Re $h_3^N(\omega)$ and Im $h_3^N(\omega)$. Re h_3^N and Im h_3^N are shown by solid curves (indicated as Re h_3^N (modified) and Im h_3^N (modified)) in figs. 2.4a and 2.4b, respectively. The corresponding values obtained by K-N, Re h_3^N (K-N) and Im h_3^N (K-N), are also shown (dash-dotted curve) in the figure.

II-3.4 Calculation of Optical Model Potential

From equation (2.8), the real and imaginary parts of the potentials are given by:

$$V_R^N(\omega) = \frac{-2\pi}{4\pi r_o^3} \frac{1}{E_\pi} \frac{W}{M} \operatorname{Re} f_o^N(\omega) \tag{2.54a}$$

$$V_I^N(\omega) = \frac{-2\pi}{4\pi r_o^3} \frac{1}{E_\pi} \frac{W}{M} \operatorname{Im} f_o^N(\omega) \tag{2.54b}$$

where, as before, quantities with the superscript N represent the quantities inside the nucleus. Re $f_o^N(\omega)$ and Im $f_o^N(\omega)$ are calculated by combining equations (2.11) and (2.12). The most important contribution in $f_o^N(\omega)$ is due to the (3,3) resonance scattering amplitude and is expected to be changed considerably inside the nucleus. In the present calculation, therefore, only the modified form of $f_{33}(\omega)$ has been used. $f_{33}^N(\omega)$ is obtained from:

$$f_{33}^N(\omega) = q^2 \, h_3^N(\omega) \tag{2.55}$$

For other amplitudes we have used the free space values of scattering amplitudes which are related to a set of pion-nucleon phase shifts δ_α's by (Geneva conf. 1958, Muirhead

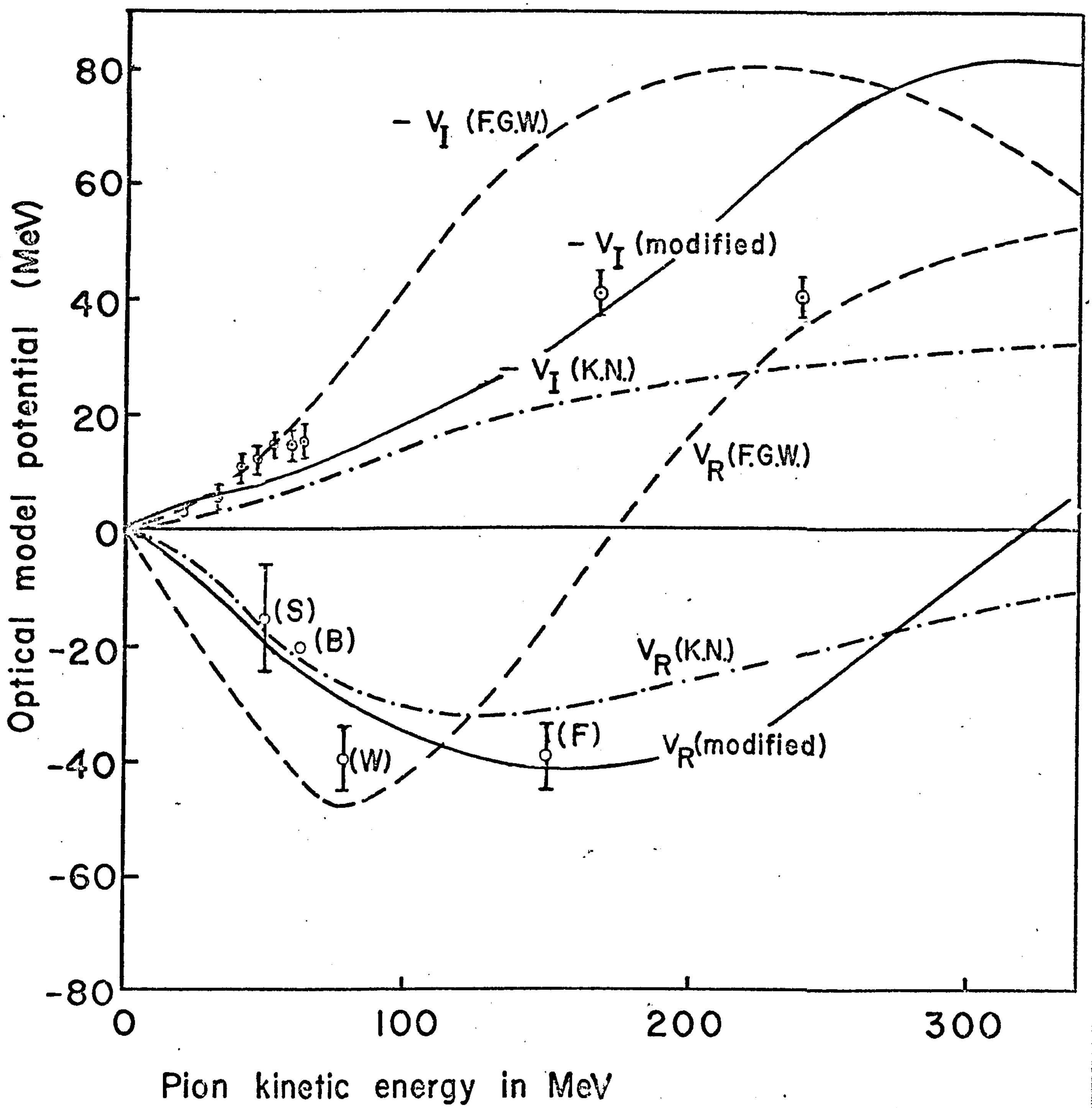

Fig. 2.5 The real and imaginary parts of the optical model potential for pion-nucleus scattering as a function of the pion kinetic energy. Experimental points are shown by vertical lines.

[The values of V_I are from our measurements: Ch.IV.and the values of V_R are taken from: S(Shapiro 1951), B(Byfield 1952), W(Williams 1956), F(Fuji 1959)]

1965):

$$f_\alpha(\omega) = \exp(i\delta_\alpha) \sin \delta_\alpha / q \tag{2.56}$$

where

$$\begin{aligned} \delta_3 &= -0.101q \quad , & \delta_1 &= 0.167q \\ \delta_{11} &= -0.016q^3, & \delta_{13} &= \delta_{31} = -0.0289q^3 \end{aligned} \tag{2.57}$$

In calculating V_I^N, we used equation 2.9 to account for the contribution due to the meson absorption term. $V_R^N(\omega)$ and $V_I^N(\omega)$, thus obtained for $r_o = 1.4F$, are shown in fig. 2.5 as functions of the incident pion kinetic energy in the laboratory system (solid curve; indicated as V_R^N (modified) and V_I^N (modified)). The corresponding values of the potentials obtained by F-G-W and by K-N are also shown in the same figure.

II-4 Discussion

In figs. 2.4 and 2.5, various results obtained for free space and for nuclear matter (both the K-N and our modified results) are plotted and compared. K-N results include the effect of the Pauli exclusion principle but neglects the Fermi motion of the target nucleons. In the present calculation (specified as 'modified' results), the momentum of the nucleon, P_L, has been properly included through equation (2.44).

In fig. 2.4, it is seen that the Pauli exclusion principle applied to the intermediate state of the nucleon remarkably changes the behaviour of the pion-nucleon scattering amplitude. The amplitude of the (3,3) resonance is reduced and the resonance energy shifts to a much higher value. From the modified calculation r_3^N was found to be 0.34, which corresponds to a total pion energy of 410 MeV in the C.M. system. Slightly different in magnitudes but similar results were obtained by K-N. They obtained $r_3^N = 0.29$, which corresponds to 480 MeV resonance energy. It was shown by Mes et al. (1966) that such a high resonance energy would cause too much pion absorption in the energy range $0 < E_\pi < 500$ MeV and would produce far too many high energy protons than are experimentally observed. It was concluded that this large disagreement was, most probably, due to the neglect of the Fermi motion of the target nucleons inside the nucleus. K-N made the effect of the Pauli exclusion principle much too severe by considering the target nucleons to be, on the average, at rest. From the modified calculation, it is found that the resonance energy, indeed, is reduced by introducing the Fermi motion of the target nucleons. The modified (3,3) resonance peak is also found to be higher than that obtained by K-N (see fig. 2.4).

In fig. 2.5, it is observed that the potentials calculated inside the nucleus significantly differs from the F-G-W potentials. It is interesting to note that the real part of the F-G-W potential goes through a maximum at about 80 MeV pion energy and changes its sign at the pion-nucleon resonance energy: This difference is due to the assumption that the two body forces are not significantly affected by the neighbouring nucleons. According to the present modified calculation, V_R^N is attractive up to about 320 MeV and changes the sign beyond that. The result of K-N is similar, but V_R^N changes its sign at a still higher energy.

In each case it is observed that our modified results lie between the K-N and the free space results: This is expected, since neglecting P_L (K-N case) is equivalent to picking out a nucleon deep in the nucleus whereas in case of F-G-W, η is effectively unity and is equivalent to picking out a nucleon on the surface of the nucleus. In our case, however, the target nucleon can have any intermediate energy between 0 to P_F and hence the results lie between the K-N and the free space results.

The experimental values of V_R & V_I are also shown in fig. 2.5 (points with error bars), for comparison. The values of V_I, at various pion energies, have been obtained from our experimentally measured cross sections. The details of the calculations are discussed in section IV-2. The values of V_R shown in the fig., have been taken from the measurements of Shapiro (1951), Byfield et al. (1952), Williams et al. (1956) and Fuji (1959). The results are plotted with the experimental errors, wherever possible. It is observed that the experimental results agree very well with the results of our modified calculations.

Chapter III

EXPERIMENTAL

III-1 Introduction

The experimental part essentially consists of the measurement of the cross sections of interactions of pions with the complex nuclei of emulsion at various pion energies up to 60 MeV and at three higher energies: 168, 225 and 254 MeV. The distributions of the energy and the opening angles of the fast protons emitted during the primary interactions have also been experimentally observed. Similar distributions have been obtained for antiproton ($\bar{p}$) annihilation stars. The experimental work involves the scanning of emulsion plates for stars, measurement of flux, and the determination of energies and angles of emitted particles. In this chapter, the actual techniques used and other experimental details will be discussed.

III-2 Irradiation of Emulsion Stacks

In the present series of measurements three different emulsion stacks were used.

Stack 1: Four pellicles from a stack of G5 emulsion, irradiated with antiproton ($\bar{p}$) were obtained from CERN. This stack was used to analyze the fast proton pairs emitted from the absorption of pions which were produced inside the nucleus by the annihilation of antiprotons at rest. The pellicles had dimensions 24 x 15 x 0.06 cm. The nominal momentum of the incident beam was 650 MeV/c corresponding to a range of 11 cms, where most of the annihilations took place.

Stack 2: This stack consisted of 13 pellicles irradiated with π^+ meson: The pellicles were obtained from the Pion physics group of the University of Stockholm and had dimensions 2 x 10 x 0.06 cm. The nominal flux and the energy were $6 \times 10^4/cm^2$ and 72 MeV, respectively. The incident beam was highly monoenergetic and was suited for our determination of π^+-nucleus interaction cross section as a function of energy.

Stack 3: In June 1968, four stacks of K5 emulsion were irradiated with π^+ beam at the CERN

Table 3.1

Characteristics of Stack 3.

Stack	No. of pellicles	Energy (MeV)	Total No. of pions (Nominal)	Angle of incidence w.r.t. the surface (Nominal)
A	12	168	$(7.74 \pm 1.5)*10^{7}$	90°
B	11	121	$(7.74 \pm 1.5)*10^{7}$	20°
C	13	254	$(1.01 \pm 0.03)*10^{8}$	90°
D	13	224	$(1.01 \pm 0.03)*10^{8}$	30°

synchrocyclotron by the University of Ottawa group. The characteristics of the stacks are given in Table 3.1.

In each stack, there were one or more boron embedded pellicles and their thicknesses varied from 200 to 400 μ. These pellicles are being used for a different experiment. Rest of the pellicles had dimensions 10 x 10 x 0.06 cm. Different energies were obtained by degrading the initial pion beam with copper blocks of suitable thicknesses. Two different irradiations, one for stack A and B (8400 seconds) and the other for C and D (4000 seconds) were made, and the geometry of the irradiations are shown in fig. 3.1

In stack A and C, the pion beam was incident perpendicular to the emulsion surface, whereas in B and D the beam was incident at angles of 20° and 30°, respectively. This differs from the usual type of irradiation in which the incident beam is always parallel to the surface. The advantage of the perpendicular beam is that the energy in any particular plate is same throughout the whole surface. Thus for a certain energy, a much larger surface area is available in a single pellicle in contrast to the pellicles which are irradiated with the incident beam parallel to the surface. Since

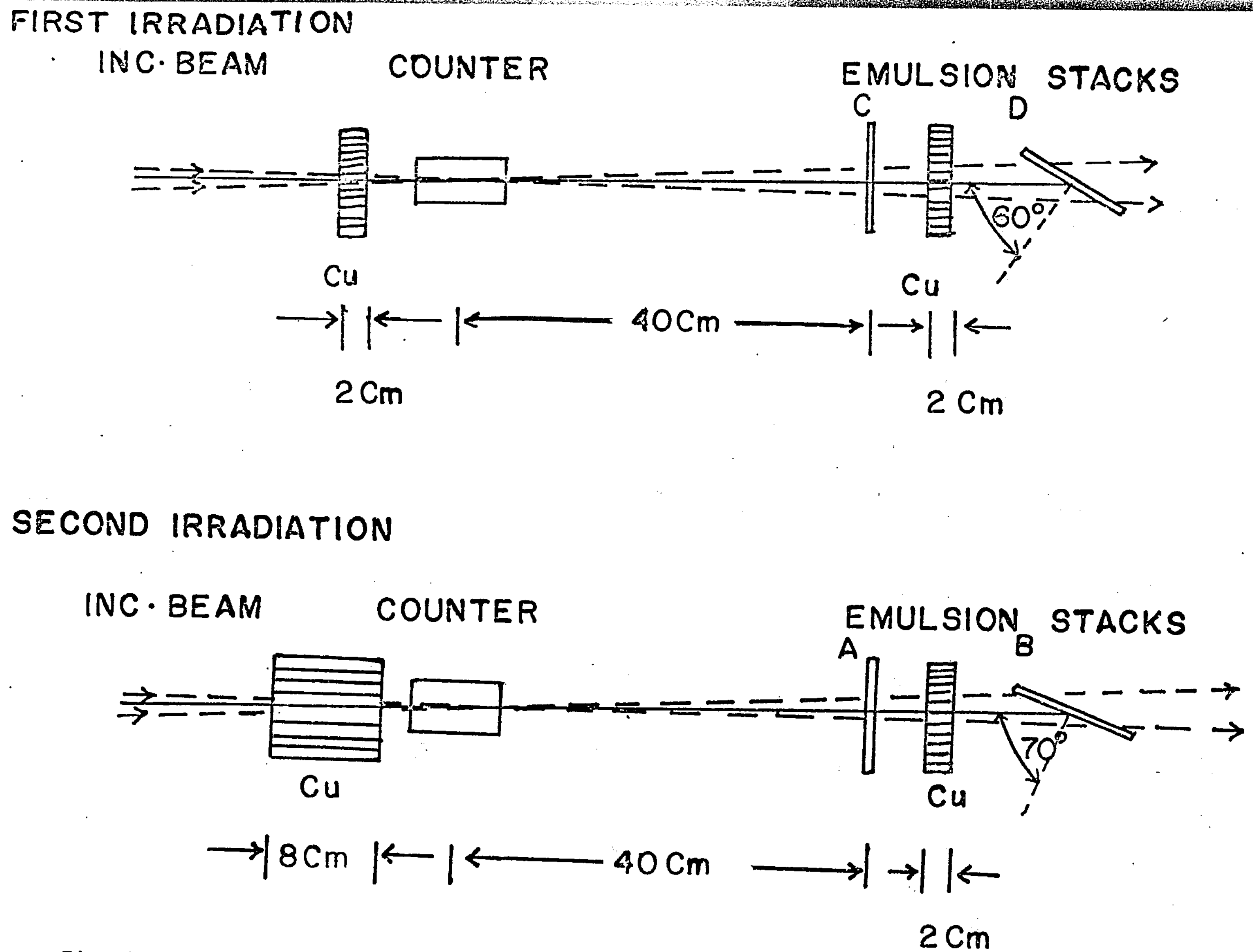

Fig. 3.1 Schematic diagram of the irradiation of Stack 3

Table 3.2

Thicknesses of pellicles in Stack 3
Unprocessed emulsion (Stack 3)

Pellicle \ Position	a	b	c	d	e	average
	(Thickness in microns)					
A5	611	634	620	609	601	615
C1	606	601	618	622	620	613
D5	620	615	620	625	620	620

the thickness of the plates are only about 600 μ, the energy does not change appreciably as the beam passes through the pellicle. This mode of irradiation is , therefore, very useful when an accurate measurement with large statistics and at a well defined energy is required.

In the case of parallel incident beam, if the plate is narrow, the statistics can only be improved by scanning a large number of pellicles in a narrow strip or by increasing the width of the strip. The latter method increases the energy width,whereas the former makes it inconvenient, and sometimes unnecessary calibration of each pellicle may be necessary. For the perpendicular beam, however, the energy of the beam cannot be measured directly and it is necessary to be able to obtain the energy from the geometry of the irradiation. Moreover, the accurate thickness of the emulsion, prior to irradiation, must be known if the length traversed by the incident beam is required. In this stack, we have used pellicles A5 (5th pellicle in stack A), C1 and D5. In each pellicle the thicknesses were measured around the center 'e' and near the four corners a, b, c and d. The pellicles were found to have uniform thicknesses and the results are shown in table 3.2.

III-3 Identification and Energy Measurements of Charged Particles in Emulsion

Nuclear emulsion is the simplest but at the same time a very powerful detector of nuclear radiations and charged particles. This consists of about equal parts by volume of silver-halide crystals, a few tenths of a micron in diameter, and a matrix material which is chiefly gelatin. An ionizing particle on encountering a crystal may render it developable. After development, followed by fixing, the silver grains become visible under high magnification. Thus, in emulsion, the path of a charged particle is recorded as a visible trail of minute black silver grains. The number of grains per unit length or the 'grain density' is related to the specific ionization. The tracks are divided into three categories based on the grain density of the track.

The grain density, g, corresponding to a particular value of ionization is not unique, but depends on the sensitivity of the emulsion and on the degree of the development. Thus it is necessary to have independant calibrations for each stack. Usually the observed grain density is expressed in terms of the the grain density g_o, for the track of a particle in the extreme relativistic region observed in the same emulsion.

The three categories of tracks are classified according to the magnitude of the normalized grain density, $g^{*}={}^{g}/g_{o}$, as follows

(i) white track or shower track: ${}^{g}/g_{o} \leq 1.4$

(ii) grey track: $1.4 \leq {}^{g}/g_{o} < 10$

(iii) black track: ${}^{g}/g_{o} \geq 10$

From the characteristics of a given track; i.e. the grain or blob density, range, scattering etc, it is possible to identify the particle and measure its energy and momentum. In most cases two or more different kinds of measurements are needed for the complete identification and specification of energy. No unique prescription can be given for the measurements and the particular method or methods must be chosen according to the specific characteristics of the track. In some cases the identity of the particle may be known either from the given conditions or from the physical considerations of the event. In these cases, the measurement of energy is simple and one type of measurement is sufficient to specify the energy.

In the present study we are mostly concerned with the measurement of energy of protons having grey tracks (with energy more than 30 MeV) and pions with energy

20-70 MeV. The important techniques used were:

a) Range measurement

b) Ionization measurement

c) Scattering measurement

a) Range measurement: This is the simplest and the most accurate method of measuring the energy of the particle. This is applicable only when the track ends in emulsion and the entire track can be followed. This is very convenient if the track is flat so that the entire track can be seen in one or two pellicles. The energy of the incident pion beam was measured from the observed range. If the track is inclined at a certain angle and can be followed from one pellicle to the other, it is possible to measure the length of the entire track. In such cases it is essential that each pellicle has well printed grid exactly in the same way. In most cases the ranges of the protons from the stars in stack 1 and 2 were measured by following the tracks from one plate to the other. From the observed range, the energy was obtained by using standard tables (Fay 1954; UCRL reports 1965).

The range of a particle is determined experimentally from the measurements of the projected range x, in the plane of the emulsion, and the vertical projection, y, of the track. The range R is given by

$$R = \sqrt{x^2 + S^2y^2}$$

where S is the shrinkage factor for the pellicle and is given by the ratio of the thicknesses of the unprocessed and the processed emulsion. The magnitude of the shrinkage factor is usually of the order of 2, and S is influenced by the temperature and humidity.

The projected range was measured by means of a precalibrated linear scale at the focus of the eyepiece. The vertical projection, y, over a distance x, was determined from the difference in the readings on the fine-focus-depth-calibration of the microscope when focussed on the first and the last grain along the length x.

b) Ionization measurement

The loss of energy per unit length traversed or the 'specific ionization' is a measure of the velocity of the particle. Since the grain density of the developed track depends on the specific ionization, it is possible to measure the velocity and hence the energy of the particle from the grain density of the track. For a relativistic particle of charge ze, passing through a medium of atomic charge Ze, the specific ionization $^{dE}/_{dx}$ is a function of the velocity, v, of the particle and is given by the Bethe-Bloch formula (Bethe 1932; Burcham 1962)

$$-\frac{dE}{dx} = \frac{4\pi e^4 z^2 NZ}{mv^2}\left\{\left[\log_n \frac{2m c^2\beta^2}{(1-\beta^2)I}\right]-\beta^2\right\} \qquad (3.1)$$

where ze = charge of the incoming particle

Ze = nuclear charge of the atom

N = atomic density of the medium

I = effective ionization potential

$\beta = {}^{v}/c$; c = velocity of light

If the medium consits of X different types of atoms, as in emulsion, then

$$-\frac{dE}{dx} = \frac{4\pi e^4 z^2}{mv^2} \sum_{i=1,\,X} N_i Z_i \left\{\left[\log_n \frac{2m c^2\beta^2}{(1-\beta^2)I}\right]-\beta^2\right\} \qquad (3.2)$$

where suffix i denotes the type of the atom, and the summation extends over all the X types of atoms present in the medium. Variation of ${}^{dE}/dx$ as a function of β for G5 emulsion, calculated from equation 3.2, is shown in fig. 3.2. The values of I and N have been taken from Powell (1959). From this curve, the variation of grain

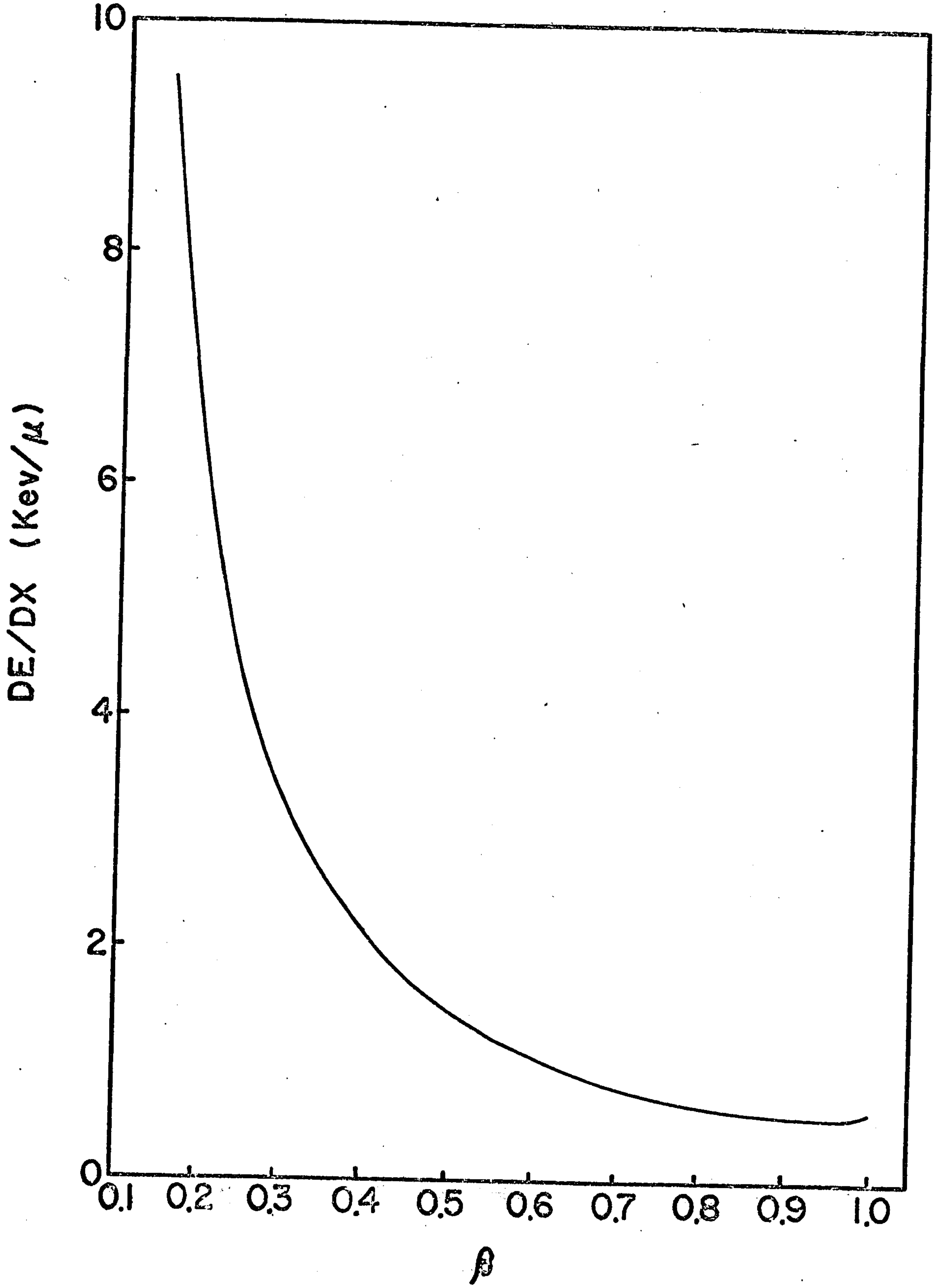

Fig. 3.2 Rate of energy loss of a singly charged particle as a function of β

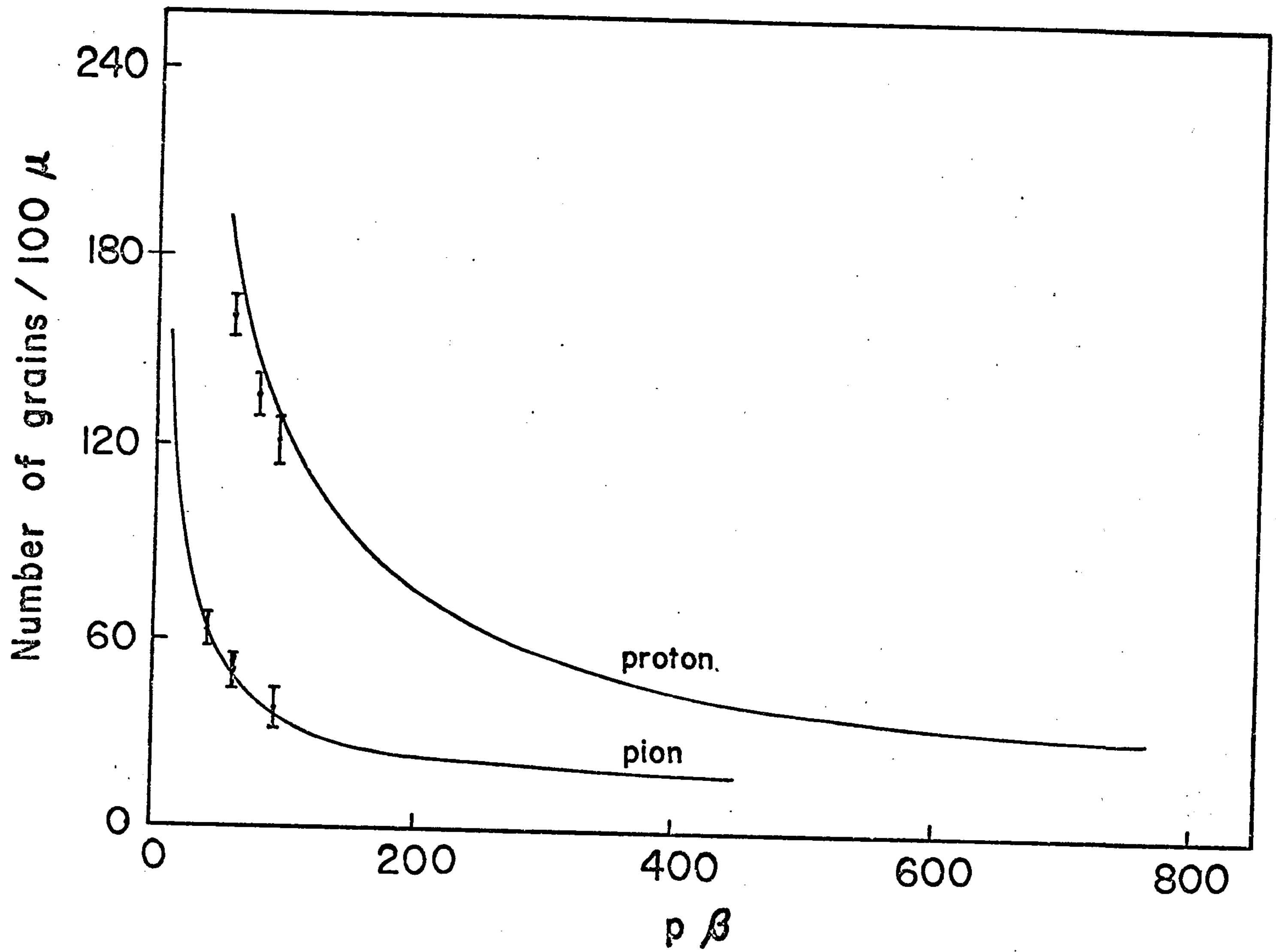

Fig. 3.3 Grain densities of pion and proton tracks in emulsion as a function of p_β. Experimental points are shown with vertical bars.

density as a function of momenta for pion and proton was obtained and the results are shown in fig. 3.3. To obtain the variation of g as a function of $P\beta$, the grain densities of pion and proton tracks at few energies were measured. Comparing these values with the specific ionization in fig. 3.2, the average energy required per developed grain was obtained. Using this value in conjunction with fig. 3.2, the variation of g as function of $P\beta$ was obtained for our range of interest. Direct experimental calibrations of grain densities were also carried out for π^+ and p at few energies where suitable tracks with known energy was available. These are shown in fig. 3.3, for stack number 2, by points with error bars. The measurements on pions were straight forward, since the incident pions were almost flat. Measurements were made on reasonable number of tracks such that the total number of the grains counted at each energy was of the order of 500 to 600. The length over which the grains were counted was kept small (300 ~ 400 μ) so that the energy was reasonably constant over the measuring length.

Similar measurements were carried out for protons (both for stack number 1 and 2) with some selected tracks which were long and flat and stopped in emulsion. In most cases the experimental calibration curve was used to obtain the energy of the particle from the measured grain density. For occassional very fast protons, however, the energy was obtained from the theoretical curve. The measurements were mostly confined to the central region as the development near the surface was usually not uniform. If the identity of the particle was known, measurement of g about one point was sufficient to specify the energy. If however the identity of the particle was not known, in most cases it was possible to obtain the energy and to identify the particle by measuring g at two different ranges.

c) Multiple scattering: When a charged particle passes through a material medium, its direction of motion changes continually as a result of frequent, small deviations due to coulomb scattering by the atomic nuclei near its line of motion. For small scattering angles, the average angular deviation , $< \alpha >$, is given by:

$$< \alpha > = k \, z \, \frac{t^{\frac{1}{2}}}{P\beta}$$

where t = cell length in microns

z = charge of the incident particle

P = momentum of the particle in MeV/c.

k is a nearly constant quantity for a given value of cell length and is taken to be 26 MeV degree/$(100\ \mu)^{\frac{1}{2}}$ for $t = 100\ \mu$ with a cut off at $<\alpha> = 4$.

By measuring $<\alpha>$ it is possible to obtain the value of $P\beta$ and hence the energy of the particle. In many cases the mass of the particle can be obtained from a combined measurement of scattering and the range of the particle.

$<\alpha>$ can be measured by two methods: in the first, which is referred to as the angular method, the direction of the tangent to the trajectory is obtained at a number of equally spaced points along the track, the deviations being deduced from the differences in successive readings. In the second, the 'co-ordinate' method, the co-ordinates of succession of points along the trajectory, separated by cell length t, are determined. In our measurements we have used the second method, and the actual measuring technique for this method is explained below (Fowler 1950).

A high precision stage microscope, built in this laboratory by Ancsin & Hébert (1964) was used for the scattering measurement. The lateral noise of the microscope was reduced to a minimum and was of the order of hundred Angstroms. To measure the lateral deviation of the track an objective with magnification 100x was used in conjunction with a Leitz precision micrometer eyepiece of magnification 12.5 x with a reference wire at the focus of the eyepiece. The reference wire could be moved by rotating the micrometer screw, each division of which corresponded to a linear displacement of 3×10^{-2} μ. The track was alligned parallel to the direction of motion of the stage and was moved along this direction. At equal intervals of t microns, the positions y_1, y_2, y_3 ... y_n of the track were read in the micrometer scale after bringing the reference wire in line with the track (see fig. 3.4).

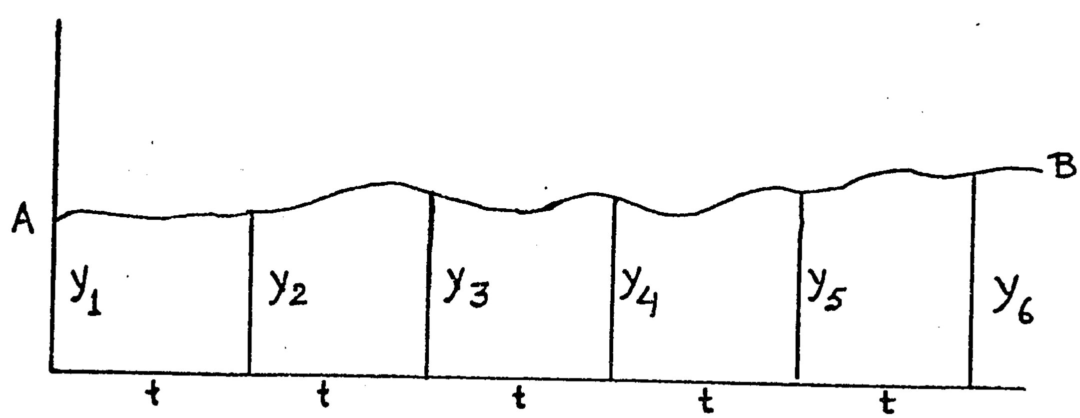

Fig. 3.4 Principle of scattering measurements.

The scattering angle $<\alpha>$ was then obtained from their second differences: e.g.

$$\alpha_1 = \left(\frac{y_3-y_2}{t} - \frac{y_2-y_1}{t} \right) * \frac{180}{\pi} \text{ in degrees}$$

$$\alpha_2 = \left(\frac{y_4-y_3}{t} - \frac{y_3-y_2}{t} \right) * \frac{180}{\pi} \qquad (3.4)$$

The average of n possible measurements were taken to obtain $<\alpha>$. Scattering angles greater than 4 $<\alpha>$ were rejected. The choice of the cell length depended on the nature of the track such that the track had a detectable deviation over that cell length. If the cell length used is different from 100 μ, then $<\alpha>_t$ can be normalized to $<\alpha>_{100}$ corresponding 100 μ cell length by using the formula

$$<\alpha>_{100} = \frac{<\alpha>_t}{\sqrt{t/100}} = \alpha_t \sqrt{\frac{100}{t}} \qquad (3.5)$$

If the identity of the particle was known, any one of the above methods, depending upon the suitability for the particular case, was used to determine the energy of the particle. An attempt was made, whenever possible, to use range measurements. In range measurement, an accuracy of 1 to 2 percent could be achieved very easily. Most of the rest were measured by grain counts, except in few cases where scattering measurements were carried out for energy determination. When the identity of the particle was not known or was ambiguous, two or more types of measurements were made on the same track. The most frequently used combinations were:

(a) Residual range and scattering

(b) Residual range and ionization

(c) Grain counts at various residual ranges along the track.

Using these techniques, it was possible to carry out the measurements in most cases, and the results of measurements are shown in Chapter V.

In addition to the techniques mentioned above, integral gap count, blob count, width measurement were used to identify and measure the energy of the very low energy particles.

III-4 Angular Measurements

Besides the energy measurements of the fast protons emitted in pion absorption, their opening angles in space were also measured. The space angle 'θ' between two tracks having azimuth and dip angles (φ_1, α_1) and (φ_2, α_2) is given by

$$\cos\theta = \cos\alpha_1 \cos\alpha_2 \left[\cos(\varphi_2 - \varphi_1) + \tan\alpha_1 \tan\alpha_2\right] \tag{3.6}$$

or in terms of the tangent of the dip angle:

$$\cos\theta = \frac{\cos(\varphi_2 - \varphi_1) + \tan\alpha_1 \tan\alpha_2}{\left[(1 + \tan^2\alpha_1)(1 + \tan^2\alpha_2)\right]^{\frac{1}{2}}} \tag{3.7}$$

To measure the azimuth angle, an eyepiece reticle with a protractor engraved on it was placed at the focus of the eyepiece. The event was moved until its centre coincided with that of the protractor. Angle φ_1 and φ_2 were read after bringing the zero degree line along the x axis of the grid which served as a reference line.

The dip angle, α, for a track is the angle between the track in the unprocessed emulsion and its own projection on the surface of the emulsion. The angle α was determined from the height z of the track at a distance x from the origin of the track. Correcting for the shrinkage factor S, the dip angle α is given by:

$$\tan \alpha = \frac{x}{Sz} \tag{3.8}$$

The angle α was taken as positive when the direction of the particle motion was upward, and as negative for particles going down towards the glass surface. Usually angles could be measured with a precision better than 1° and z within about 1 to 2 percent.

III-5 Calibration of Development with the Depth in the Emulsion

In thick emulsion, it is usually found that there is a variation in the degree of development with depth. The development is more near the top and the bottom and remains reasonably uniform in the middle. For reliable measurements, therefore, it is necessary that the development is uniform throughout the depth in which ionization measurements are carried out. The region of uniform development can be found either i) from the variation of the grain density (for same energy of the same type of particle) as a function of depth or ii) from the variation of the average grain size at different depths in the emulsion. The results of measurements of grain sizes as a function of the depth in the emulsion, for stack 1 and 2, are shown in fig. 3.7. The results are based on the measurement of 1000 grains at each depth. In each case, the average size was obtained by fitting the histogram of grain size with suitable gaussian curves. The sample results of grain size measurements at two depths are shown in fig. 3.5 and 3.6 for stack 1 and stack 2, respectively. The results show that the devel-

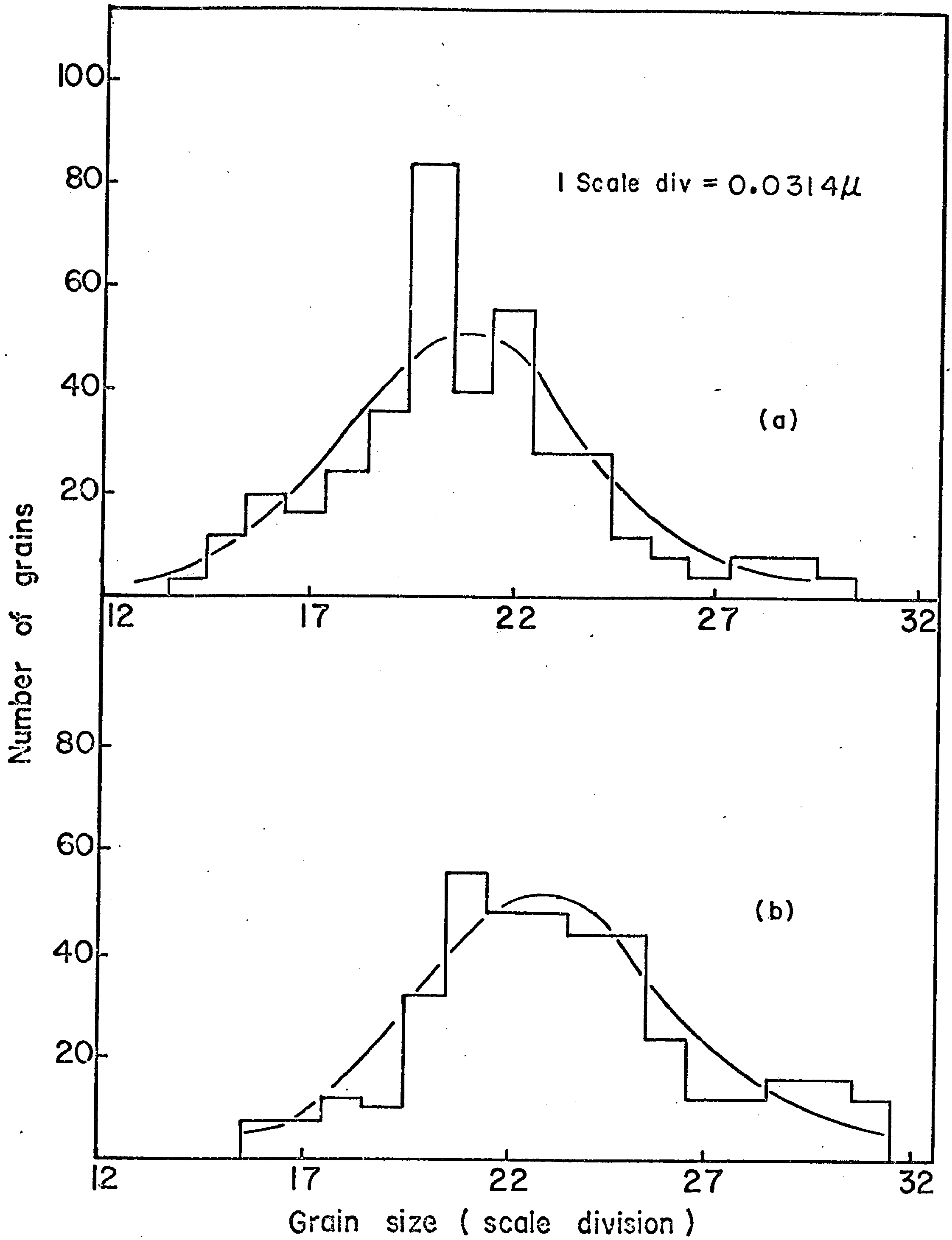

Fig. 3.5 Grain size distribution in Stack 1: at depths (a) 500 μ (b) 50 μ

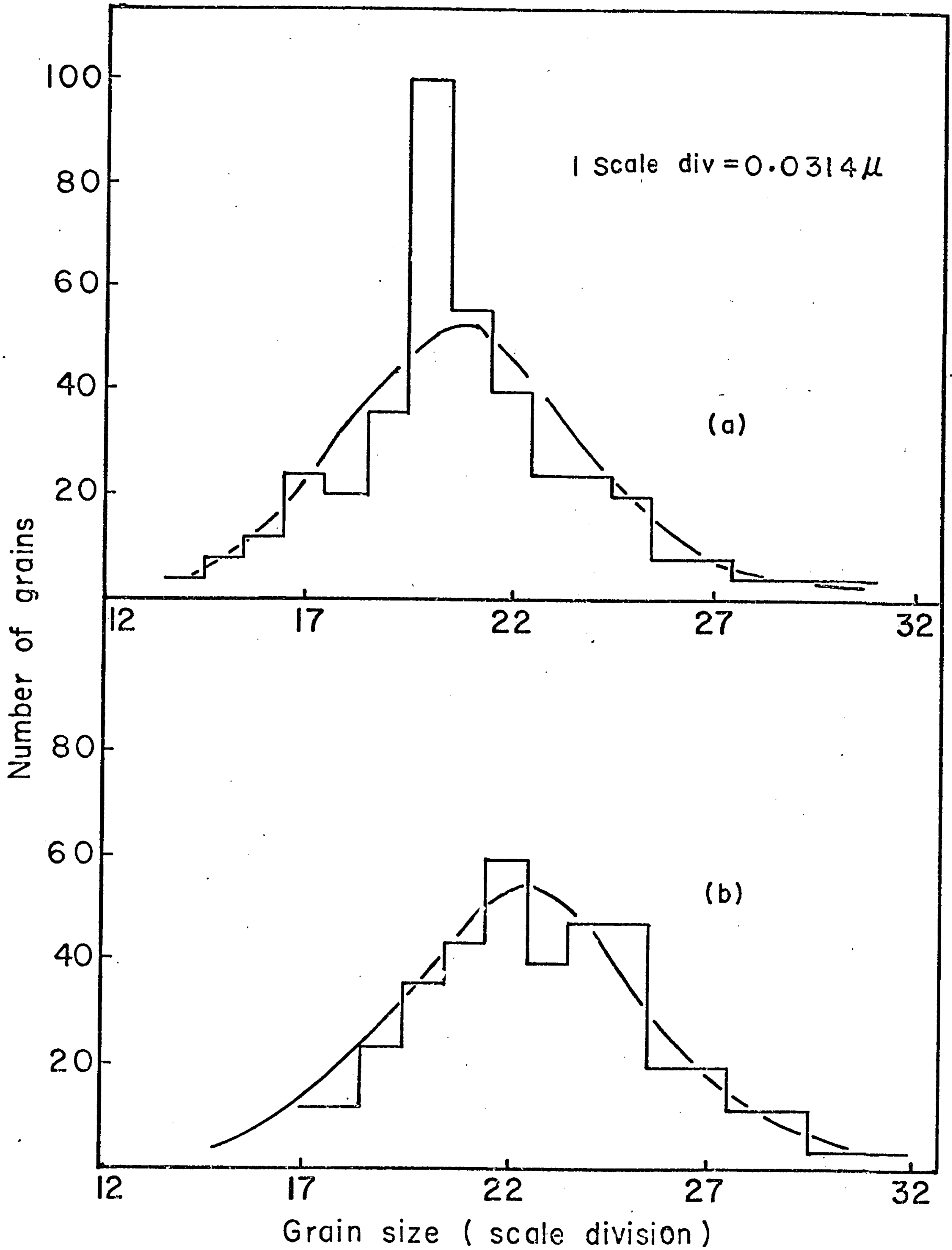

Fig. 3.6 Grain size distribution in Stack 2 at depths (a) 200 μ (b) 550 μ

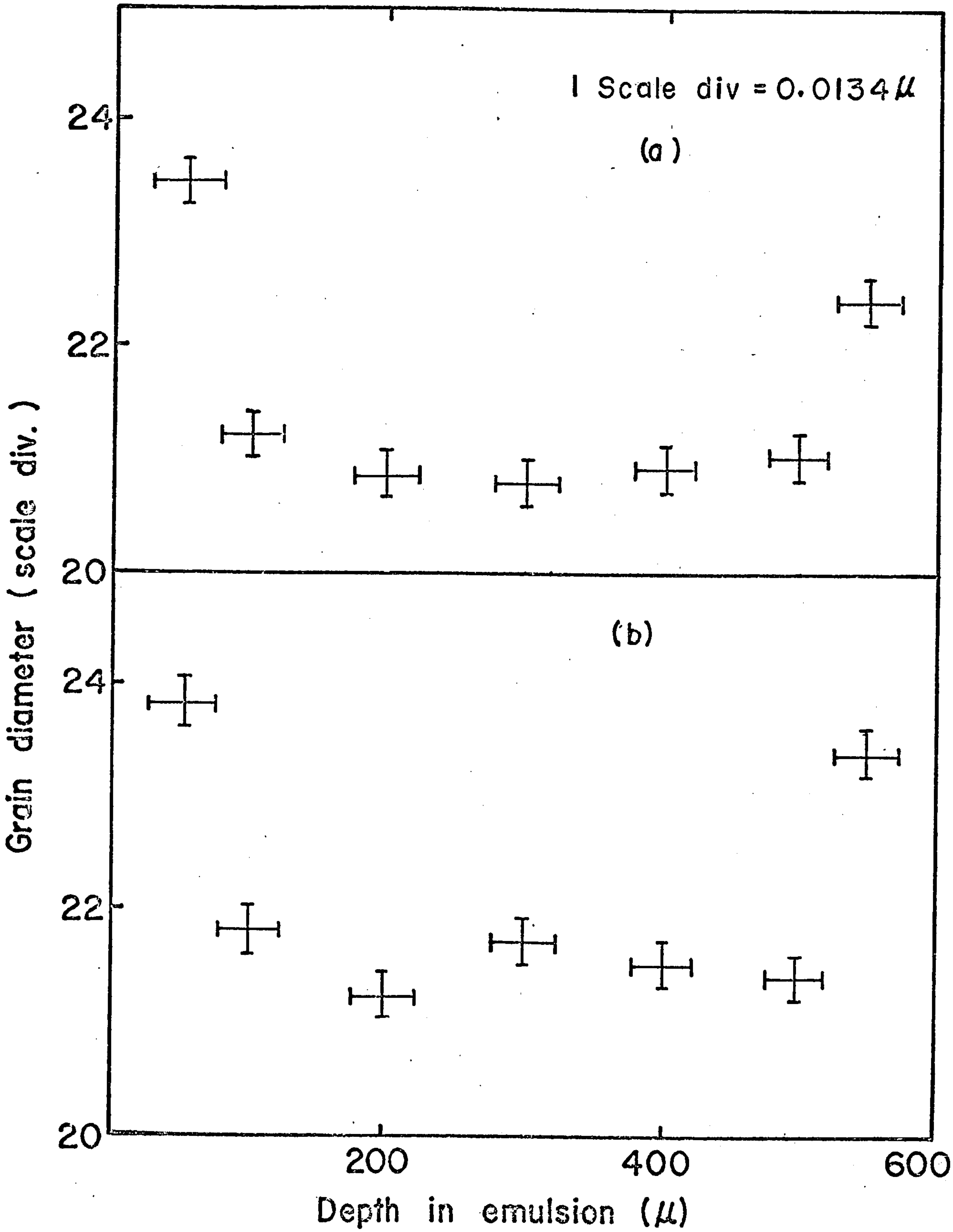

Fig. 3.7 Variation of grain size with depth in (a) Stack 1 (b) Stack 2

opment was practically uniform from about 100 μ to 500 μ measured from the top. Most of the ionization measurements were, therefore, performed in that region.

III-6 Measurements of Pion Flux and Energy

To determine the star formation cross section at a given energy, it is necessary to determine the flux at that energy and the density of the stars. Stacks 2 and 3 were used for the determination of the cross sections and hence the flux was measured in these two stacks.

Measurements of Flux and Energy in Stack 2:

Since in this stack pions were parallel to the surface of the pellicle, it was possible to follow the pions from the beginning to the end of their range where they decayed into μ^+; i.e. $\pi^+ \to \mu^+ + \nu$. Flux, at different energies, was measured by two independent methods

i) from the area of the $\pi^+ \to \mu^+$ decay curve

ii) direct counting of pions.

i) The nominal energy of the pion beam in this stack was 72 ± 3 MeV. Most of the pions decayed, with the characteristic $\pi^+ \to \mu^+$ decay, at a distance of about 6.4 cm. from the entering edge of the plate. Number of $\pi^+ \to \mu^+$ decays were counted from a distance of 59 mm to about 69 mm using a magnification of 100×10. The experimental results and the corresponding gaussian fit are shown in fig. 3.8. From the area of the curve, the number of pions stopping in emulsion were obtained. (The energy and the width of

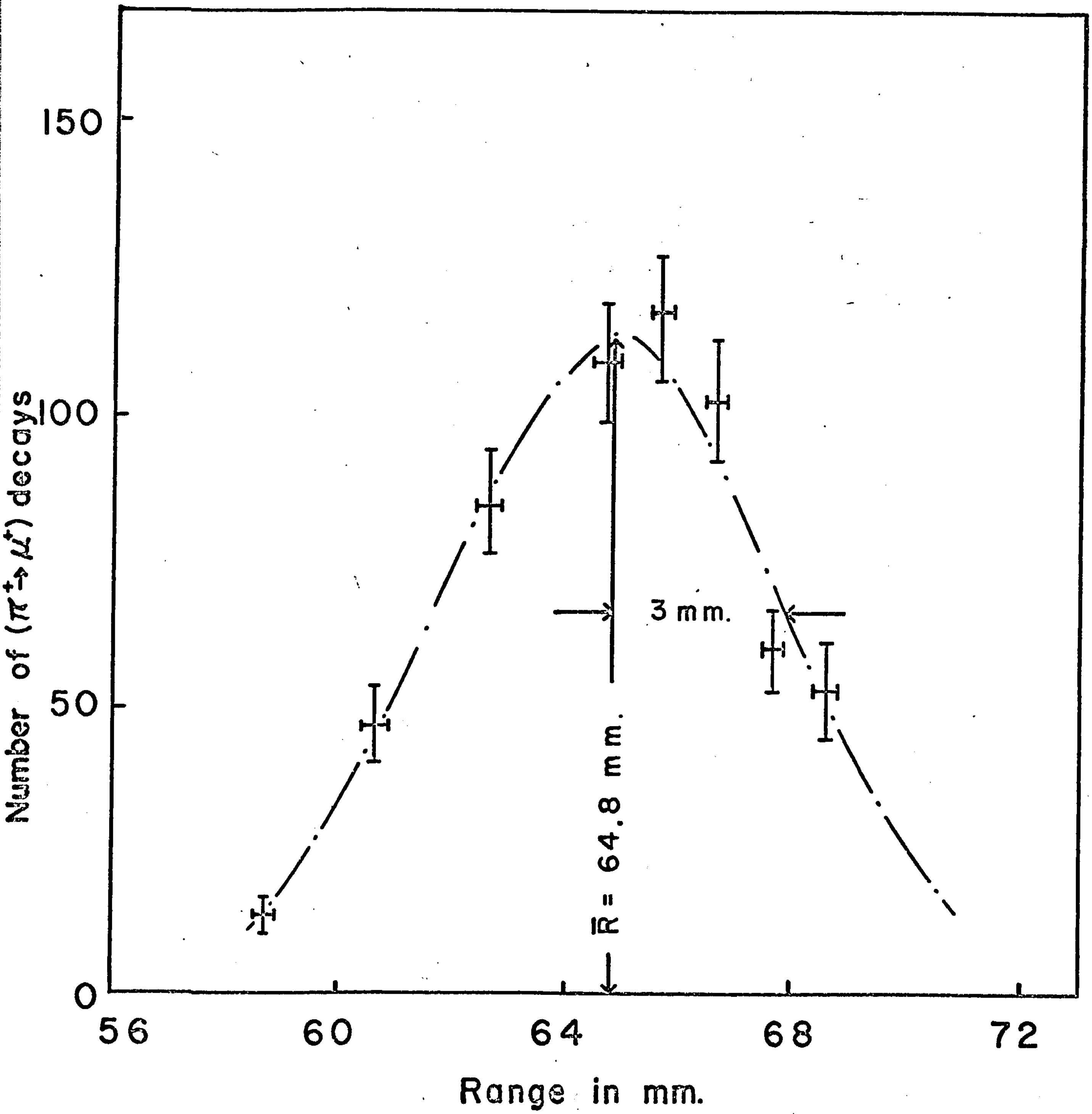

Fig. 3.8 Range distribution of 70 MeV π^+- meson beam.

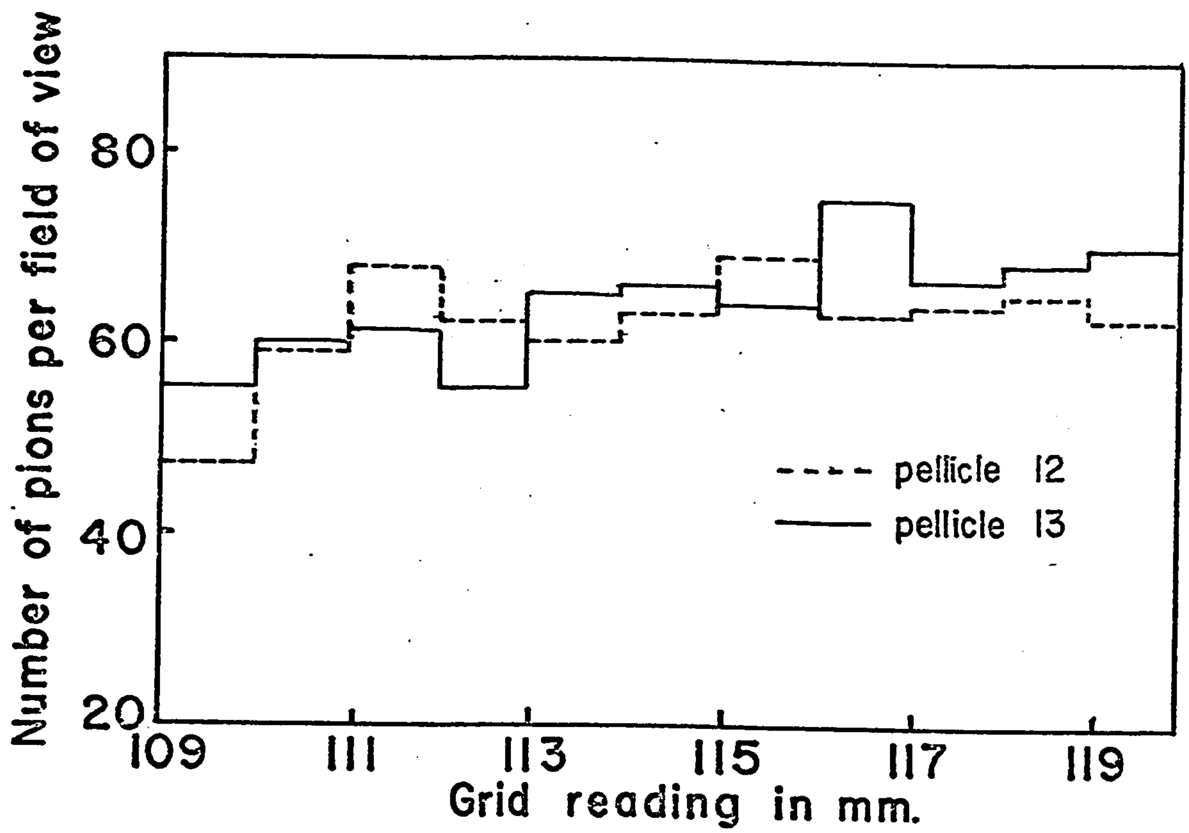

Fig. 3.9 (a) Transverse distribution of $\pi^+ \to \mu^+$ decays in pellicle. 12 and 13 of Stack.2

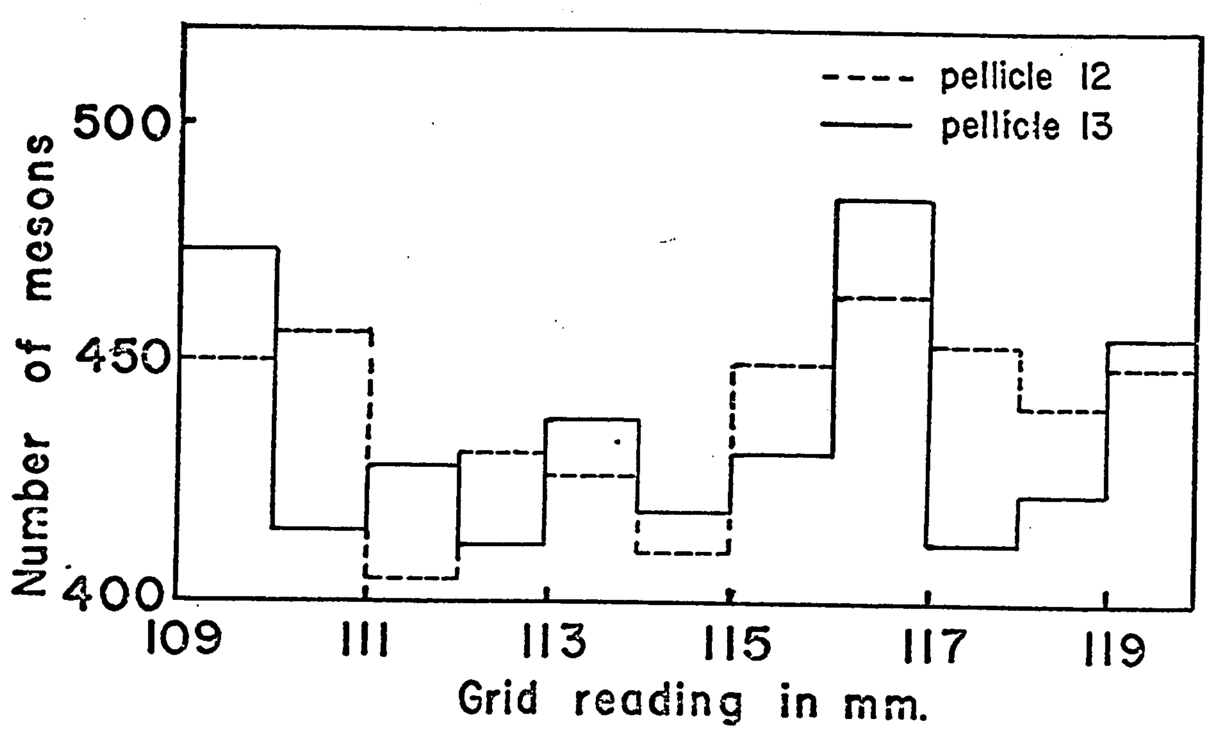

Fig. 3.9 (b) Transverse distribution of the meson flux at 12 mm from the entrance.

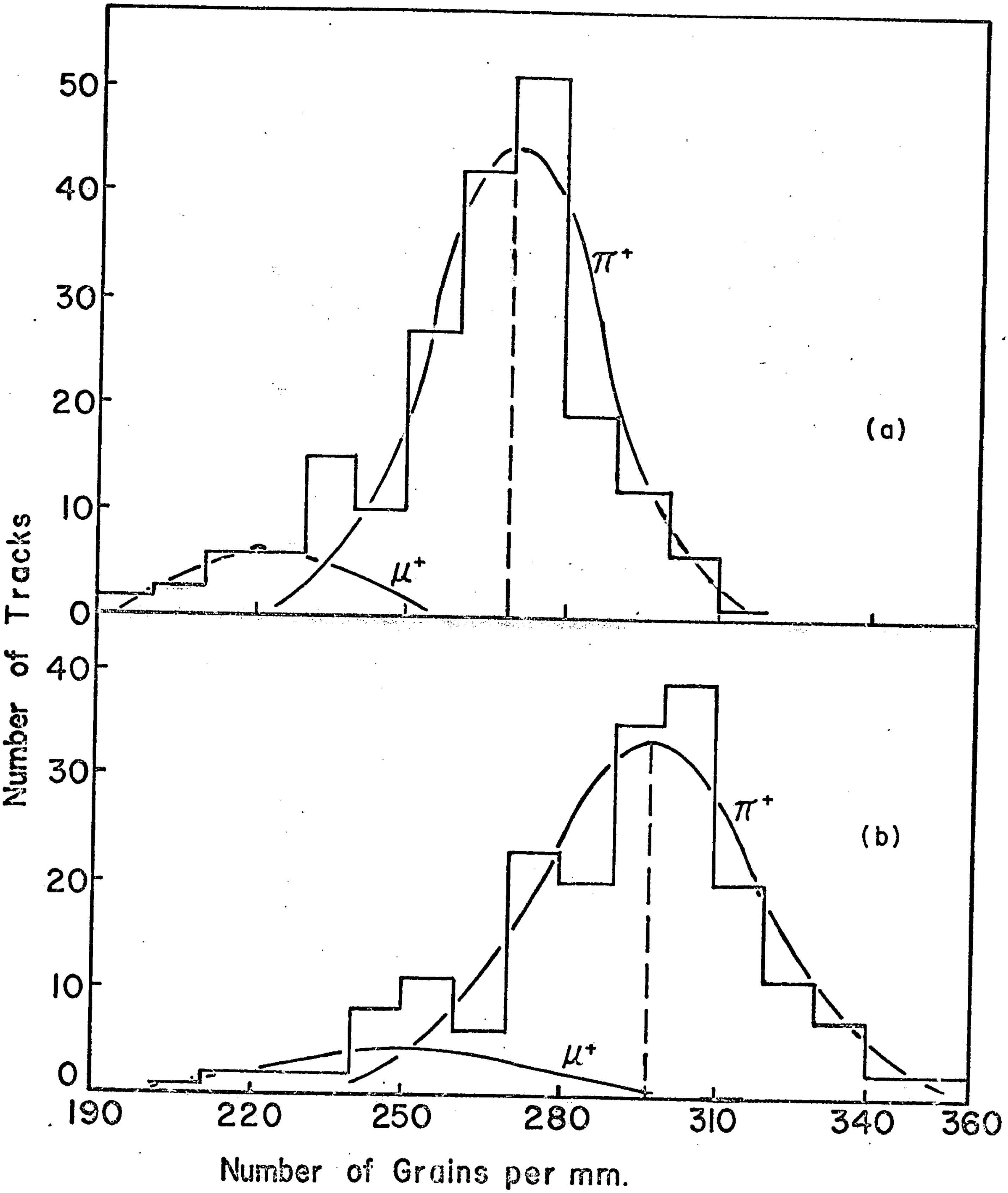

Fig. 3.10 Determination of Muon contamination in pellicle - 13 at residual ranges (a) 49.8 mm. (b) 29.8 mm.

the incident beam was obtained from the peak and the width of the gaussian distribution and was found to be 72.5 ± 2.5 MeV corresponding to a range of 64.8 mm.). The flux at any energy (corresponding to a certain value of the range) was obtained by applying corrections for the loss of π^+ due to absorption and scattering between the energy of interest and the mean peak position.

In each pellicle, various necessary characteristics of the incident beam were obtained. The transverse distribution of the incident beam was found to be uniform. Fig.3.9a shows the transverse distribution of the number of $\pi^+ \rightarrow \mu^+$ decays at the end of their ranges. Fig. 3.9b is that for mesons at a distance of 1.2 cms. from the entering edge and corresponds to an energy of 58 MeV. In both these cases, the dotted and the solid lines represent the distributions in pellicles: number 12 and13, respectively. Figs 3.11 show the distribution of the angle of incidence of the pion beam in pellicle 13 of stack 2. In fig. a the distributions have been plotted at three different residual ranges, where as in b the average of them is shown. The mean angle of incidence was found to be $- 3^\circ \pm 3^\circ$ with respect to the grid axis parallel to the longer edge of the pellicle.

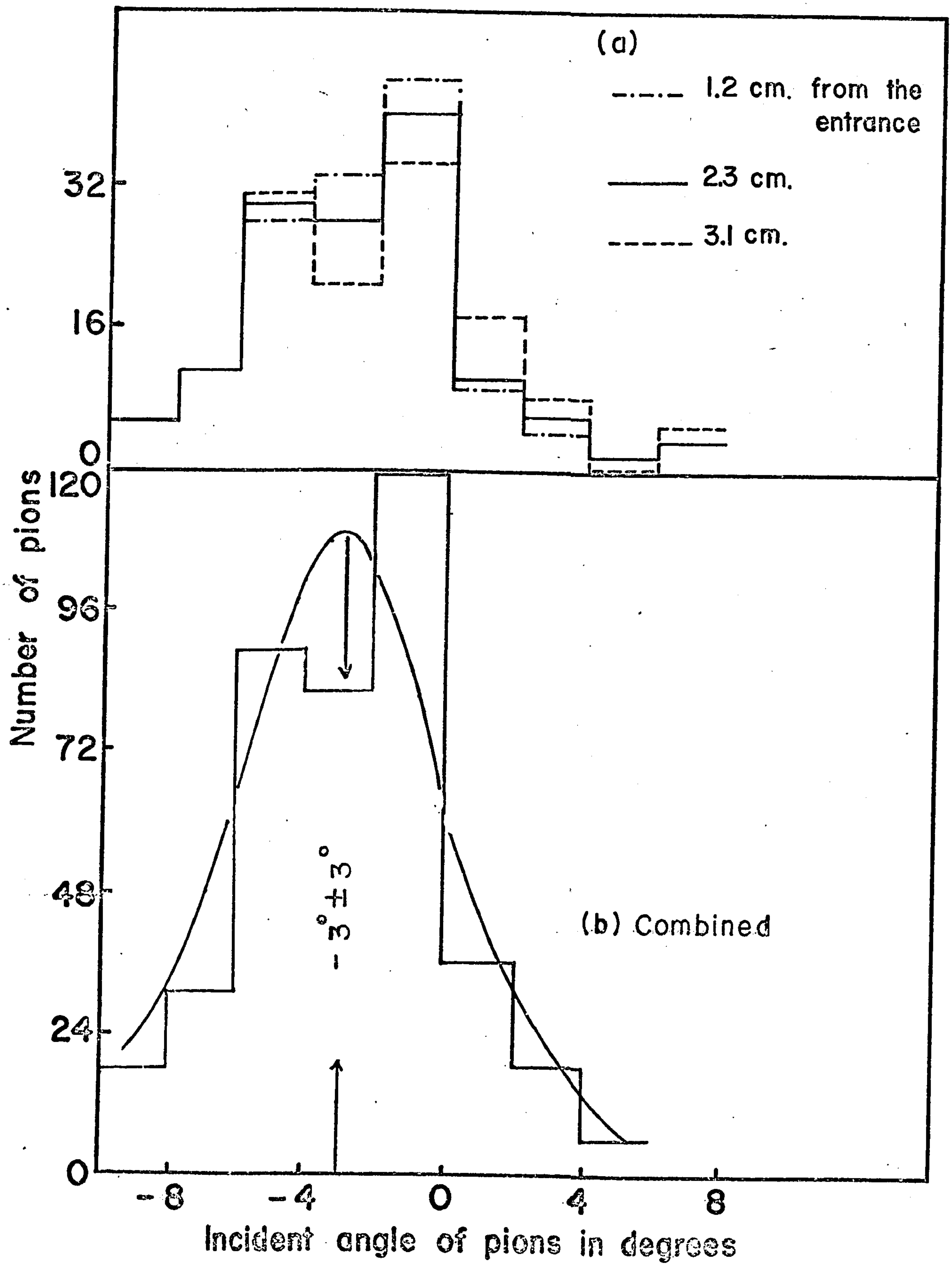

Fig. 3.11 Distribution of the incident angles of pions in pellicle - 13

ii) In the second method, the flux was measured by actually counting the number of meson tracks (in pellicle number 13) per unit area in the region corresponding to each of the experimental point. The tracks having grain densities from g^* to $1.5g^*$ were considered as meson tracks which also included muons. Muons were separated on the basis that, at these energies, pion grain densities are 20 to 30 percent higher than that of muons. Measurements of grain densities were carried out at two points, at residual ranges of 29.8 and 49.8 mm, and the gaussian distribution of grain densities were obtained by minimizing χ^2. Each histogram was fitted by superimposing two gaussian curves (fig. 3.10a and 3.10b). The curves with larger areas represent the distribution of pion and the ones with smaller area represent that due to muon. From the ratio of these areas, the percentages of muons were calculated and were found to be 11.5% ± 2.5% and 12% ± 1.5% at residual ranges of 29.8 mm and 49.8 mm, respectively.

<u>Measurements of flux and energy in stack 3</u>:

In these stacks pions were incident either normally or at an angle and hence it was not possible to use the techniques previously mentioned for the measurement of flux. In this case, flux was obtained by counting the number of meson tracks leaving unit area on the surface of the

Table 3.3

Characteristics of pellicles A5, C1 and D5

Pellicle	Energy (MeV)	Meson flux	pion flux	incident angle w.r.t. the normal to the surface
A5	168	$0.366 \times 10^6/cm^2$	$0.3 \times 10^6\ /cm^2$	4 ± 2^o
C1	254	$1.69 \times 10^6/cm^2$	$1.57 \times 10^6/cm^2$	2.5 ± 1^o
D5	224	$0.321 \times 10^6/cm^2$	$0.29 \times 10^6/cm^2$	30.5 ± 2^o

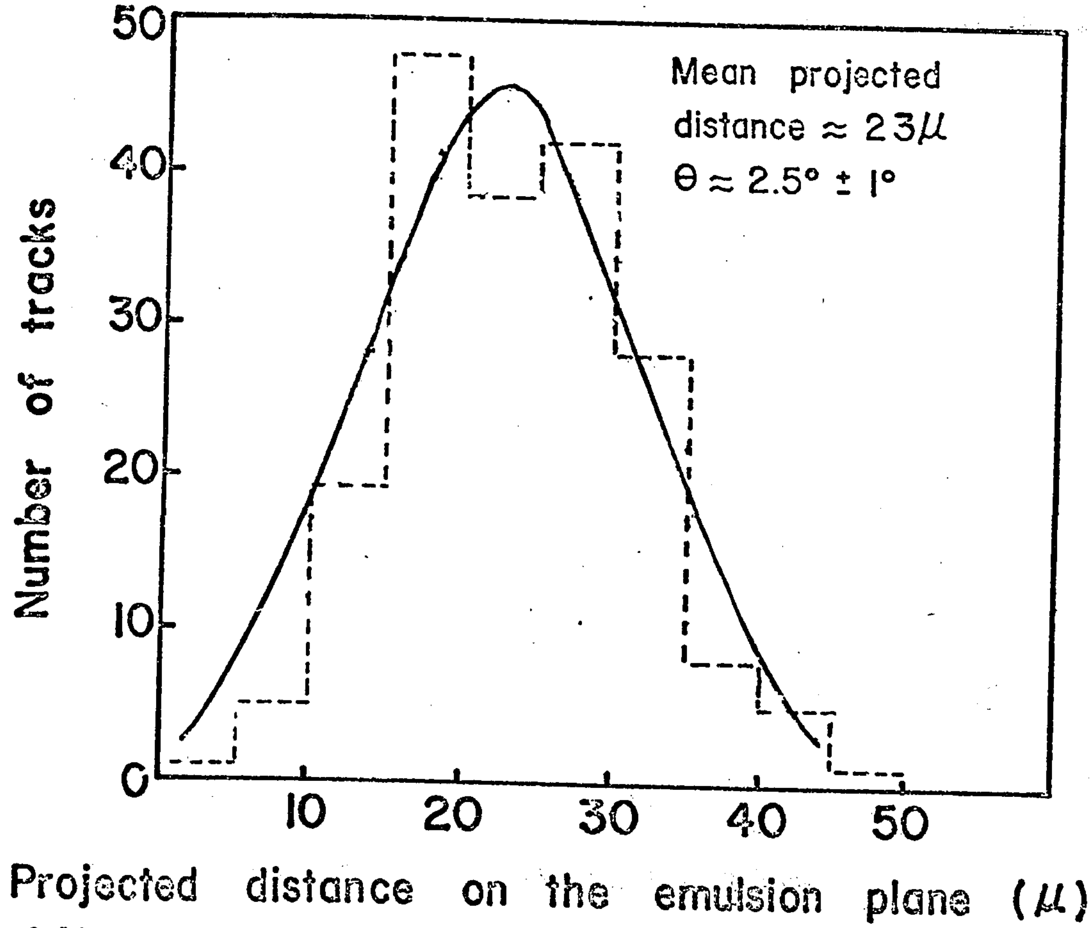

Fig. 3.12 Distance traversed by pions in the pellicle C-1

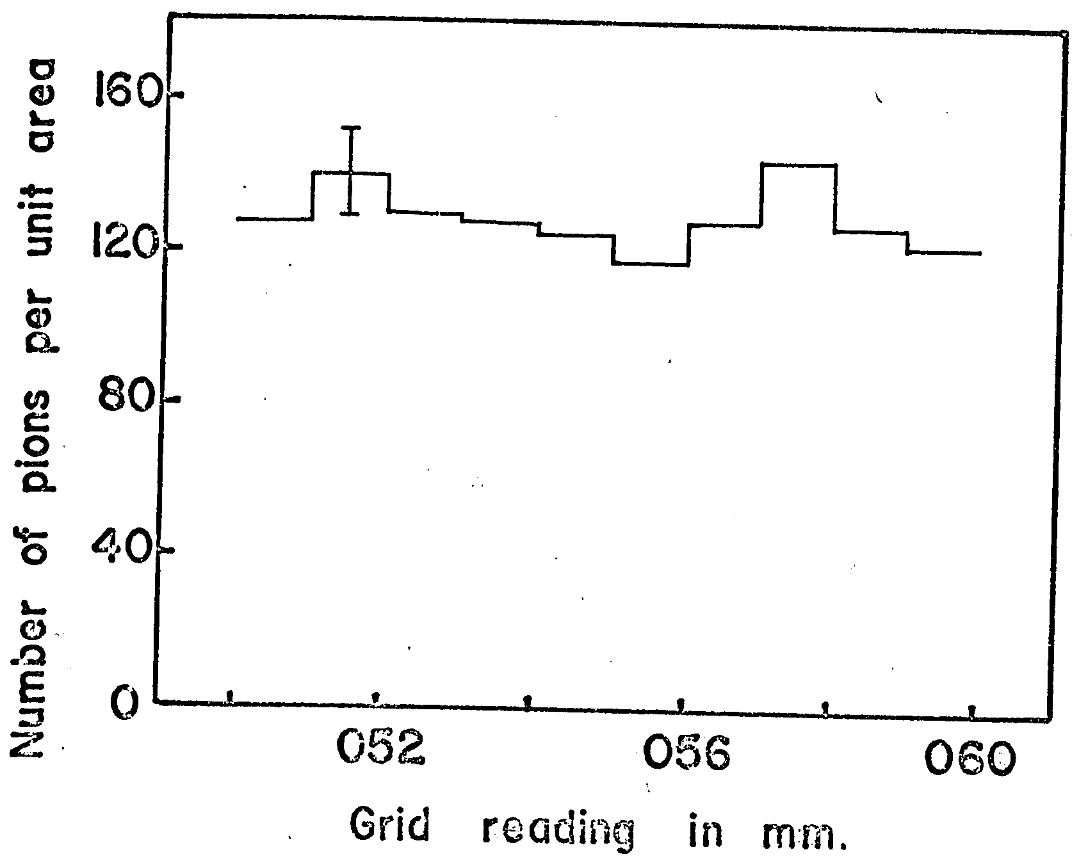

Fig. 3.13 Transverse distribution of the meson flux in pellicle C-1

pellicle. For this purpose small areas at equal intervals were chosen in the region where the stars were scanned. The mean incident angle for each of the pellicles used, were determined from the projected distances traversed by the pions. The sample distribution of the projected distances and the flux distribution in the transverse direction are shown for pellicle C1 in fig. 3.12 and 3.13, respectively. The results of the calibration and other characteristics for the pellicles A5, C1 and D5 are given in table 3.3.

III-7 Detection of Stars

The stars were obtained by area scanning using suitable magnification to suit the condition of the particular pellicle concerned. Stack 1 and 2, were scanned with magnification 25 x 10, and stack 3 with magnification 43 x 10. For greater efficiency, each area was scanned twice, and the stars which were not observed in the previous scanning were added to obtain the total number of stars. The efficiency of star detection was determined by comparing the results with that obtained by scanning, very carefully, a limited area with a magnification of 100 x 10. Efficiency was found to be (85 ± 5) percent and (82.5 ± 5) percent for the stacks 2 and 3, respectively.

To calculate the cross section, secondary stars were eliminated and suitable selection criteria were imposed on the stars. Stars with the incident tracks inclined not more than 10^{o} from the mean incident direction were accepted. In stack 2 and 3; 783 and 645 stars were scanned in which 554 and 551 stars, respectively, satisfied the selection criteria. The break down of the data are shown in table 6.2. In stack 1, 520 primary stars due to $\bar{p}$ annihilations were obtained, and were used only for the analysis of the fast proton pairs.

Chapter IV

PION-NUCLEUS INTERACTION

IV-1 Introduction

The interaction cross sections of the pion with free nucleons are well established from about one GeV pion-energy down to the lowest possible energies. It is observed that the behaviour of cross sections is characterized by sharp peaks. The most predominant and important peak occurs at about 180 MeV of pion energy, and is interpreted as an unstable resonance state between pion and nucleon. This resonance state or isobar, $N^{*3/2,\,3/2}$, has intrinsic angular momentum $J = {}^{3}/2$ and a mass of 1236 MeV.

The cross sections for elastic scattering of π^+ and π^- with proton are shown in fig. 4.1 (solid and dashed curve, respectively) (Anderson et al. 1955; Focacci et al. 1966). From the conservation of isospin, the positive pion-neutron cross section, $\sigma_{\pi^+ n}$, and the negative pion proton cross section, $\sigma_{\pi^- p}$, are equal. If the nucleus is made up of an equal number of neutrons and protons, and the interaction inside the nucleus is similar to that of the nucleons, then the general behaviour of the π-nucleus interaction cross

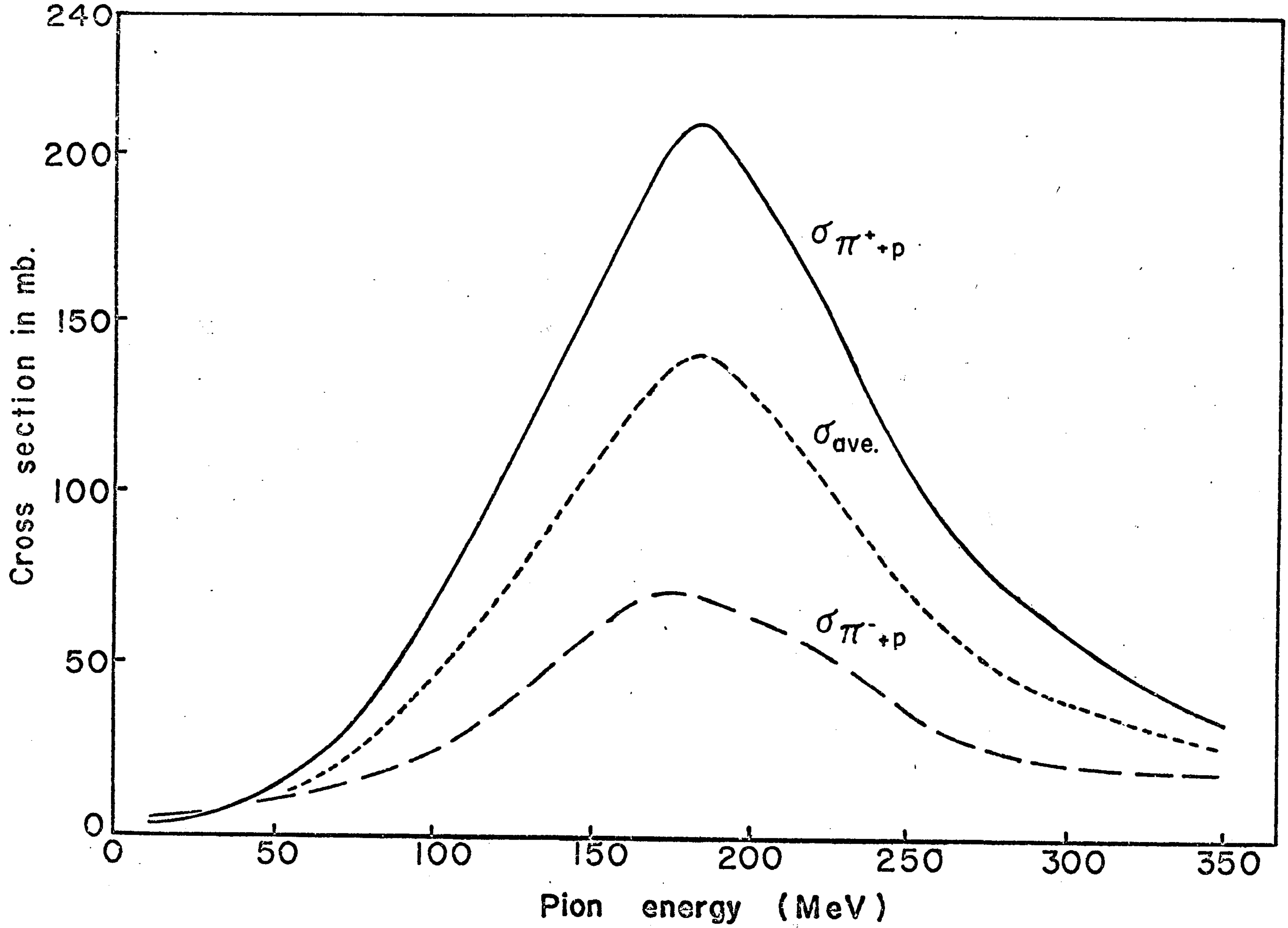

Fig. 4.1 Total cross section for pions on protons versus pion K-E in the lab. system.

section is expected to be similar to that of the average cross section (average of $\sigma_{\pi^+ p}$ and $\sigma_{\pi^- p}$) which is shown by the dashed curve in fig. 4.1. It is possible, therefore, to explain the π-nucleus interaction cross section in terms of the average free space π-nucleon cross section. The effect of the presence of other nucleons inside the nucleus, however, can be accounted for by using suitable model which can describe the effect. Thus in the frame work of the optical model, it is possible to account for the effect in a gross manner by introducing the optical model potential.

From a different view point, however, one can start with the pion-deuteron interaction cross section and obtain the cross section according to the quasi-deuteron model of B-S-W.

In this chapter the results of the experimental measurements, described in Chapter III, are given and the cross sections at various energies are calculated. The results have been analysed by:

i) Optical model calculation through isobar formation.

iii) Quasi-deuteron model.

IV-2 Experimental results and cross sections

From the observed number of stars and the incident pion flux, the interaction cross section was obtained from

$$\sigma = \frac{N_S}{f * A * d * N_e} \qquad 4.1$$

where

A = Area of the face in which pion is incident

N_S = Number of stars, in area A, due to the complex nuclei.

f = pion flux/cm^2

d = distance traversed by pion

N_e = number of atoms of complex nuclei per c.c.

Since σ is the cross section due to the complex nuclei only, it is necessary to eliminate the hydrogen stars to obtain N_S. An unambiguous separation is, however, not always possible. For this reason, the expected number of hydrogen stars in each case was obtained from the known $\pi^{\pm}p$ cross section using equation 4.1. For energies up to about 60 MeV, $\sigma_{\pi^{\pm}p}$ is small and the contribution of hydrogen stars was calculated to be less than 1 percent. At

Table 4.1

Experimental Cross Sections of π^+ Interaction

Pion energy E_π (MeV)	Face Area A (sq. mm)	Vol. scanned (mm^3)	d (mm)	N_s (corrected for efficiency and hydrogen stars)	Pion flux/cm^2 (corrected for efficiency)	cross section σ(mb)
10.7 ± 7	19.8	120	6	17	5.51×10^4	55 ± 18
21.4 ± 6	19.8	120	6	34	5.69×10^4	107 ± 22
31.2 ± 4.3	19.8	120	6	73	5.77×10^4	224 ± 31
40.5 ± 3.5	13.2	80	6	83	5.93×10^4	377 ± 52
46.5 ± 3.5	13.2	80	6	98	6.06×10^4	435 ± 61
52 ± 3	13.2	80	6	112	6.17×10^4	492 ± 64
58 ± 3	13.2	80	6	106	6.25×10^4	457 ± 63
62 ± 2.5	13.2	80	6	129	6.35×10^4	548 ± 69
168 ± 2.5	30	18	0.6	188	3.0×10^5	730 ± 75
224 ± 1.1	15	9	1.2	162	2.9×10^5	652 ± 72
254 ± 0.5	10	6	0.6	215	1.35×10^6	565 ± 59

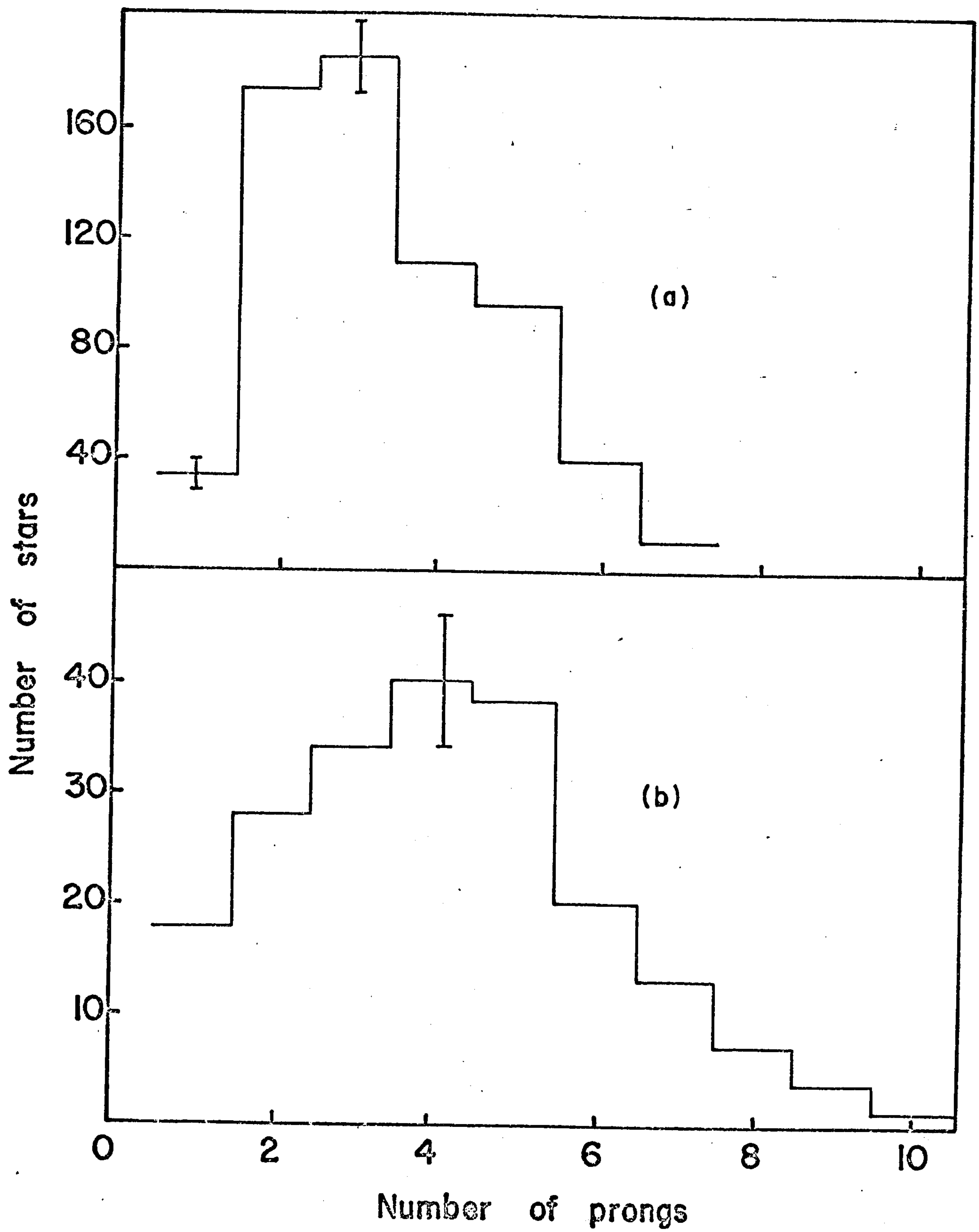

Fig. 4.2 Prong distribution of stars induced in emulsion nuclei by π^+- meson of energies (a) 50 MeV (b) 254 MeV

pion energies 168, 224 and 254 MeV, the contributions are 16.5, 13.5 and 12 percent, respectively. The results of the experimental measurements and the cross sections obtained by using equation 4.1 is shown in table 4.1.

The experimental cross sections are also used to calculate the imaginary part of the optical model potential, V_I. From the measured cross section, the mean free path $\lambda_{em.}$ for inelastic interaction of pions with complex nuclei of emulsion is obtained. The corresponding mean free path in nuclear matter, λ_n, is given by:

$$\lambda_n = \lambda_{em.} \frac{\rho_{em.}}{\rho_n}$$

where ρ_n and $\rho_{em.}$ are the densities of the nuclear matter and the emulsion, respectively.

The absorption coefficient, K, is then given by

$$K = \frac{1}{\lambda_n} = \frac{\rho_n}{\lambda_{em.} \cdot \rho_{em.}}$$

This value of K is finally used in equation 2.4, to obtain V_I. V_I, thus obtained, are shown in fig. 2.5 by small circles with error bars. The results have already been discussed and compared with theoretical results in Chapter II.

The prong distributions of the stars for average incident pion energies 40 MeV and 240 MeV are shown in figs 4.2a and 4.2b, respectively. It is seen that the average number of prongs in stars induced by the higher energy pions are somewhat larger than those induced by the lower energy pions. This is evident, since the energy available for evaporation in the former case is more compared to the latter.

IV-3 Isobar model

IV-3.1 Theory

This is essentially a model in which the absorption of 'pi-meson' takes place on two nucleons. In contrast to the quasi-deuteron model of B-S-W, this is a two stage process in which the pion first interacts with one of the nucleons to form an isobar. The interaction probability is determined from the pion-nucleon interaction cross section. The isobar may, then, either interact with another nucleon and is absorbed, or decay. The process can be most conveniently described as

$$\pi + N_1 \rightarrow N^* \text{ (isobar)}$$

$$N^* + N_2 \rightarrow N_3 + N_4 \text{ (absorption)}$$

or

$$N^* \rightarrow N + \pi \text{ (charge exchange or scattering)}$$

The outgoing pion and the nucleons can further interact with the nucleons and may lead to the excitation and subsequent evaporation of the residual nucleus. In any case, a visible star is expected as a result of the collision of the pion with one of the nucleons inside the nucleus. It is possible, therefore, to obtain the interaction cross section of the pion with complex nuclei, from the average π^+-nucleon interaction cross section, $\bar{\sigma}$, inside the nucleus.

Following Bethe (1938), Fernbach et al.(1949), the inelastic interaction cross section σ_i, in terms of $\bar{\sigma}$, is given by

$$\sigma_i = \pi R^2 \left(1 - \frac{V_c}{E}\right) \left[1 - \{(1 + 2KR)e^{-2KR}\}/2K^2R^2\right] \quad 4.2$$

where

V_c =coulomb barrier of the nucleus

E = incident energy of the pion

A = mass number of the nucleus

R = nuclear radius

K = absorption coefficient = $\dfrac{3\bar{\sigma}A}{4\pi R^3}$

The factor ($1 - V_c/E$) is the correction factor due to the coulomb barrier V_c at the incident energy E.

It is to be noted that $\bar{\sigma}$ must be evaluated at the energy of the particle inside the nucleus. Thus, if the pion sees a potential V_R, then $\bar{\sigma}$ has to be evaluated at an energy $E + V_R$, where E is the incident pion energy. In the present calculation V_R has been taken from our calculations (Chapter II, hereafter referred to as V_R modified). For comparison, the results have also been shown with the Frank-Gammel-Watson's values of V_R (referred as V_R-F-G-W) and for the case when pion does not see any potential.

If the medium contains two or more different types nuclei (as is the case with the emulsion), the cross section σ_i must be calculated for each type of atoms and the results have to be suitably averaged over. In our calculation, the emulsion has been considered to be made up of two groups of nuclei with average mass number 14 and 94, corresponding to the light group (consisting of C, N, O ~ 15.8% by weight) and the heavy group (Ag, Br ~ 84.2% by weight), respectively.

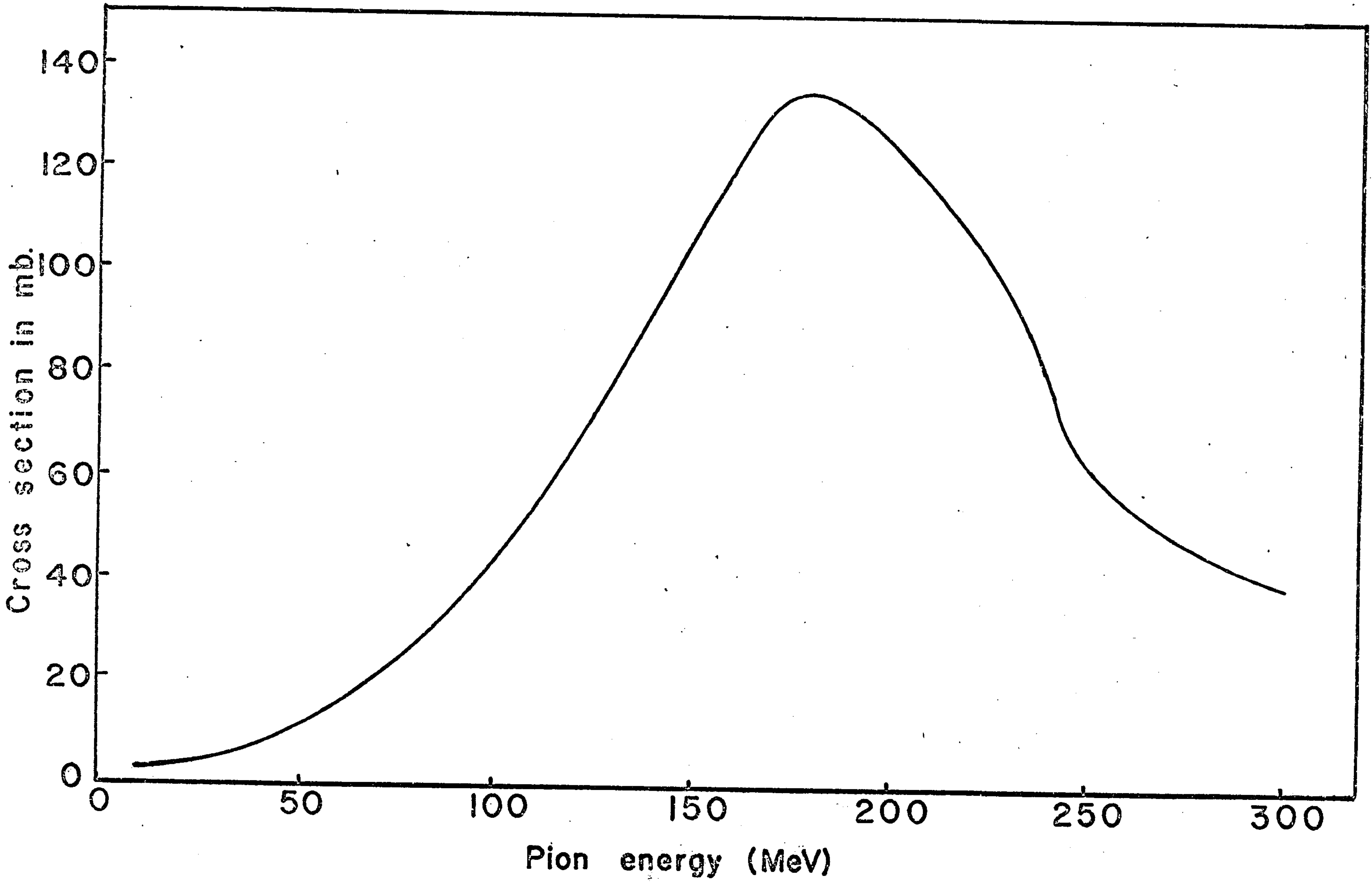

Fig. 4.3 Average total cross section for pions on nucleons in the nuclear medium of emulsion.

IV-3.2 Pion-Nucleon Interaction Cross Section

The average values of the pion-nucleon interaction cross sections, $\bar{\sigma}$, used in equation 4.2, were taken from the pion-nucleon interaction cross sections shown in fig. 4.1. For the target nucleus with equal number of protons and neutrons a simple average of σ_{π^+-p} and σ_{π^--p} can be taken (curve c in fig. 4.1). For heavier atoms, however, there are more neutrons than protons and hence the average must be taken, accordingly. Thus, if there are x protons and y neutrons in a given nucleus, then the cross section $\bar{\sigma}$ is given by:

$$\bar{\sigma} = \frac{x\sigma_{\pi^+-p} + y\sigma_{\pi^--p}}{x + y} \qquad (4.3)$$

Finally, this is averaged over the percentage abundances of the two groups of nuclei present in the emulsion. The average cross section, calculated on this basis, is shown in fig. 4.3. These cross sections are applicable if the target nucleons are at rest. The target nucleons, however, move in all directions inside the nucleus, and change the effective cross section. At lower pion energies, the corresponding changes were found to introduce a difference in the σ_i calculated from the equation 4.2. For this reason, the average pion-nucleon interaction cross section, $\bar{\sigma}$, in the region up to about 100 MeV, was corrected for the Fermi motion of the target nucleons inside the nucleus. The nucleons were assumed to form a Fermi gas with a maximum momentum of 225 MeV/c. A simple Monte-carlo type calculation was performed in which the target nucleons, approaching from different directions, were made to collide with the incident pion. For each collision, the effective incident energy in the rest frame of the target nucleon was calculated. The corresponding cross section was obtained from the pion-nucleon interaction cross section. For a particular incident energy of the pion, the calculations were repeated many times with various values of the energy and the direction of the target nucleon. The result was finally averaged to obtain the desired corrected cross section. The scheme of the program used for this calculation is given below:

For a given energy of the incident pion:

a) a suitable energy was attributed to the target nucleon

b) A direction was given to the nucleon chosen in "a".

c) The total C.M. energy, E*, was obtained

$$E^{*2} = 2E_\pi E_N + (m_\pi^2 + m_N^2) \mp 2\sqrt{(E_\pi^2 - m_\pi^2)(E_N^2 - m_N^2)} \qquad (4.4)$$

where E_π and E_N are the total pion and nucleon energy in the laboratory system, respectively; m_π and m_N are the corresponding masses.

d) The equivalent laboratory energy of the incoming pion, ϵ', which produces the above total C.M. energy E* on a nucleon at rest, was calculated from:

$$E^{*2} = 2\epsilon' m_N + (m_\pi^2 + m_N^2) \qquad (4.5)$$

e) The cross section corresponding to ϵ' was obtained.

f) The direction of the target nucleon was changed by 5° and the steps 'c' to 'e' were repeated. This was repeated to cover the whole solid angle.

g) The energy of the target nucleon was changed by 2.5 MeV and the steps 'b' to 'f' were performed. This was repeated to cover the momentum up to 225 MeV/c.

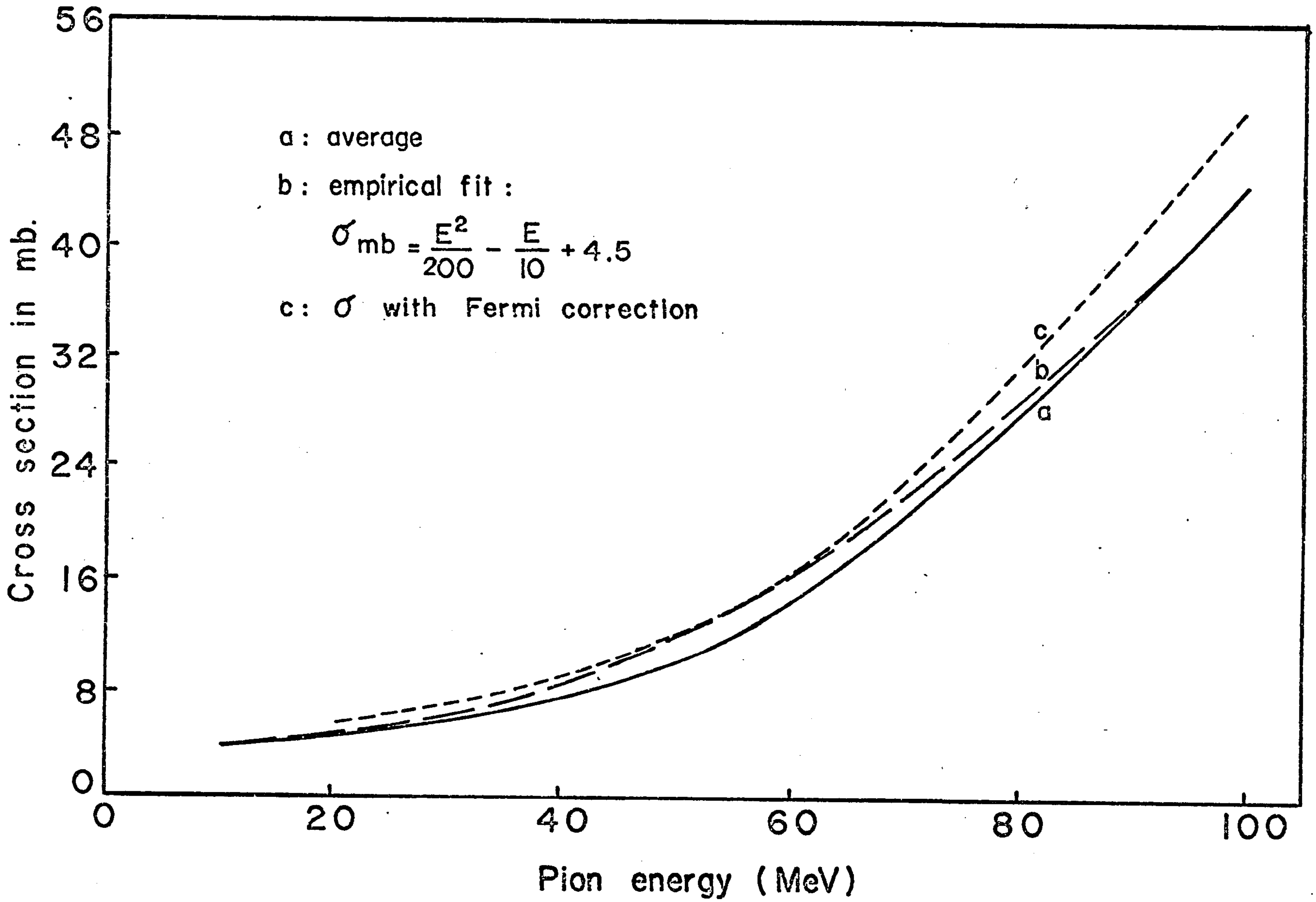

Fig. 4.4 Empirical fit of the total cross section for pions on nucleons in the nuclear medium of emulsion

These cross sections were averaged.

To perform the step 'e', the energy dependence of the cross section was supplied to the machine in the form of the empirical equation

$$\sigma_{mb} = \frac{E^2}{200} - \frac{E}{10} + 4.5 \text{ (up to about 100 MeV)} \tag{4.6}$$

This equation, however, gives cross sections which are slightly higher than the experimental values (fig. 4.4: curve 'a' is the average pion-nucleon cross section, and the curve 'b' is the closest analytic fit). This was accounted for by introducing a correction in the calculated cross section, and the corrected values are shown by the curve 'c'.

IV-3.3 Comparison of the Experimental and Theoretical Results

Using equation 4.2, the cross sections, σ_i, were calculated for the entire (3,3) resonance energy region. In fig. 4.5, the results for r_o = 1.3F, 1.4F and 1.5F (without any potential) are shown. The experimental results are also shown in the same figure with

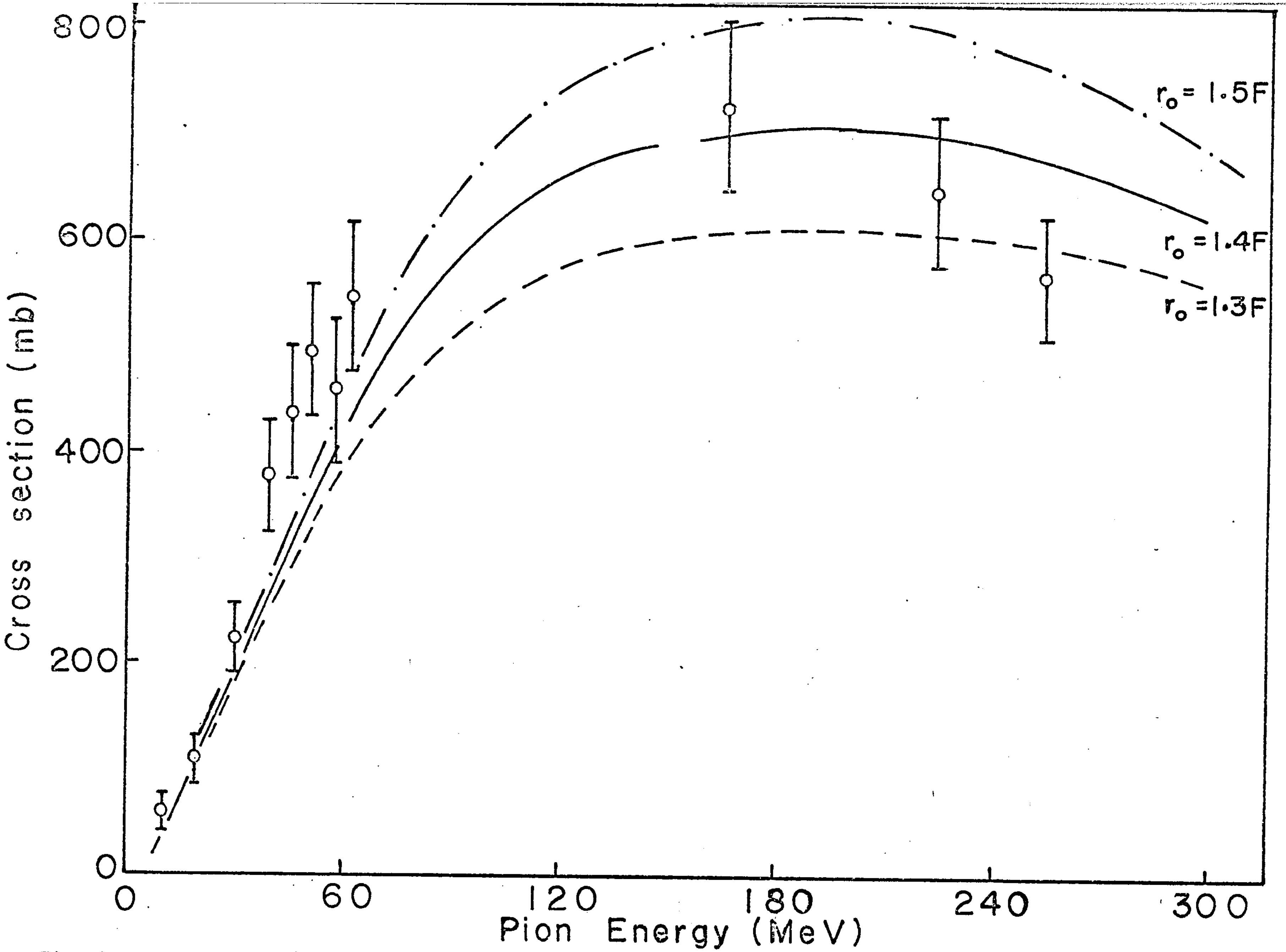

Fig. 4.5 Experimental (vertical lines) and calculated (with r_0 = 1.3F, 1.4F and 1.5F; but no potential) energy dependence of the inelastic interaction cross section of π^+- mesons in emulsion in the energy range up to 300 MeV.

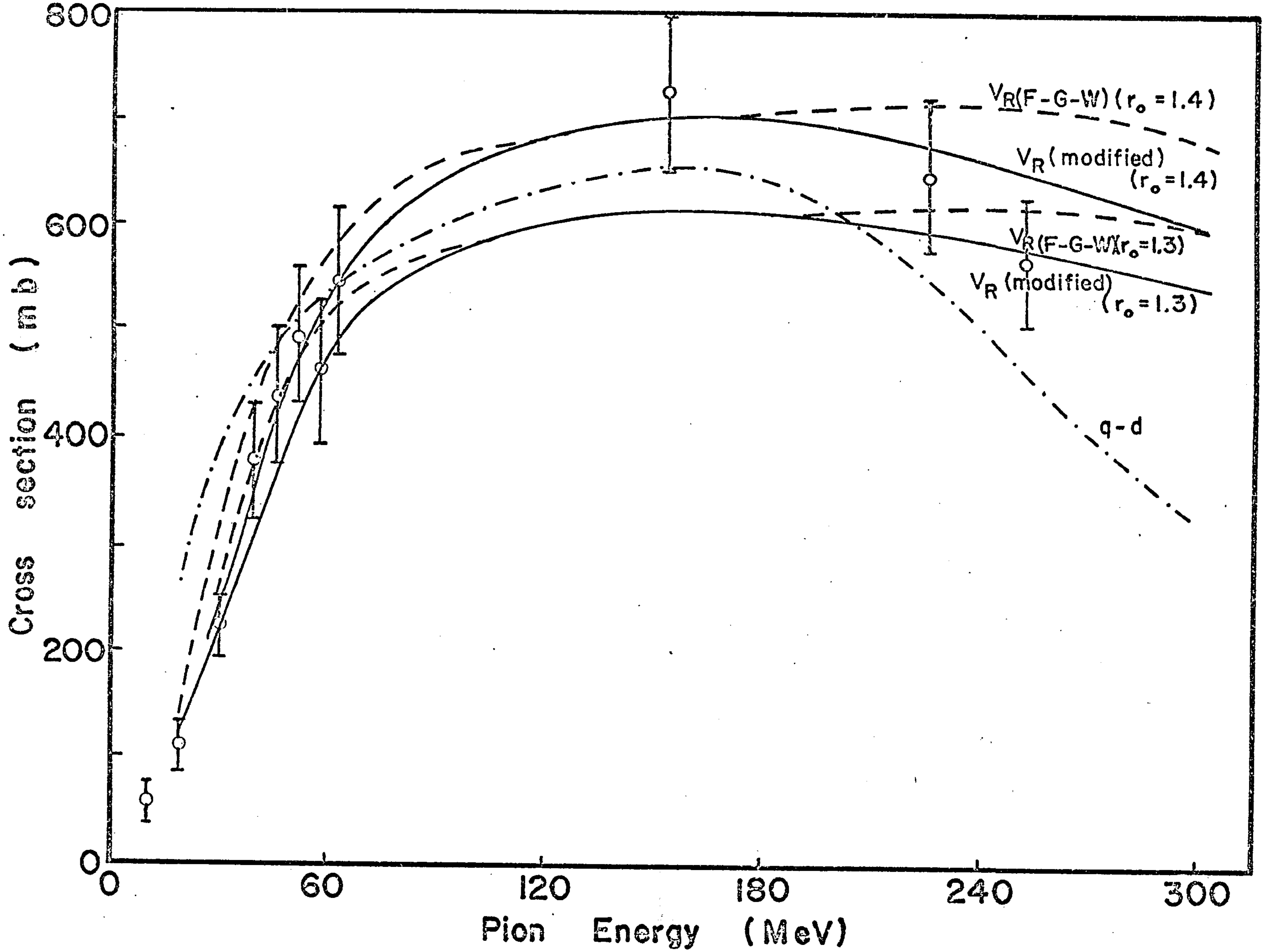

Fig. 4.6 (a) Experimental (shown with vertical lines) and calculated (r_0 = 1.3F, 1.4F and with V_R - modified and V_R-F.G.W.) energy dependence of the inelastic interaction cross section of π^+- mesons in emulsion in the energy range up to 300 MeV.

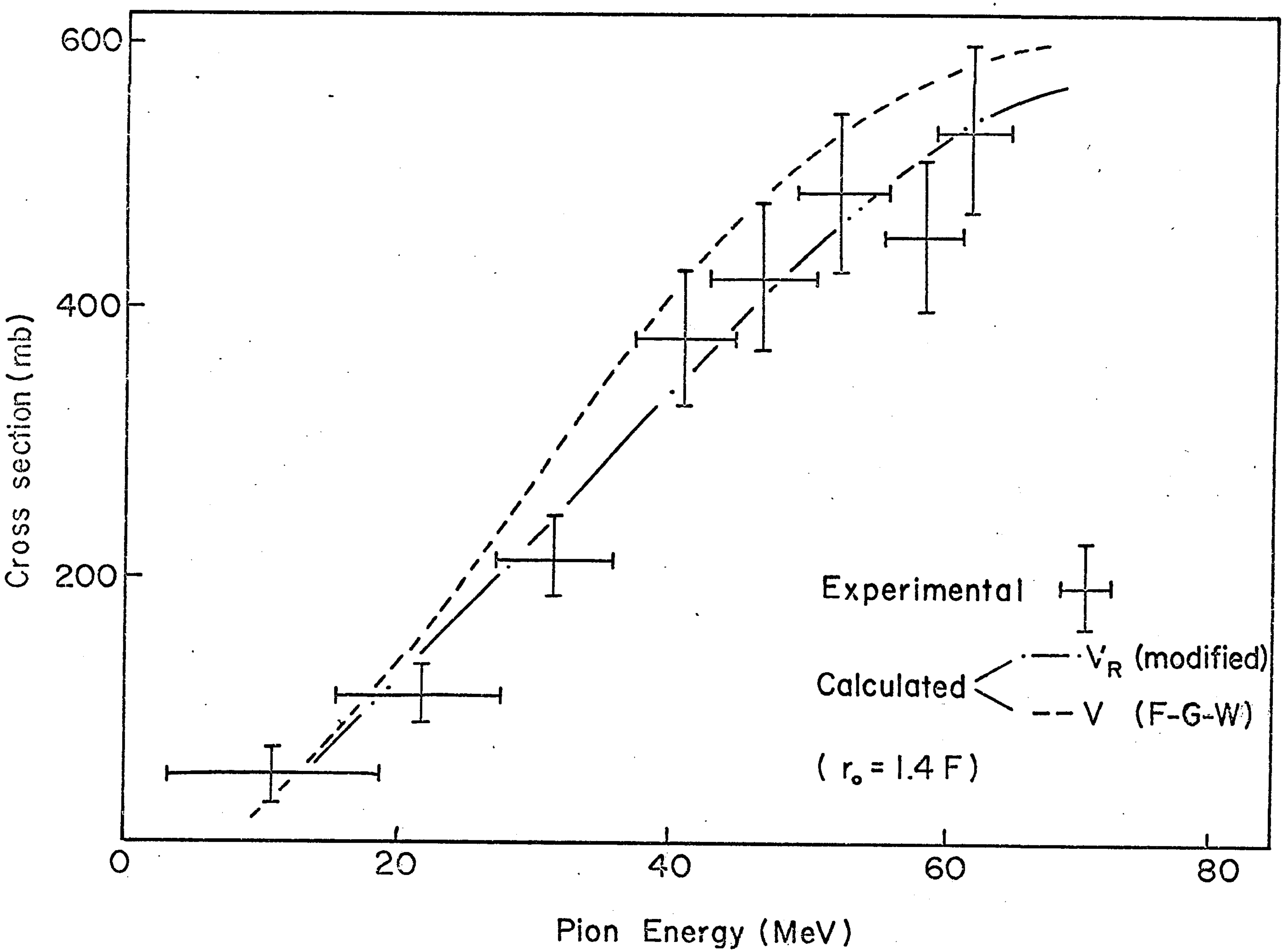

Fig. 4.6 (b) Inelastic interaction cross section of π^+- meson in emulsion (up to 70 MeV)

the error bars. It is observed that a very large value of r_o will be required to obtain any agreement between the experimental and the calculated values in the low energy region. No satisfactory agreement can, however, be obtained over the entire range. A much better agreement can be obtained if a pion-nucleus potential is introduced. In fig. 4.6a, the results of calculations are shown for both the potentials V_R; i.e. V_R calculated in Chapter II (V_R-modified) and that calculated by F-G-W (V_R-F-G-W). The results are shown for r_o = 1.3F & 1.4F and are again compared with the experimental results. The experimental results have good general agreement with the calculated values for r_o = 1.4F and our values of V_R. The experimental cross section at 254 MeV, is, however, somewhat lower than the predicted cross section. For comparison, the results obtained on the basis of quasi-deuteron model of B-S-W are also shwon in fig. 4.6a (dash-dotted line).

In fig. 4.6b, the results for the energy region up to about 70 MeV (Stack 2) are shown separately for r_o = 1.4F. A very good agreement is quite apparent in this region with V_R-modified. The results with V_R-F-G-W are also shown for comparison.

In the preceding section, it has been noted that the emulsion was considered to be made up of two groups of nuclei; a light group with mass number A = 14 and a heavy group with A = 94. Equation 2, however, is not strictly applicable for very light nuclei, particularly at low energies, where KR < 1 and kR ~ 1, ($k = (2mE)^{\frac{1}{2}}/\hbar$ and is the propagation vector). To check its applicability for the present case, the experimentally obtained ratio of the cross section due to the light nuclei to the total cross section was compared with the predicted values on the basis of equation 4.2. At 20 MeV, equation 4.2 gives, σ_i (total) = 128 mb, σ_{light} = 34 mb. Thus the contribution due to the light nuclei is 27 percent of the total cross section. The experimental ratios were obtained by separating the stars due to light and heavy nuclei by using the criteria of Blau, Oliver and Smith (1953). The ratios were found to be 30 ± 6 percent and 25 ± 5 percent at energy ranges between 15 to 30 MeV and 40 to 60 MeV, respectively, and compare fairly well with the calculated values. This indicates that the equation 4.2 still yields acceptable values for light nuclei at these low energies and can be accepted within the experimental errors.

IV-4 Quasi-deuteron Model for Pion Absorption

In the previous section it has been seen that the isobar model of pion interaction can, very well, explain the energy dependence of the pion-nucleus interaction. The quasi-deuteron model of Brueckner-Serber and Watson (B-S-W) is also a two nucleon interaction process, and is based on the fact that the pion is absorbed on a close proton-neutron pair. According to this model, the cross section σ_i , can be obtained from the pion-deuteron cross section, $\sigma(\pi^+ + d \rightarrow 2p)$. Following B-S-W, the interaction cross section per proton can be written as:

$$\frac{1}{Z}\,\sigma\,[\pi^+ + \text{nucleus} \rightarrow \text{star}] = \Gamma \,.\, \sigma\,(\pi^+ + d \rightarrow 2p) \qquad (4.7)$$

where Z = number of protons in the nucleus. The proportionality factor, Γ , is essentially a correlation factor, and is measure of the probability for a given nucleon of forming a deuteron with another nucleon in the nucleus. B-S-W prescribe a value of $\Gamma \sim 10$.

The cross section $\sigma(\pi^+ + d \rightarrow 2p)$, for the entire (3,3) resonance region was obtained from its inverse cross section $\sigma(p + p \rightarrow \pi^+ + d)$ using detailed balance,

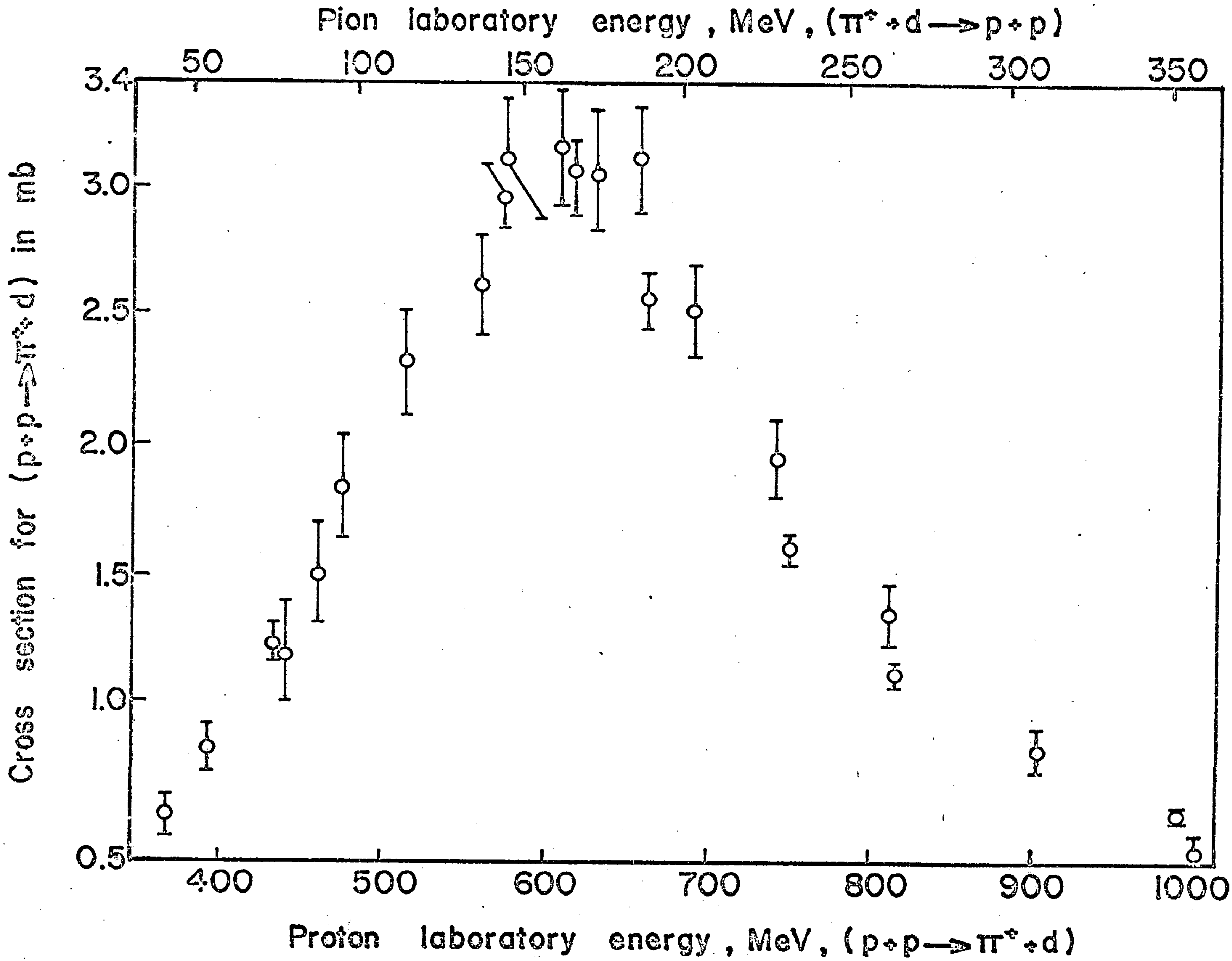

Fig. 4.7 Energy dependence of the cross section, σ ($p + p \rightarrow \pi^+ + d$)

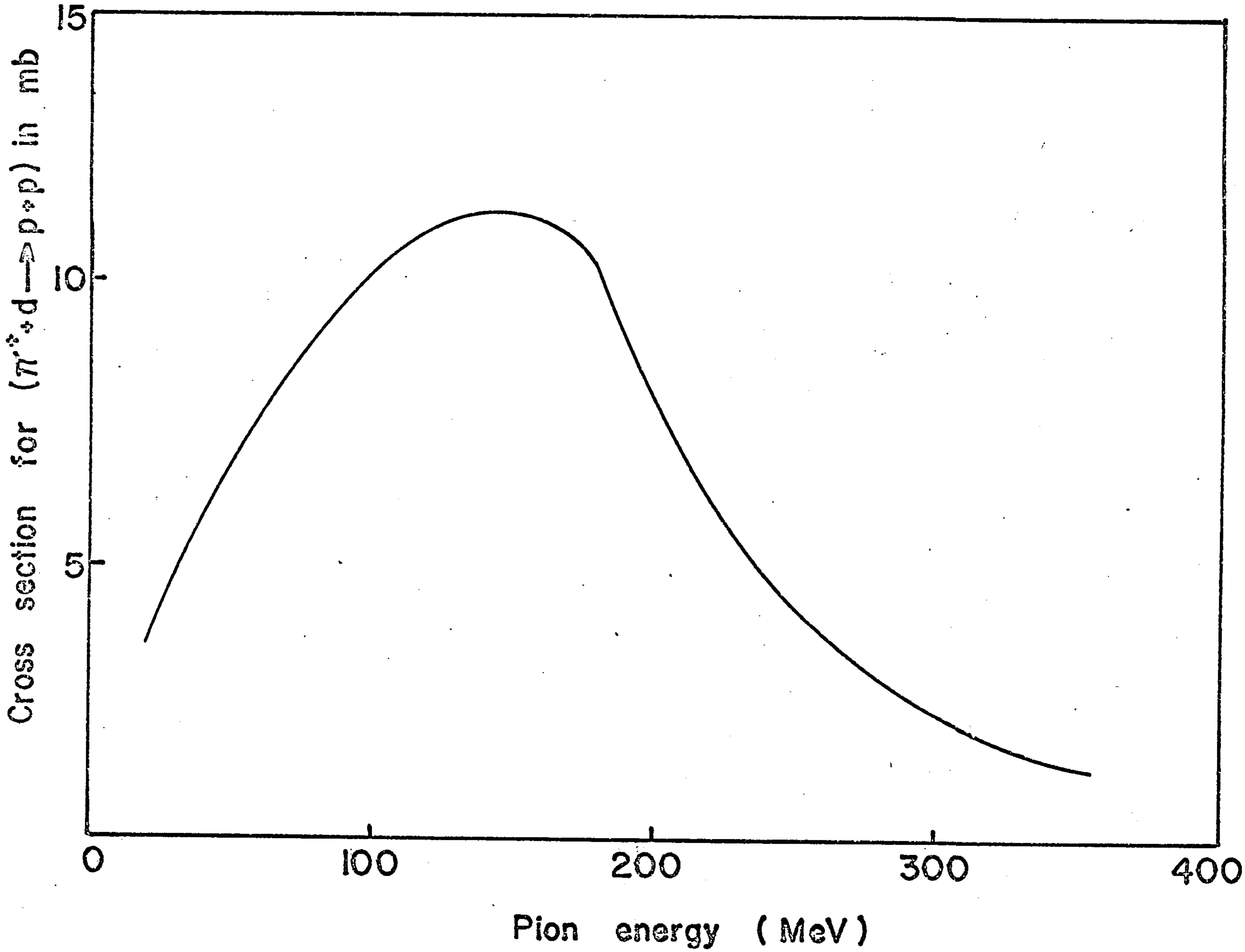

Fig. 4.8 Energy dependence of the cross section, σ (π^{+}+ d→ p + p)

(Fig. 4.7, Hirt et al. 1968). From the detailed balance, the cross section $\sigma(\pi^+ + d \rightarrow 2p)$ is given by: (Nishijima 1964):

$$\sigma(\pi^+ + d \rightarrow p + p) = \sigma(p + p \rightarrow \pi^+ + d)\ \frac{2}{3(2S_\pi + 1)}\ \frac{P_p^{*2}}{P_\pi^{*2}} \tag{4.8}$$

where S_π is the spin of the pion = 0; P_p^* and P_π^* are the momenta of the proton and the pion in the C.M. system, respectively. The cross sections $\sigma(\pi^+ + d \rightarrow p + p)$ thus obtained are shown in fig. 4.8.

It is to be noted that the quantity $\Gamma.\sigma(\pi^+ + d \rightarrow p + p)$ is equivalent to the interaction cross section per deuteron (since the number of protons determines the number of deuterons) inside the nucleus. The nucleus can be considered as a sphere of radius R with Z deuterons and equation 4.2 can be used to obtain σ_i. In this case the absorption coefficient K is given by:

$$K = \frac{3Z\Gamma\sigma(\pi^+ + d \rightarrow p + p)}{4\pi R^3} \tag{4.9}$$

The cross-sections thus obtained with $r_o = 1.4F$ and $\Gamma = 10$, are shown by curve 'e' in fig. 4.6. The cross sections are much larger in the low energy region, although comparable values are obtained around 160 MeV. In general, the results do not agree very well with the experimental values. The results can, however, be fitted to the experimental values by adjusting Γ. This can be achieved by reducing Γ at lower incident energies. This is contrary to the fact that Γ is expected to be larger at smaller energies. At low energy, the pion remains inside the nucleus for larger period of time, and hence the probability of finding two nucleons together is greater. Moreover, a precise knowledge of nuclear correlation is needed for a more rigorous defination of Γ.

IV-5 Other Available Data of π^+-nucleus Interactions

On the basis of the isobar model, presented in section IV-3, some existing data of the interaction of positive pions with complex nuclei have been interpreted. The experimental data consist of (a) The measurement of Blinov et al. (1958) of π^+ on freon from 77 to 285 MeV; (b) The measurement of Tracy (1953) of π^+ on aluminum from 25 to 80 MeV.

The results of Blinov et al. are based on the bubble chamber study of 4600 pairs of photographs. The working liquid was a mixture of freon 12, (CCl_2F_3) and freon 13, ($CClF_3$). They used three different beams having energies 320, 234 and 130 MeV to cover their experimental range. Use of different beams reduced the uncertainty due to straggling. The beams were fairly monoenergetic; the range of 130 MeV beam was (38 ± 3) cm.on freon. The muon contamination was 13 percent.

The interpretation of the results are somewhat difficult as the experimental results do not have the explicit values of the total inelastic cross sections. The values for the absorption and the charge exchange cross sections are given, whereas the equation 4.2 predicts the total cross section for the inelastic processes. For

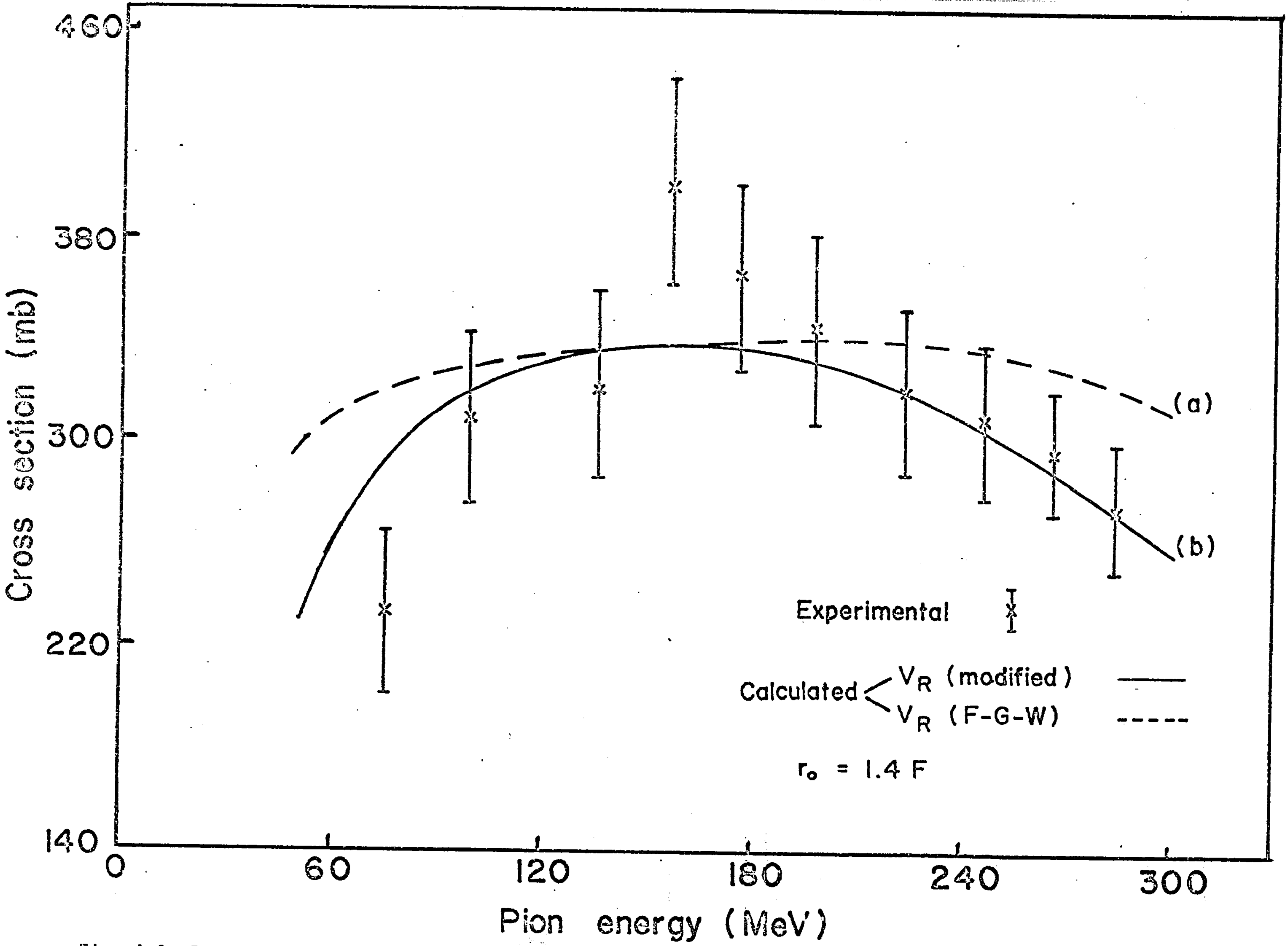

Fig. 4.9 Interaction cross section of π^+- meson, ($\sigma_{ch.ex.} + \sigma_{abs.}$), with freon nuclei

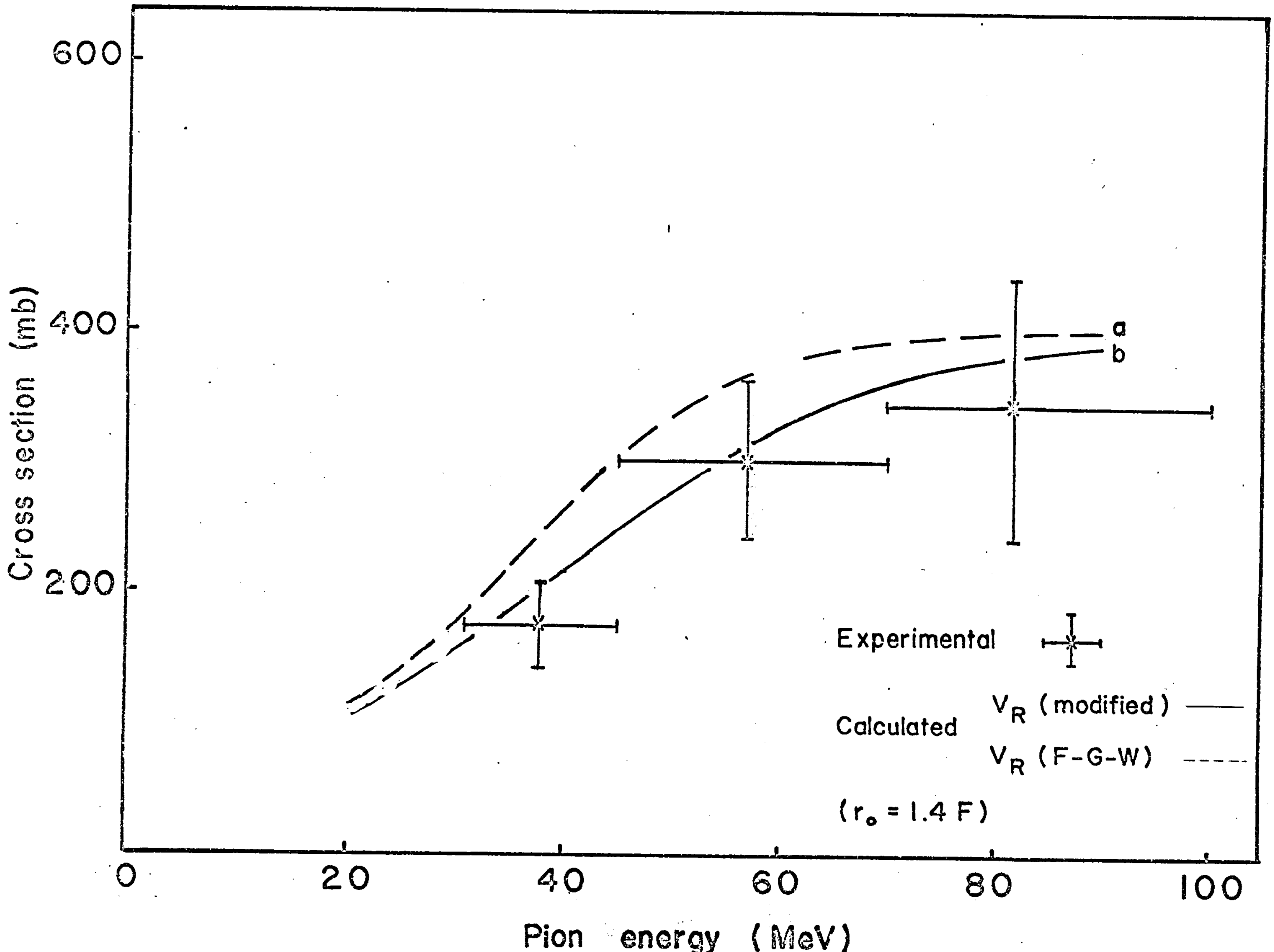

Fig. 4.10 Interaction cross section of π^+- meson, ($\sigma_{ch.ex} + \sigma_{abs.}$), with aluminum.

this reason, a Monte-Carlo calculation, similar to the one explained in Chapter VI, was performed to obtain the fraction in which an inelastically scattered pion comes out. This cross section was subtracted from the cross section obtained by using equation 4.2. The results, with $r_o = 1.4F$, are shown for both the F-G-W and the modified potential (fig. 4.9) by curves a and b, respectively. These are compared with the experimental values of $\sigma_{ch.\ ex.} + \sigma_{abs}$ which are shown by points with error bars. A good agreement is obtained and in both cases a peak at about 160 MeV is observed.

The results on aluminum are taken from the cloud chamber study of Tracy. He used a magnetic cloud chamber containing five $1/8''$ aluminum plates as the target. The usefulness of these results are, however, somewhat limited due to the large energy width and the probable loss of small tracks inside the aluminum plates for which a suitable correction was applied. Moreover, the energies are not well defined. The range of 100 MeV pions was divided into three ranges to obtain three wide energy bands; e.g. 25 to 45 MeV, 45-70 MeV and 70-100 MeV, corresponding to the mean energies of 38, 57, 82 MeV. The results were interpreted as in the case of freon, and are shown in fig. 4.10. Again the general agreement is good, although not much can be concluded due to the large uncertainty and wide spread of the energy.

IV-6 Discussion

From the foregoing discussions, it is seen that the pion-nucleus interaction cross section can be well explained by optical model through the isobar formation. The advantage of this mechanism over the quasi-deuteron model, is attributed to the fact that according to this mechanism the π-nucleus interaction can be described on the basis of the well known π-nucleon interaction. The use of isobar model does not require a nucleon pair to form a deuteron within a very short time and thus avoids the use of any uncertain correlation factor. Moreover, the quasi-deuteron model require a p-n pair, whereas in the isobar model the absorption can take place with any two nucleons provided the charge is conserved. The relative ratio of the n-n/n-p pairs, produced in π^- capture can be well explained by isobar model (Mes. H. 1968), which the quasi-deuteron model fails to explain. Further studies in Chapter V and VI, also indicate the applicability of the isobar model.

Chapter V

PIONS FROM ANTIPROTON ANNIHILATION

V-1 Introduction

An antiproton ($\bar{p}$) is an antiparticle of proton (p) and hence, has the same mass but opposite charge (-1) as that of a proton. Like proton, this is a Fermion and has a spin (J) $\frac{1}{2}$. It has a negative charge and odd parity. Like antiproton, antineutron is an antiparticle of neutron. Antiproton forms an isospin doublet with antineutron.

The antinucleon-nucleon system has a total mass of 1880 MeV and baryon number zero. The system is identical to a heavy meson and is highly unstable and breaks up into a number of mesons (Baltay 1966, Cresti 1963) through strong interactions. Ninety six percent of the mesons are pions and the remaining four percent are kaons, which also eventually decay into pions through weak interactions. The kaons form only a small fraction of the total and, therefore, can be neglected. Since the antinucleon-nucleon system has a total mass of 1880 MeV and pion mass of about 140 MeV, a maximum of about 13 pions can be produced in an annihilation. Such a high pion multiplicity, however, is

Table 5.1

Observed and Calculated Pion Multiplicities for $\bar{p}$
Annihilations with Proton, Neutron and Emulsion

	$\bar{p}$-emulsion	p-$\bar{p}$ annihilations		n-$\bar{p}$ annihilations	
	(observed)	observed	calculated	observed	calculated
$\langle N_{\pi}\rangle$		4.83 ± 0.07	4.86 ± 0.07	5.07 ± 0.09	4.90 ± 0.20
$\langle N_{\pi^+}\rangle$				1.08 ± 0.03	1.07 ± 0.04
	2.44 ± 0.07	2.95 ± 0.04	2.91 ± 0.04		
$\langle N_{\pi^-}\rangle$				2.07 ± 0.03	2.05 ± 0.08
$\langle N_{\pi^0}\rangle$		1.88 ± 0.05	1.95 ± 0.04	1.92 ± 0.08	1.78 ± 0.08

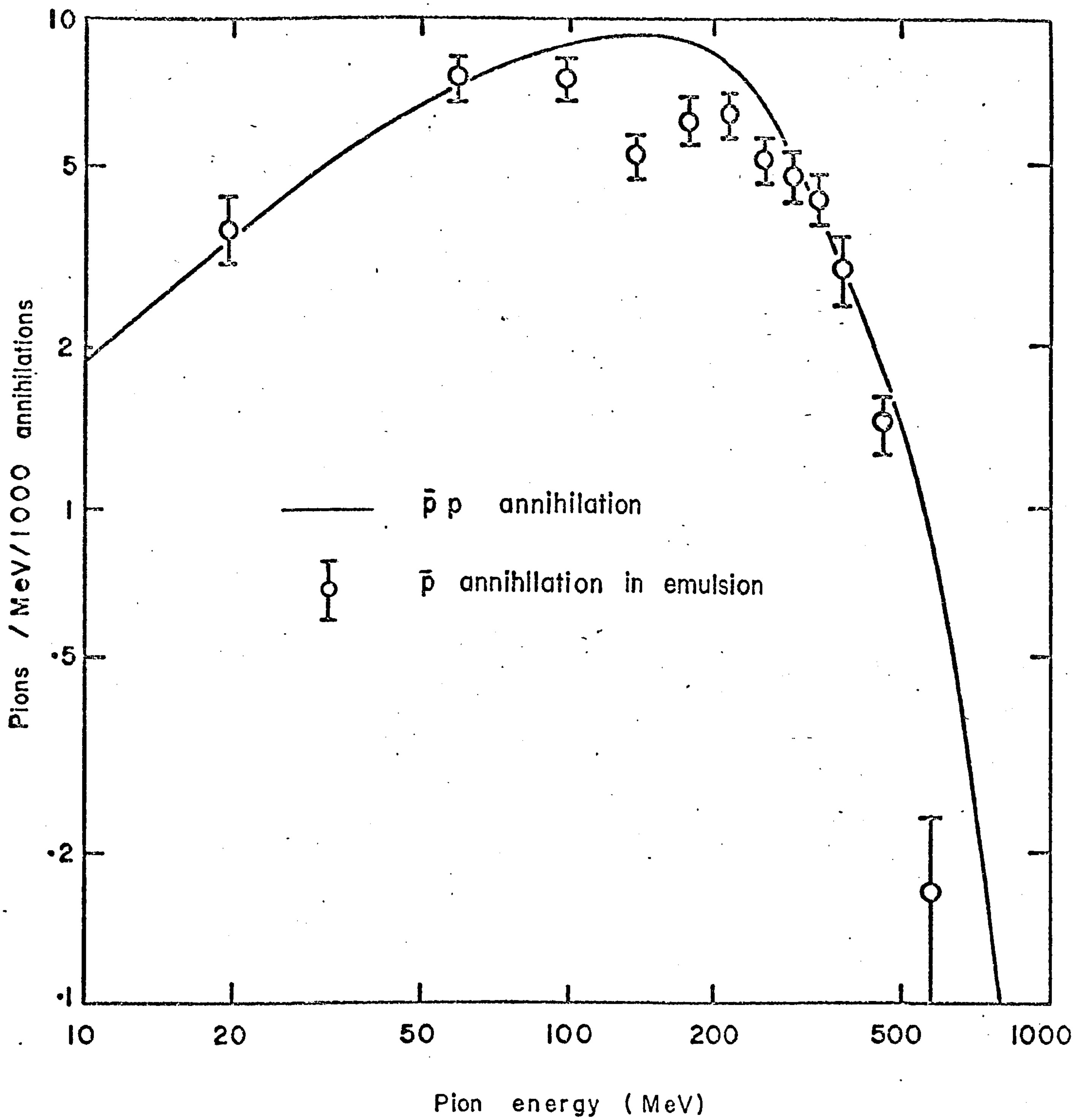

Fig. 5.1 Energy distribution of charged pions in $\bar{p}$ - annihilation.

not observed and rarely more than 7 pions are produced. In most cases 4, 5, 6 pions are produced with an average multiplicity 5. Various pion multiplicities, both observed and calculated, in antinucleon annihilations are given (Hébert et al.1968) in table 5.1. The experimental energy distribution of the charged pions produced in $\bar{p}$-p annihilation is also shown on a log-log scale by the solid curve in fig. 5.1.

If however, an antiproton annihilates on a nucleus, it does so with one of the nucleons at the surface of the nucleus (Barkas 1957, Chamberlain 1959). The annihilation process is, therefore, similar to the antiproton-nucleon annihilation and emits pions in all directions. These pions travel through the nucleus and can interact with other nucleons, thus decreasing the total pion multiplicity observed in annihilation with free nucleons. The observed multiplicity and the energy distribution of the charged pions produced in $\bar{p}$ annihilation on emulsion nuclei are shown in column 2 of table 5.1 and in fig. 5.1 (circles with vertical bars), respectively. The averaged charged pion multiplicity, $\langle N_{\pi}\pm\rangle$, is 2.44 ± 0.07, which is about 20 percent less than that observed in annihilation on free nucleons.

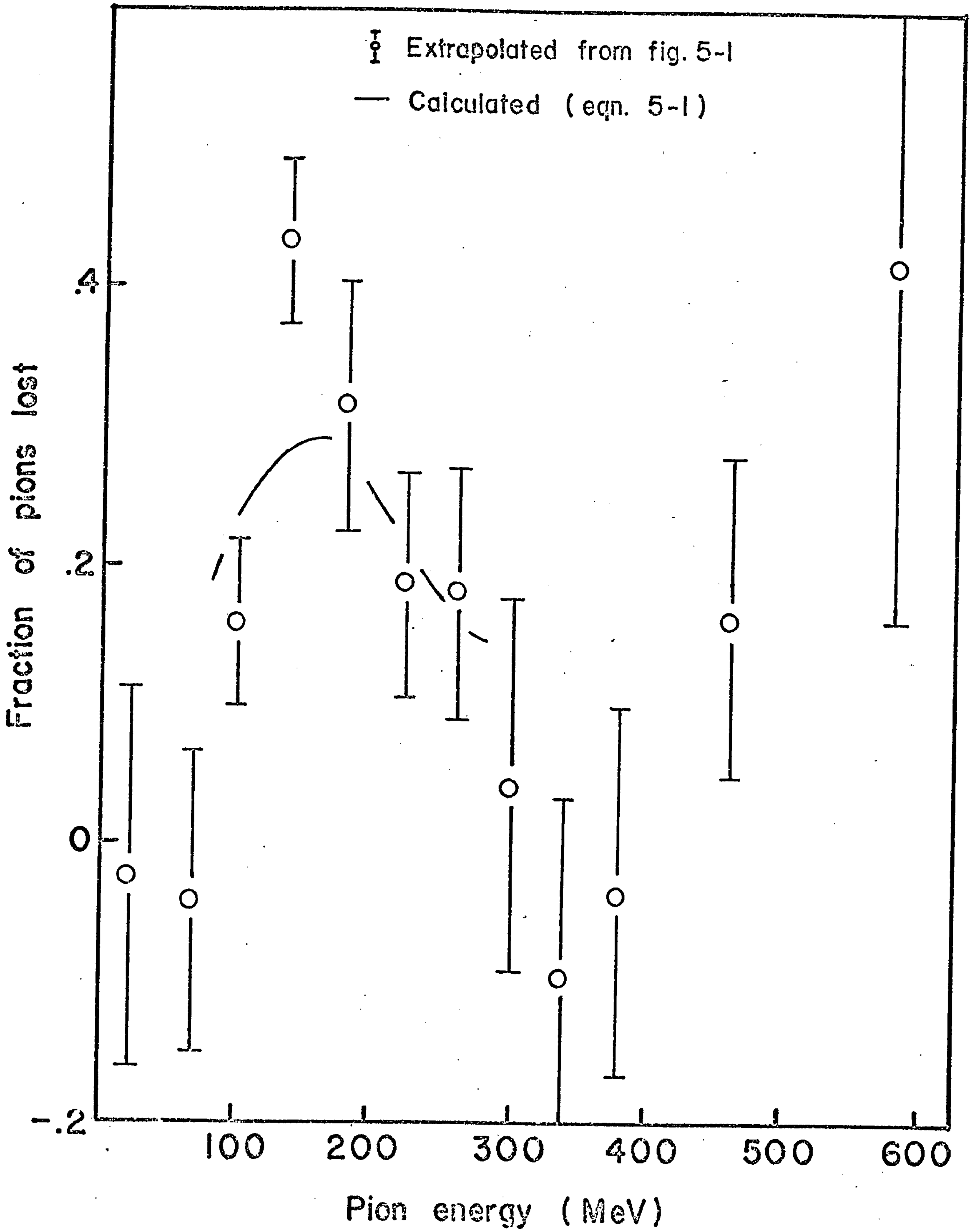

Fig. 5.2 Charged pions lost in nuclear matter following $\bar{p}$ - annihilation in emulsion.

V-2 Absorption of Pions

From the foregoing discussions, it is seen that a fraction of the pions produced inside the nucleus gets absorbed before coming out of the nucleus. In fig. 5.1, a large difference between the two distributions is apparent between 100 and 200 MeV of pion energy. The fractional difference between these two distributions are plotted (circles with vertical error bars) in fig. 5.2. A striking energy dependence of the absorption fraction is quite obvious and has a peaking at about 160 MeV. In Chapter IV, similar energy dependence and a peaking at about 160 MeV was found in the pion-nucleus interaction cross section. From this it can be inferred that a similar mechanism prevails in the interaction of these pions inside the nucleus. Assuming that the interaction takes place through the isobar formation, the absorption fraction 'f' can be written as (see appendix 2):

$$f = \frac{1}{2}\,\{1 - \frac{1}{2KR}\,(1 - e^{-2KR})\} \qquad (5.1)$$

where K ($K = \frac{3A\bar{\sigma}}{4\pi R^3}$) and R have the same meaning as in equation 4.2.

The equation 5.1 is derived on the assumptions:

1) Antiproton annihilates at the surface of the nucleus.
2) Nucleus behaves as a sphere.
3) Isotropic angular distribution for the pions.

In calculating the absorption fraction, the emulsion has been considered to be made up of two groups of nuclei (light and heavy) as in equation 4.2. The effect of the optical model potential has been accounted for, as before. Thus a pion having observed energy E, outside the nucleus, would have an energy $E + V_R$ at the time of production. This is the energy of the pion at the time of interaction and hence $\bar{\sigma}$ at that energy was used for calculating K in equation 5.1.

The calculated absorption fraction is shown by the solid curve in fig. 5.2, for the energy region 80 to 300 MeV. A fair agreement seems to have been obtained between the experimental and the calculated absorption fractions. The calculated absorption fraction reproduces the peak roughly at the right energy where the experimental peak is observed.

Equation 5.1, however, is based on the assumptions which are not strictly satisfied. It may be possible to improve the results by removing some of the assumptions. This will, however, complicate the calculations and is not expected to change the results significantly. Moreover, the experimental results have large errors and hence such a calculation is not considered worthwhile. In any case, the agreement is fair and the fraction of pions absorbed (pions from antiproton annihilation on emulsion nuclei) is satisfactorily explained by the optical model formulation through isobar formation.

Chapter VI

ANALYSIS OF PRIMARY PROTONS IN PION INDUCED STARS

VI-1 Introduction

In the absorption of a pion by a pair of nucleons, the rest mass energy (~140 MeV) released is shared more or less equally by the two absorbing nucleons. Thus in low energy pion absorption both the nucleons will have energies of the order of 70 MeV. The study of these fast pairs can, therefore, yield information on the absorption process as well as on the behaviour of the nucleons inside the nucleus. These nucleons, however, interact with other nucleons in traversing through the nucleus, and hence change their initial energies and directions. The presence of other evaporated particles makes it difficult to distinguish the primary nucleons from the secondaries. A selection criteria is, therefore, imposed on the energy of the protons under investigation. It is seen in the following section that most of the evaporated particles will have energies less than 30 MeV. The nucleons with energy greater than 30 MeV, therefore, can be considered as coming from the primary interaction.

In this chapter, the energy and the angular distribution of these fast protons have been studied and have been compared with the results of the M.C. calculations. The experimental results consist of

i) The analysis of the fast protons emitted due to the absorption of pions which are produced inside the nucleus due to $\bar{p}$ annihilation (Stack 1)

ii) The analysis of the protons emitted due to the direct absorption of pions which are incident on emulsion (Stack 2)

VI-2 Energy Spectrum of Evaporated Particles

Due to frequent collisions of the two outgoing fast nucleons and knock on nucleons, the whole nucleus becomes excited. In a very short time the excitation energy of the nucleus distributes itself in a statistical manner among all other nuclear particles. In other words, the temperature of the nucleus as a whole increases which may lead to the explosion of the nucleus emitting a number of low energy particles. Most of the evaporated particles are usually protons, neutrons and α-particles. The average energy of the emitted particles is of the order of 10 MeV; their number and the energy distribution being dependent on the temperature of the nucleus.

The energy spectrum of the evaporated particles can be obtained from the statistical thermodynamics. The number of charged particles with energy E in a width dE is given by (Rossi 1956):

$$N(E)dE = \text{const.} \frac{E - V_c}{T^2} e^{-\frac{(E - V_c)}{T}} dE \qquad (6.1)$$

Table 6.1

Fraction of Evaporated Particle with Energy less than $(E-V_c)$

$E-V_c$ (MeV)	T (MeV)	Fraction with energy < $(E-V_c)$
30	3	1.000
30	5	0.995
30	6	0.979
25	3	1.000
25	5	0.988
25	6	0.973
20	3	0.999
20	5	0.971
20	6	0.931

where T and V_c are the temperature of the nucleus and the height of the coulomb barrier in energy units, respectively. $(E - V_c)$ is the energy which is observed outside the nucleus. For a high energy interaction, T is of the order of 3 to 5 MeV.

The fraction, N, of particles having energy up to E is then given by:

$$N = 1 - e^{\frac{-(E - V_c)}{T}} \left(1 + \frac{E - V_c}{T}\right) \qquad (6.2)$$

Using equation 6.2, the fractions of evaporated particles with energy less than $(E - V_c)$ have been calculated and are shown in table 6.1, for T = 3, 5, 6 and an average $V_c \sim 6$ MeV.

These results show that for typical values of V_c and T, more than 98 percent of the evaporated particles have energies less than 30 MeV. On this basis, a cut off value of 30 MeV was chosen and the protons with higher energies were considered as the primary nucleons coming out of the nucleus.

VI-3 Interaction of Pions Produced in Antiproton Annihilation

VI-3.1 Pions from Antiproton Annihilation Stars

Preliminary experiments were carried out with the pions which were produced inside the nucleus by the annihilations of antiprotons at rest. Due to the annihilation, pions are produced with a definite energy spectra, the characteristics of which have already been described in Chapter V (fig. 5.1, table 5.1). It was concluded that the charged pion multiplicity in emulsion stars was 20 percent less than the average multiplicity observed with free proton and neutron. Obviously these pions are absorbed inside the nucleus. Thus on the average 0.6 pions get absorbed before coming out of the nucleus. Hence two fast protons, coming out from some of these stars are expected to be from the absorption of a single pion inside the nucleus. The study of such protons is, therefore, equivalent to the study of protons coming out from the direct absorption of pions. It is possible, however, that the two fast protons are due to the absorption of two pions in the same nucleus, each emitting a proton and a neutron. This probability is small since the statistical probability of two pions being absorbed in the same nucleus is small. Moreover, as is shown below from the various modes of absorptions, the probability of emission of similarly charged particles are much higher compared to the neutron-proton pairs. The various absorption modes and their frequencies are:

$\pi^+ + p \rightarrow N^{*++}$	75%
$\pi^+ + n \rightarrow N^{*+}$	25%
$N^{*+} + p \rightarrow p + p$	12%
$N^{*+} + n \rightarrow n + p$	12%
$N^{*++} + n \rightarrow p + p$	75%
$\pi^- + n \rightarrow N^{*-}$	75%
$\pi^- + p \rightarrow N^*$	25%
$N^{*-} + p \rightarrow n + n$	75%
$N^* + p \rightarrow n + p$	12%
$N^* + n \rightarrow n + n$	12%

Thus in about 12 to 13 percent cases a proton-neutron pair is emitted. From this, together with the fact that only rarely more than one pion is absorbed in the same nucleus, it can be concluded that the fast proton pairs coming out in the $\bar{p}$-annihilation stars are in most cases due to one single pion absorption. In the following section the experimental study of these fast proton pairs are reported.

Table 6.2

Breakdown of the Data of $\bar{p}$ Annihilation Stars

	Plate No.	Area scanned	No. of stars	No. of pairs with $E_p > 30$ MeV
	88	4 cm x 1 cm	101	20
	89	4 cm x 1 cm	119	20
	90	2 cm x 1 cm	70	9
	91	4 cm x 1 cm	115	17
Total	4 pellicles	14 sq. cm	405	66

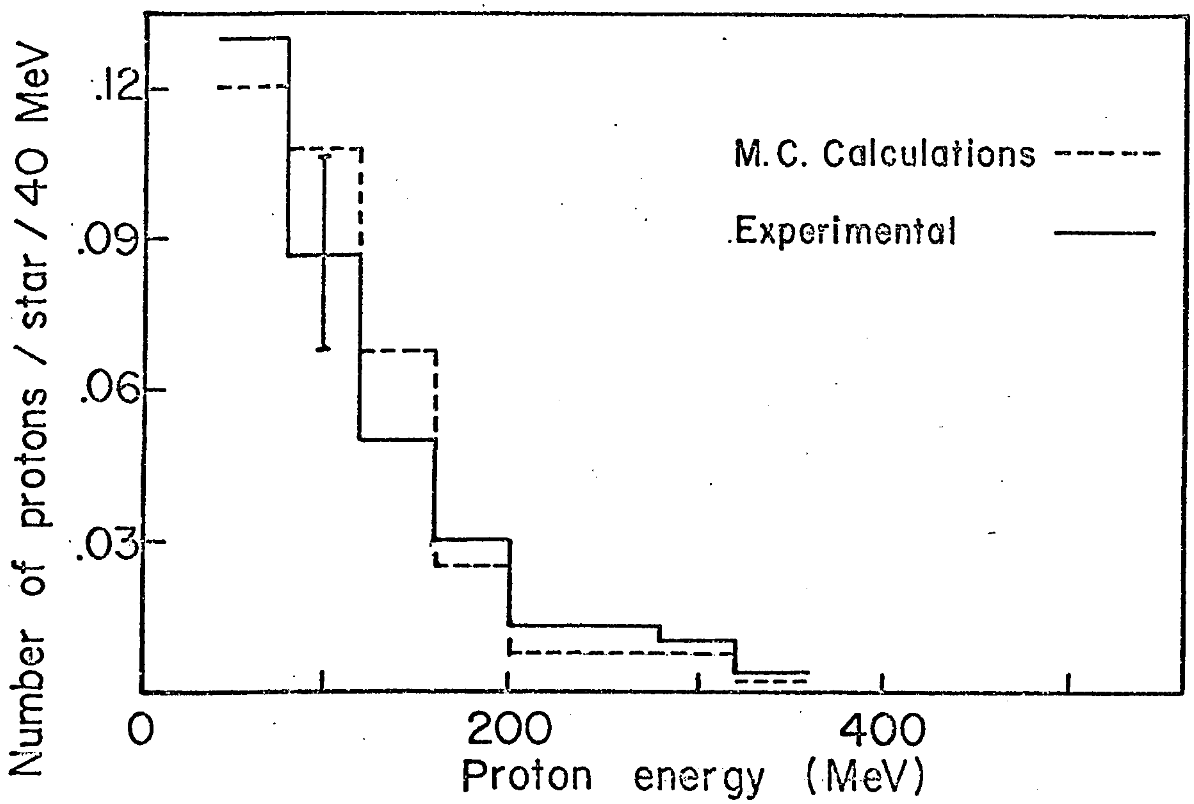

Fig. 6.1 Energy (lab) spectrum of the fast protons (Ep>30 MeV) produced in $\bar{p}$ annihilation.

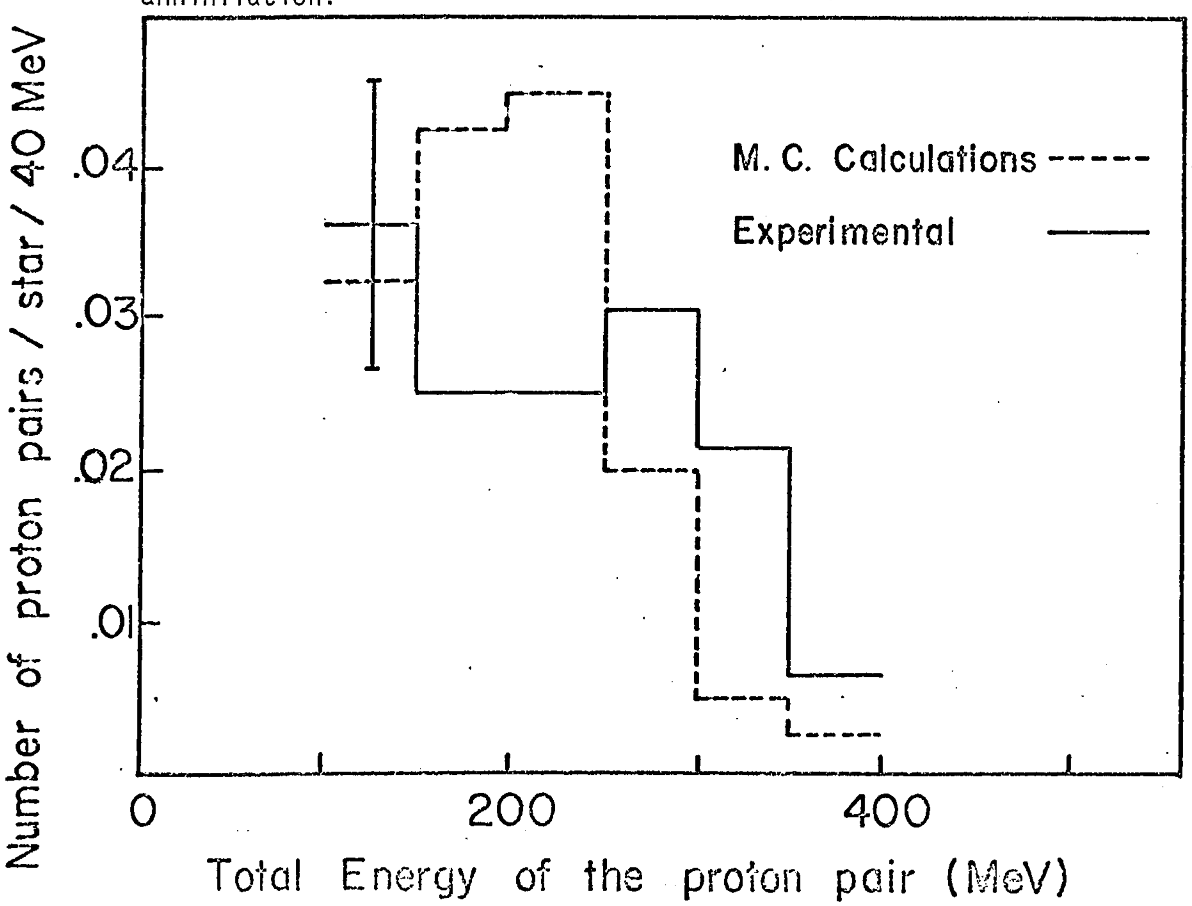

Fig. 6.2 Number of fast proton pairs produced in $\bar{p}$ annihilation stars versus total

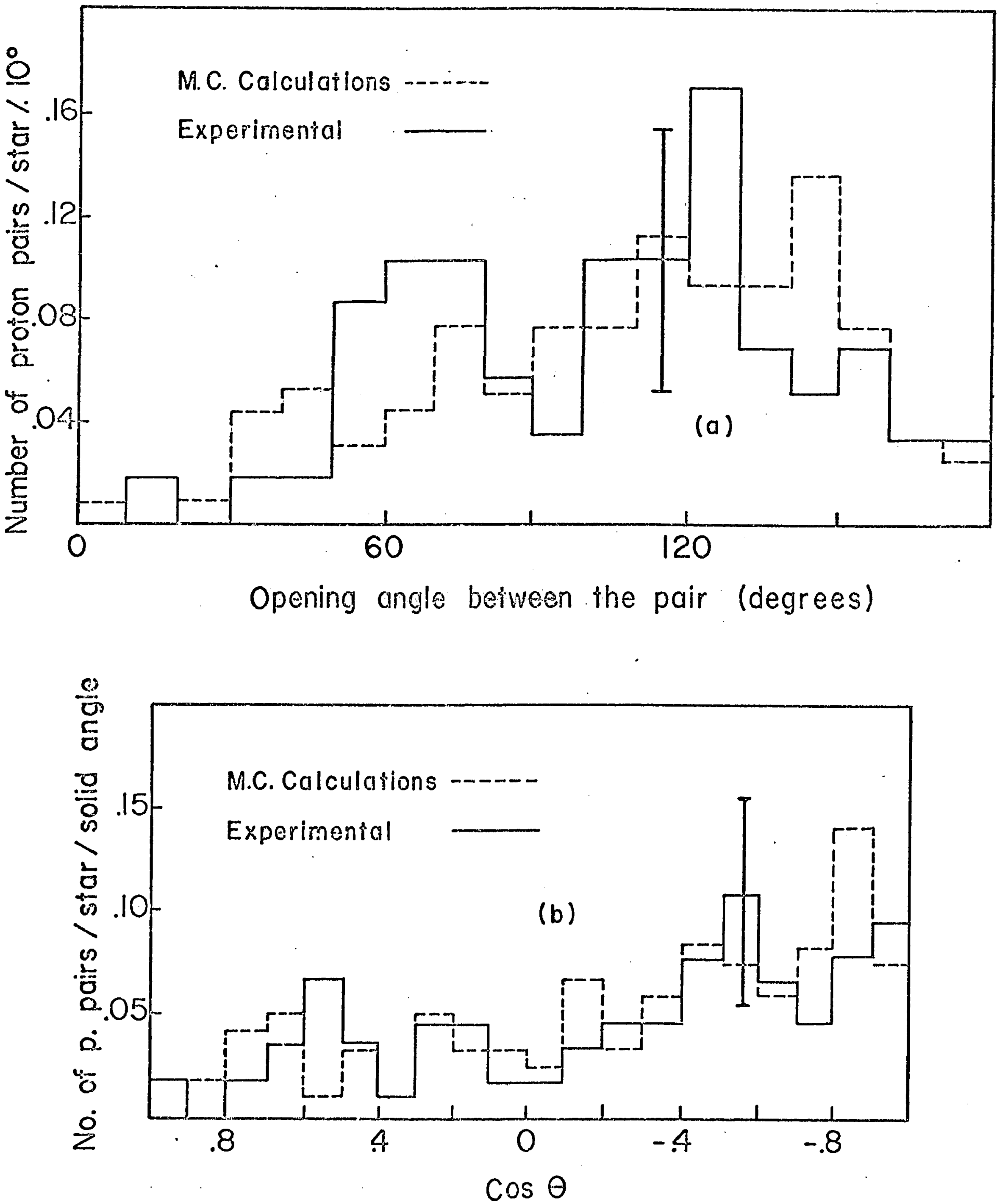

Fig. 6.3 Distribution of the fast proton pairs produced in $\bar{p}$ -annihilation stars as a function of their opening angles (lab): (a) θ (b) cos θ.

VI-3.2 Experimental

The experimental measurements were carried out in the emulsion stack which was irradiated with a beam of antiprotons. The details of the stack are given in section III-2.

405 $\bar{p}$-annihilation stars were obtained by scanning a total area of 14 sq. cm. in four pellicles: 88, 89, 90, 91. Of these 66 stars were found to have fast proton pairs. The breakdown of the data of the $\bar{p}$-annihilation stars are given in table 6.2.

The energies of these protons and the opening angles between the two nucleons were measured using the techniques explained in section III-4 and III-5. The experimental results are shown in the form of histograms by solid lines in figs. 6.1, 6.2, 6.3a and 6.3b.

Fig. 6.1: The distribution of the individual fast protons (in terms of the fraction of the total number of fast protons) as a function of the proton energy.

Fig. 6.2: The distribution of the fractional number of proton pairs as a function of the total energy of the pair.

Fig. 6.3: The distribution of the fractional number of pairs as a function of

(a) the opening angle θ (laboratory system) between the two protons.

(b) $\cos\theta$.

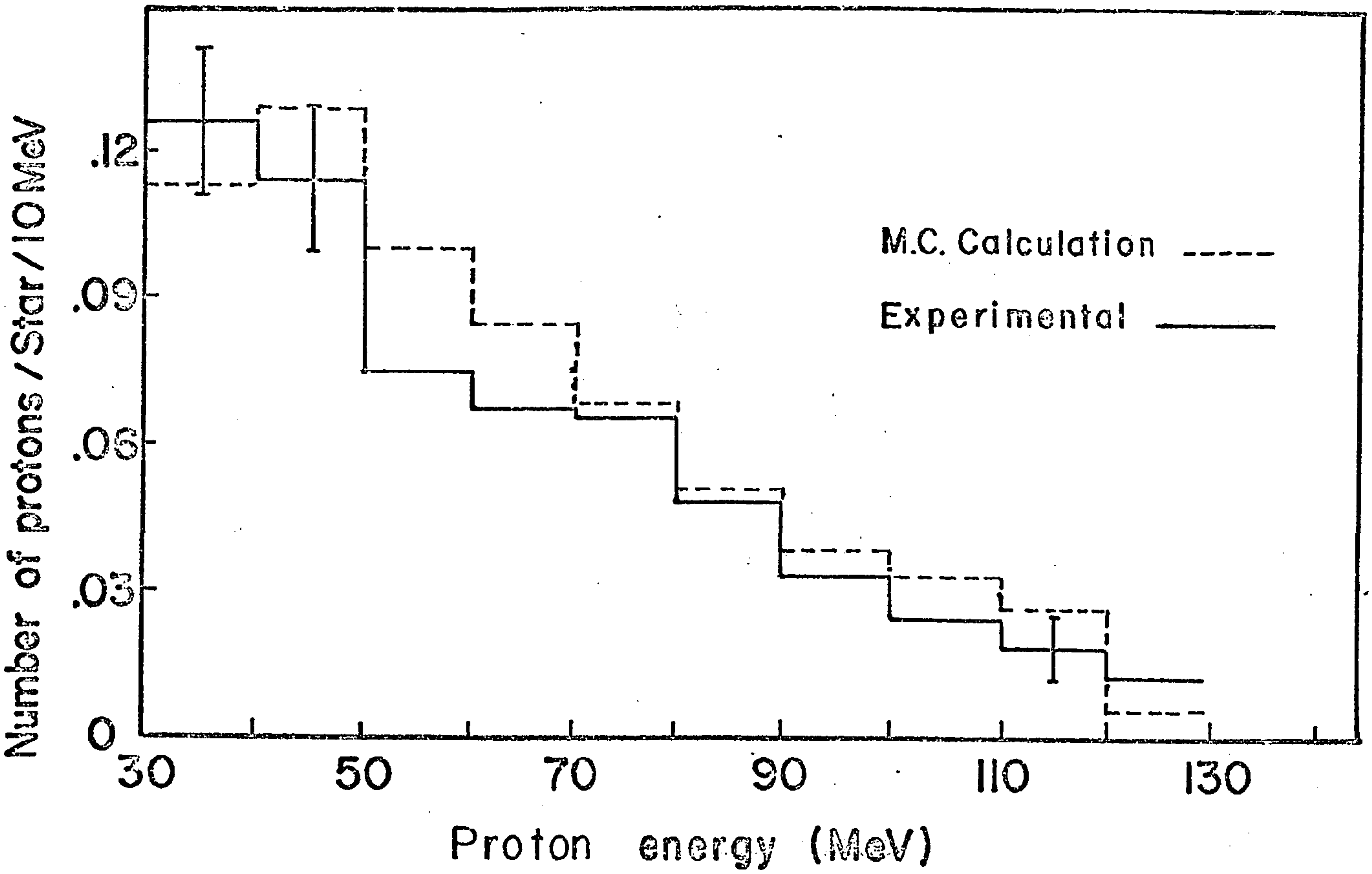

Fig. 6.4 Energy(laboratory) spectrum of the fast protons produced in positive pion absorption stars. ($E_{\pi^+} \sim (45 \pm 15)$ MeV)

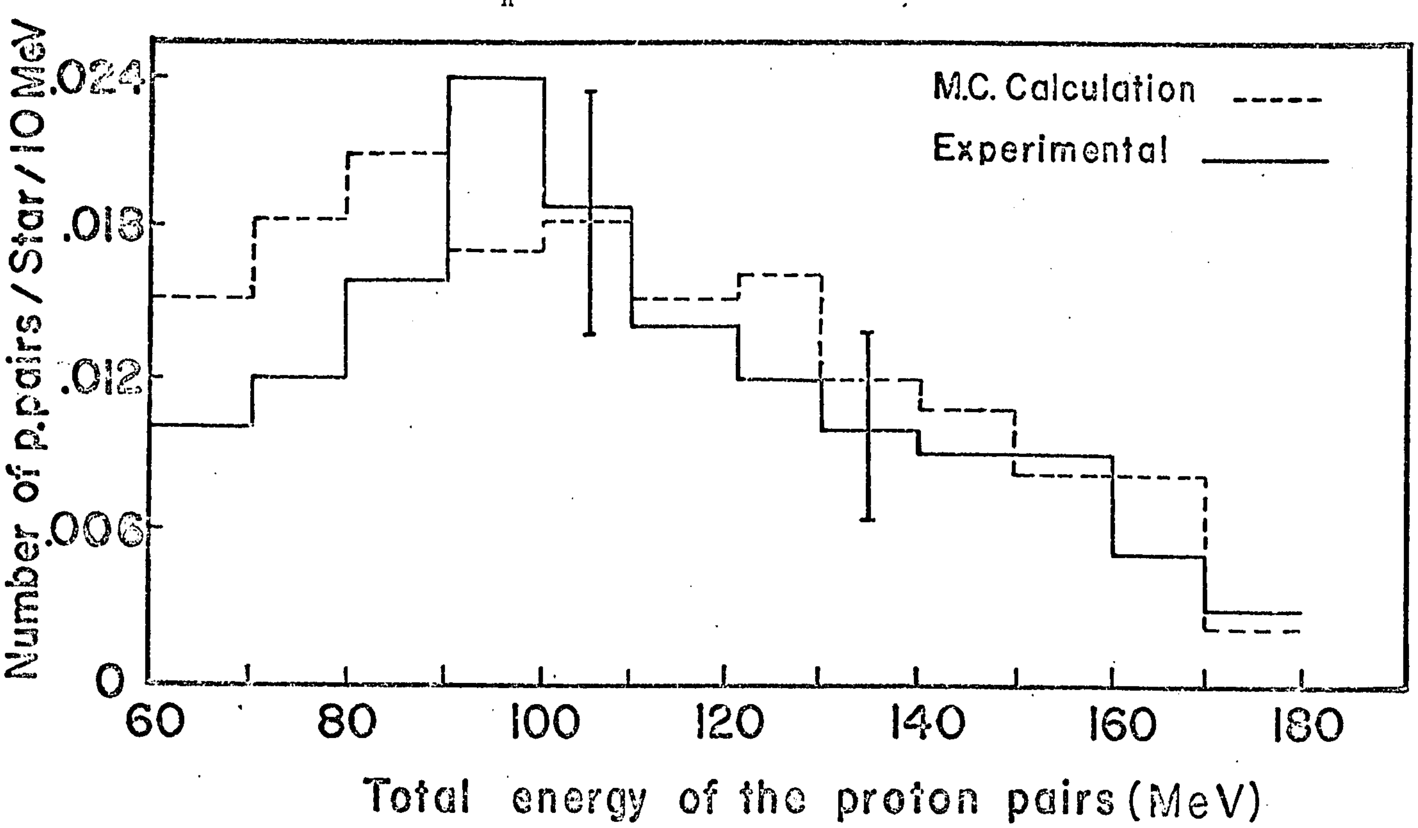

Fig. 6.5 Number of fast proton pairs produced in positive pion absorption stars versus the total kinetic energy (lab) of the pair. ($E_{\pi^+} \sim (45 \pm 15)$ MeV)

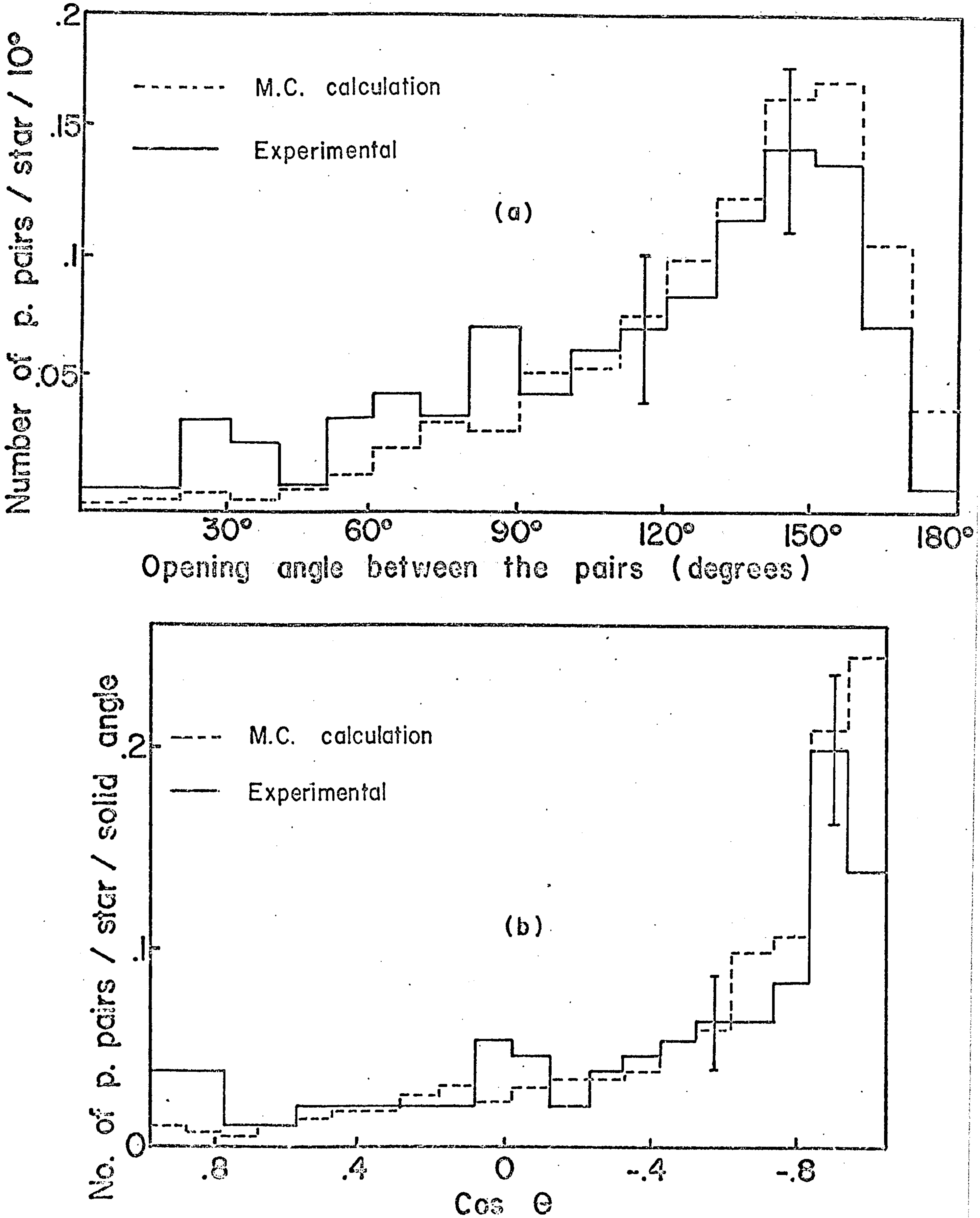

Fig.6.6- Distribution of the fast proton pairs produced in positive pion absorption stars (E ~45 MeV) as a function of their opening angles (lab):

VI-4 70 MeV Pion Induced Stars

In stack 2, 882 pion induced stars, in the energy range up to 60 MeV, were examined for fast protons with energy greater than 30 MeV. A total of 530 fast protons were found and 108 stars had fast proton pairs. Energies of these fast protons as well as the opening angles between the two protons of the pairs were measured. The experimental results are shown by solid lines in histograms 6.4, 6.5, 6.6a and 6.6b.

VI-5 Monte Carlo Calculations

VI-5.1 Monte Carlo Technique

The experimental results obtained in sections VI-3 and VI-4 have been interpreted by Monte Carlo calculations based on the isobar formation. The Monte Carlo method is essentially a technique in which a given physical process, having one or more random variables, is simulated in the same prescribed manner in which the process is expected to proceed. The process is completely determined by choosing random numbers associated with proper weighting factors determined by the physical process under consideration. The calculations are repeated many times with different random numbers and the results are statistically analysed. These results can then be compared with the experimental results. The scheme of the Monte Carlo calculation and the program used for pion interaction in the complex nuclei of emulsion is explained in the next section.

VI-5.2 Programme

The Monte Carlo calculation used is similar to that of Metropolis et al. (1958) and of Werbrouck (1964). In the calculation, the nucleus has been considered as a spherical potential well in which neutrons and protons form two Fermi gases. The characteristics of the Fermi gas, such as the nuclear potential and the Fermi level were taken from Metropolis et al.

In stack 2, the pions are the incident particles and the energy and the direction of the incident beam is known. This direction and the energy can be taken as the starting point in the programme. In case of $\bar{p}$ as incident particle, (Stack 1), the charges, energies and the directions of the produced pions are not uniquely known and have to be determined from the characteristics of the annihilation process. It is assumed that the $\bar{p}$ annihilation takes place on the surface of the nucleus and has equal probability of annihilating on any one of the nucleons. Once the direction and the energy of the pion is determined, the rest of the mechanism is identical to the former case.

The pions traversing the nucleus can interact with the nucleons to form an isobar which in turn can interact with another nucleon to get absorbed and emit two fast nucleons or may be de-excited to a pion and a nucleon. The emitted nucleons can set up a cascade. The scheme of the programme is as follows.

A) Initialization: The relevant cross sections, distributions and constants are read in and all counters are set.

B) Start: By means of random numbers, the incident energy, position, direction and charge of the pions are determined. This is necessary when pions are produced due to $\bar{p}$ annihilation. For monoenergetic incident pion, these quantities are known from the intial condition.

C). Penetration: From the input pion-nucleon cross section, the mean free path of the pion in the nuclear matter is calculated and by using a random number the distance of the collision is obtained. From the previous position, the direction of motion and the collision distance, the position of the collision is obtained. If the new position is inside the nucleus, the programme proceeds with the next step otherwise it continues at step H.

D) Collision: By using random numbers, the charge of the target nucleon, its momentum, direction and the type of interaction (i.e. charge exchange, absorption etc.) are determined. The calculations are done in the centre-of-mass (C.M.) system and the outgoing direction of the scattering particles is obtained by using another random number. The use of random number is described in section VI-5.3.

The outgoing direction and energy of the scattered and the target particles (in the laboratory system) are calculated using relativistic mechanics. The energies of the outgoing nucleons are tested to ensure that the Pauli exclusion principle is not violated.

The scheme of the kinematics used for the collision process is given below.

The energy, the direction and other characteristics of the interacting particles are known. In the laboratory frame, both the particles are moving but not generally along the same line or along any one of the axes. Thus to accomplish an easy calculation, it is necessary to perform a series of rotations and relativistic transformations. In the first rotation the target nucleon is made to move along the x-axis and is followed by a transformation of both the particles to the rest frame of the target nucleon. Under this condition, one of the particles is at rest while the other approaches from some general direction. Another rotation is performed, in the rest frame of the struck nucleon, to bring the incident particle along the x-axis. The particles are then transformed to the centre-of-mass system so that they approach each other with equal momenta and along the x-axis. The energy of each of the particles in the centre-of-mass system is calculated. After the collision, they move along directions determined by the random numbers and have equal and opposite momenta. Finally, the inverse transformations and rotations are applied to obtain the energy of the outgoing particles in the laboratory system. The various transformations are given in appendix 4 .

E) Struck particle: If the struck nucleon is sufficiently energetic after the collision, it is stored in the memory to be followed later.

F) Incident particle: The energy of the incident particle is tested to determine whether it is sufficiently energetic to be followed. If so, the programme proceeds with the step C, otherwise the particle is abandoned and the programme executes step G.

G) If there is any particle stored in the memory, its position, direction and other characteristics are taken as those for a new incident particle and the programme executes step C. If not, step H is performed.

H) The energies and directions of the outgoing particles are printed and a new event is started with step B.

At the end of the programme, when the required number of events have been simulated, the energy and the angular distribution of all the incident and the outgoing particles are printed.

A schematic flow chart of the program is shown in fig. 6.7.

VI-5.3 Random Number and its Use

From the foregoing discussions it is evident that most of the decisions are taken by using random numbers. The random numbers were generated by using the subroutine 'Randu' supplied by IBM. A multiplicative congruential method, having a period of 5×10^8 numbers, was used for generating the numbers. Once the random number is generated, it is necessary to use the number properly, very often with a proper weighting factor. The use of random numbers is illustrated by considering the step C and D.

In step D, the nature of the target nucleon is to be found from the given random number. From physical considerations, it may be known that the probability, or the weighting factor, of collision with a neutron is x. The probability of collision with a proton is, therefore, 1-x. If the random numbers are uniformly distributed between 0 and 1, then for a random number (R) less than x, the target particle is taken as a neutron. On the other hand, the target particle is taken as a proton if the random number is greater than x. If the operation is repeated many times, the ratio of the neutron to proton is expected to correspond, statistically, to the physical ratio.

The above procedure can be extended to the case of a multiple choice and for continuous probability functions. For a multiple choice, consider n possibilities having probabilities $x_1, \ldots x_n$. The i^{th} possibility would be chosen if the random number, R, lies between the sum of the probabilities up to $i-1^{th}$ and i^{th} possibility, i.e.; if

$$\sum_{j=1}^{i-1} x_j \leq R \sum_{j=1}^{n} x_j < \sum_{j=1}^{i} x_j \qquad (6.3)$$

The factor $\sum_{j=1}^{n} x_j$ is the total probability of choosing any one of the possibilities and is normalized to unity. The choice is repeated many times to obtain correct frequency.

For continuous probabilities, the probability x_j is replaced by a continuous function and the sum by integration: Thus if P(x)dx is the probability for a variable to have a value between x and x + dx, where dx is infinitesimal, then for a random number R the choice of the point x' is made from the equality:

$$R \int_{x_{min}}^{x_{max}} P(x)dx = \int_{x_{min}}^{x'} P(x)dx \qquad (6.4)$$

If the left hand integral is normalized to unity, then x' can be obtained by solving the right hand integral. This equation has been used to obtain the collision distance (penetration) in step C. If λ is the mean free path of interaction, then the probability of interaction within a distance 'ℓ' is given by

$$\int_0^{\ell} P(x)dx = 1 - e^{-\ell/\lambda} \tag{6.5}$$

since the total normalized probability of interaction is:

$$\int_0^{\infty} P(x)dx = 1 \tag{6.6}$$

we have, using 6.4, 6.5 and 6.6

$$1 - R = e^{-\ell/\lambda} \tag{6.7}$$

Since (1 - R) is also a random number between 0 and 1, it may be replaced by R, i.e.

$$R = e^{-\ell/\lambda} \tag{6.8}$$

$$\text{or } \ell = -\lambda \log_e R \tag{6.9}$$

Thus knowing R and λ, the distance of collision 'ℓ' can be chosen for a particular event.

TABLE 6.3

Energy Distribution of the Fast Protons (Energy $E_p > 30$ MeV) Produced in Pion Induced Stars

E_p (MeV)	Monte Carlo Calculations: Total number of stars = 2000 — No. of protons ($E_p > 30$ MeV)	fraction of stars with fast protons	Experimental: Total number of stars = 520 — No. of protons ($E_p > 30$ MeV)	fraction of stars with fast protons
31-40	230	0.115	65	.125
41-50	246	0.123	60	.115
51-60	200	0.100	39	.073
61-70	164	0.082	35	.068
71-80	134	0.067	34	.065
81-90	98	0.049	25	.048
91-100	78	0.039	17	.033
101-110	60	0.030	12	.023
111-120	54	0.027	9	.017
121-130	16	0.008	6	.012
131-140	14	0.007	7	.013

Table 6.4

Energy Distribution of the Fast Proton Pairs Produced in Pion Induced Stars

$E_{p1} + E_{p2}$ (MeV)	Monte Carlo calculation Total number of stars=N=2000 Number of stars with fast proton pairs=n=340 No. of stars having fast pairs=Δn	fraction $\Delta n/N$	Experimental Total number of stars=N=750 n=109 Δn	$\Delta n/N$
61 - 70	30	0.015	8	0.010
71 - 80	37	0.018	9	0.012
81 - 90	42	0.021	12	0.016
91 - 100	35	0.017	18	0.024
101- 110	37	0.018	14	0.019
111- 120	30	0.015	10	0.013
121- 130	32	0.016	9	0.012
131- 140	25	0.012	8	0.011
141- 150	23	0.011	7	0.009
151- 160	17	0.008	7	0.009
161- 170	16	0.008	4	0.005
171- 180	4	0.002	3	0.003

TABLE 6.5

Opening Angles of the Fast Proton Pairs Produced in Pion Induced Stars

Opening angle	Monte Carlo Calculations Total number of stars = 2000 No. of stars with fast proton pairs=n=340		Experimental: Total number of stars = N = 750 No. of stars with fast proton pairs=n=108	
	No. of stars having fast pairs = Δn	Fraction: $\Delta n/n$	Δn	$\Delta n/n$
$0^{\circ}-10^{\circ}$	0	-	1	0.0092
$11^{\circ}-20^{\circ}$	1	0.0029	1	0.0092
$21^{\circ}-30^{\circ}$	2	0.0058	4	0.0370
$31^{\circ}-40^{\circ}$	1	0.0029	3	0.0277
$41^{\circ}-50^{\circ}$	2	0.0058	1	0.0092
$51^{\circ}-60^{\circ}$	4	0.0117	4	0.0370
$61^{\circ}-70^{\circ}$	8	0.0234	5	0.0462
$71^{\circ}-80^{\circ}$	12	0.0352	4	0.0370
$81^{\circ}-90^{\circ}$	10	0.0294	8	0.0740
$91^{\circ}-100^{\circ}$	18	0.0529	5	0.0462
$101^{\circ}-110^{\circ}$	18	0.0529	7	0.0648
$111^{\circ}-120^{\circ}$	25	0.0735	8	0.0740
$121^{\circ}-130^{\circ}$	33	0.0970	9	0.0833
$131^{\circ}-140^{\circ}$	42	0.1235	12	0.1111
$141^{\circ}-150^{\circ}$	55	0.1617	15	0.1388
$151^{\circ}-160^{\circ}$	57	0.1676	14	0.1296
$161^{\circ}-170^{\circ}$	36	0.1058	6	0.0555
$171^{\circ}-180^{\circ}$	16	0.0470	1	0.0092

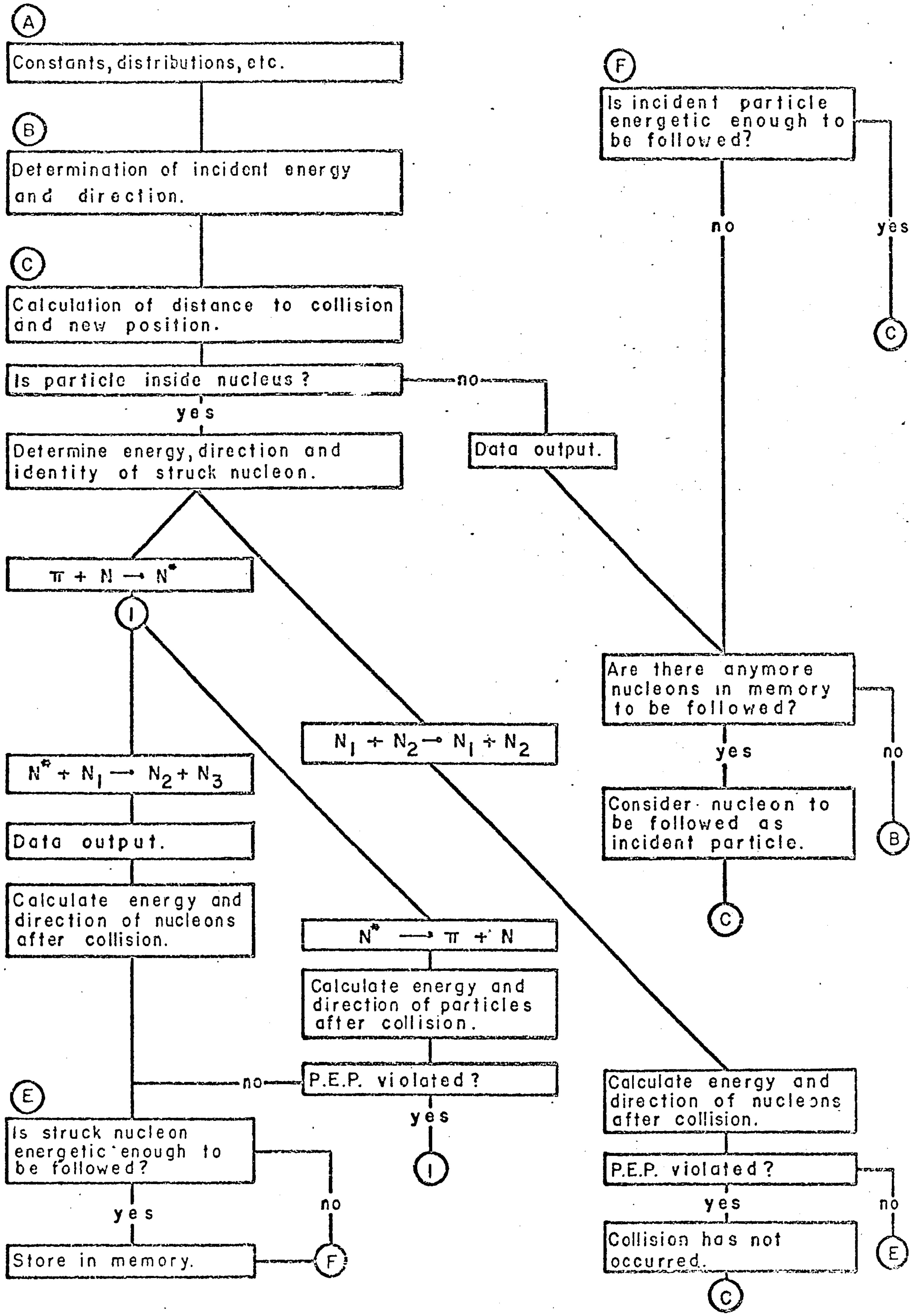
A
Constants, distributions, etc.
B
Determination of incident energy and direction.
C
Calculation of distance to collision and new position.
Is particle inside nucleus?
no
yes
Data output.
Determine energy, direction and identity of struck nucleon.
$\pi + N \rightarrow N^*$
I
$N_1 + N_2 \rightarrow N_1 + N_2$
$N^* + N_1 \rightarrow N_2 + N_3$
Data output.
Calculate energy and direction of nucleons after collision.
$N^* \rightarrow \pi + N$
Calculate energy and direction of particles after collision.
P.E.P. violated?
no
yes
I
E
Is struck nucleon energetic enough to be followed?
yes
no
Store in memory.
F
F
Is incident particle energetic enough to be followed?
no
yes
C
Are there anymore nucleons in memory to be followed?
yes
no
Consider nucleon to be followed as incident particle.
B
C
Calculate energy and direction of nucleons after collision.
P.E.P. violated?
yes
no
Collision has not occurred.
E
C

VI-6 Results and Discussions

The output of the program contained a listing of the energy and direction of the outgoing particles. From this, suitable statistical distributions of the energy and opening angles of the fast pairs were obtained.

For the antiproton annihilation, 2000 events were calculated and the results are shown by dotted lines along with the experimental results in fig. 6.1, 6.2, 6.3a and 6.3b. A general agreement is obtained, although nothing definitely can be concluded due to the poor statistics of the experimental results.

With the pion induced stars, the experimental results consist of events produced by pions with a maximum energy of 60 MeV. Most of the stars, however, were with pions having energy more than 30 MeV. The Monte-Carlo calculations were, therefore, performed for 2000 monoenergetic pions with energies 30, 50 and 60 MeV and was properly averaged over for obtaining the distributions. The results obtained from the Monte Carlo calculations are summarized in tables 6.3, 6.4 and 6.5 and are shown by dotted histograms in figs. 6.4, 6.5, 6.6a and 6.6b and are compared with the corresponding experimental results shown by solid histograms.

It is observed that there is a very good agreement between the experimental and the Monte Carlo results. From the single proton spectrum (figs. 6.1 and 6.4) it is seen that the number of protons having energies greater than 80 MeV falls rapidly and have a flat spectrum from about 50 to 80 MeV. This is what is expected if the pion rest mass (140 MeV) is divided more or less equally between the two interacting nucleons. In the energy spectrum of the proton pairs, the total kinetic energy of the pairs predominently lies between 80 to 130 MeV and is close to the rest mass of the pion.

The agreement for the distribution of the opening angles is also fairly good (fig. 6.6). The experimental and the Monte Carlo results (fig. 6.6a), both show a peaking between 140° and 160°.

Chapter VII

CONCLUSION

It is found that the isobar model of pion interaction is quite successful in explaining the interaction of pions with complex nuclei. The advantage of this model is due to the fact that only well known pion-nucleon interaction cross section is necessary to explain the pion-nucleus cross section. This model avoids the use of any uncertain nuclear correlation factor as was used by Bernardini and Levy (1951) in the interpretation of their pion interaction results with complex nuclei.

It has been seen (Chapter IV) that the isobar model reproduces very well the experimentally measured cross section of positive pion interaction with complex nuclei in the entire (3,3) resonance energy region. The results tend to favour a value of $r_o = 1.4F$ and show the presence of the pion-nuclear potential. Due to the presence of the nuclear potential, the peak in the pion-nucleus interaction cross section occurs at a lower energy than the (3,3) resonance energy. This is indicated by a considerably higher cross section at 168 MeV. Similar results are also obtained (reference Chapter V) in the study of the fraction of pions absorbed (where pions are produced inside the nucleus) inside the nucleus in antiproton annihilation. Maximum absorption occurs at about 160 MeV. Also the observed absorption fraction agrees satisfactorily with the isobar model calculations. The experimental distribution (Chapter VI) of the opening angles between the two fast nucleons produced in the π^+ absorption is also well reproduced by the Monte Carlo calculations based on isobar model. In both cases a peaking around 150^o is observed.

According to the isobar model, the interaction of negative pions with complex nuclei is expected to be similar and, hence can be treated similarly. The interaction cross section can be obtained by changing the sign of the coulomb barrier in equation (4.2). Thus the π^--nucleus cross section is expected to be larger than the corresponding π^+-nucleus results. This was observed by Bernardini in his work with 35 and 70 MeV pions. At higher energies, however, the difference between the two is expected to be negligible. A systematic measurement of the cross section of interaction of negative pion with the emulsion nuclei will, therefore, be very useful for further verification of our model. A comparison between the two results may also be very useful. It will also be worthwhile to carry out similar experiments in the entire (3,3) resonance energy range with positive and negative pions on given complex nuclei like lead or aluminum. The analysis of stars produced with a given type of nuclei is much easier and more reliable than the analysis of the results with emulsion or freon where more than one types of nuclei are involved.

Appendix 1 Some Expressions Used in Chapter II

(a) Properties of Projection Operator

The important properties of projection operators used in Chapter II are:

$$P_\alpha^2 = P_\alpha \; ; \quad P_\alpha P_\beta = 0 \text{ for } \alpha \neq \beta \qquad \text{A.1.1}$$

Similar relations hold good for the isospin and spin components of the projection operator.

(b) Derivation of Equation 2.29

The L.H.S. of the equation 2.29

$$= \sum_{t_n} \Gamma_{3/2} (\vec{p},\vec{n}) \, \Gamma_{3/2} (\vec{n},\vec{q})$$

$$= \sum_{t_n} (\delta_{pn} - \tfrac{1}{3} t_n t_p) (\delta_{nq} - \tfrac{1}{3} t_p t_n)$$

$$= \sum_{t_n} (\delta_{pn} - \tfrac{1}{3} t_n t_p)\delta_{nq} - \sum_{t_n} (\delta_{pn} - \tfrac{1}{3} t_n t_p) (\tfrac{1}{3} t_q t_n)$$

$$= (\delta_{pq} - \tfrac{1}{3} t_q t_p) - \sum_{t_n} (\delta_{pn} - \tfrac{1}{3} t_n t_p) (\tfrac{1}{3} t_q t_n)$$

$$= (\delta_{pq} - \tfrac{1}{3} t_q t_p) - \sum_{t_n} \Gamma_{3/2} (p,n) \, \Gamma_{\frac{1}{2}} (n,q)$$

$$= \Gamma_{3/2} (p,q) \quad [\because \Gamma_{3/2} \Gamma_{\frac{1}{2}} = 0]$$

(c) Angle Between Two Vectors

The addition theorem for spherical harmonics is given by:

$$P_\ell(\cos \theta_{pn}) = \frac{4\pi}{2\ell + 1} \sum_{m=-\ell}^{\ell} Y_\ell^m (\theta_p, \varphi_p) \, Y_\ell^{m*} (\theta_n, \varphi_n)$$

where P_ℓ is the Legendre function and Y_ℓ^m is the spherical harmonics of degree ℓ. The angles are defined in fig. 2.1. For $\ell=1$

$$P_1(\cos \theta_{pn}) = \frac{4\pi}{3} \sum_{m=-1}^{1} Y_1^m (\theta_p, \varphi_p) \, Y_1^{m*} (\theta_n, \varphi_n)$$

But

$$P_1(x) = x$$

Hence $$\cos \theta_{pn} = \frac{4\pi}{3} \sum_{m=-1}^{1} Y_1^m (\theta_p, \varphi_p) \, Y_1^{m*} (\theta_n, \varphi_n) \quad \text{A.1.2}$$

using the following values of Y_ℓ^m:

$$Y_1^1 (\theta, \varphi) = -\sqrt{\frac{3}{8\pi}} \sin \theta \, e^{i\varphi}$$

$$Y_1^0 (\theta, \varphi) = \sqrt{\frac{3}{4\pi}} \cos\theta$$

$$Y_1^{-1} (\theta, \varphi) = (-1)^1 [Y_1^1 (\theta)]^* = \sqrt{\frac{3}{8\pi}} \sin\theta\, e^{-i\varphi}$$

we obtain from A.1.2

$$\cos\theta_{pn} = \cos\theta_p \cos\theta_n + \sin\theta_p \sin\theta_n \cos(\varphi_p - \varphi_n) \qquad \text{A.1.3}$$

This relation has been used in equation 2.31a and is also the same as relation 3.6.

Appendix 2 Absorption Fraction of Pions in $\bar{p}$ Annihilation

The following assumptions are made in the $\bar{p}$ annihilation:

(1) $\bar{p}$ annihilates on the surface of the nucleus

(2) Nucleus is spherical

(3) Isotropic angular distribution for the pions produced.

Let an antiproton annihilate at the point I on the surface of the nucleus. Since the pions produced have isotropic distribution, only the pions in the upper half plane will enter the nucleus. Hence the absorption fraction:

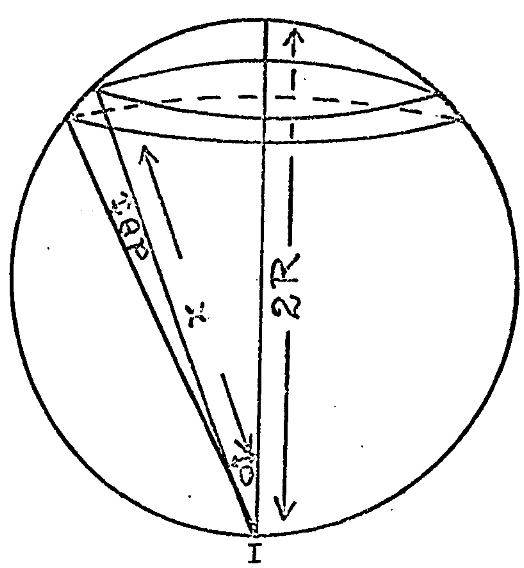

Fig. A.1 Geometry used in calculating the pion absorption fraction.

$$f = \frac{1}{2} \int (1 - e^{-Kx})\, d(\cos\theta)$$

where K = interaction co-efficient = $\frac{3A\bar{\sigma}}{4\pi R^3}$, R = nuclear radius and x = distance traversed by pion.

$$f = \frac{1}{2} \int_0^{2R} (1 - e^{-Kx}) \frac{dx}{2R} \qquad [\ \cos\theta = \frac{x}{2R}\ ]$$

$$= \frac{1}{4R}\left[x + \frac{1}{K} e^{-Kx}\right]_0^{2R}$$

$$= \frac{1}{2}\left[1 - \frac{1}{2KR}(1 - e^{-2KR})\right]$$

Appendix 3 Sample Programme

In this appendix a copy of the Monte Carlo programme, used in Chapter VI, is shown. The last page shows a sample of the output data.

The following are the important conventions used in the programme:

1) All symbols starting or ending in X, Y, Z refer to space positions or directions.

2) Symbols starting in T, E or W refer to kinetic energy in MeV, momentum in MeV/c and mass in MeV/c^2; respectively.

3) Symbols starting with NUCL refer to pions if their value is negative, neutrons if there value is zero and protons if their value is positive.

4) Symbols with SEC or SIG refer to cross sections measured in millibarns.

5) Symbols ending in CHAR refer to the charge of the pion.

6) In the subroutine CMSLOB, symbols starting with U refer to total energy in MeV and symbols starting with P refer to a component of momentum measured in MeV/c.

7) RZERO refers to the radius parameter r_o.

8) RANDU is the subroutine for generating random numbers.

```
//GDS2036 JOB  SJSCC029,'S.C.CHAKRAVARTTY   ',PRTY=08,MSGLEVEL=1,
//               CLASS=A              STANDARD RUN
//FORTRAN EXEC PROC=FORTFCLG,REGION=100K
XXFORT   EXEC  PGM=IEYFORT,REGION=100K,PARM=BCD                          00020000
XXSYSPRINT   DD   SYSOUT=A,DCB=(RECFM=FBA,BLKSIZE=1320,LRECL=120)        00040000
XXSYSLIN    DD   DSNAME=&LOADSET,DISP=(MOD,PASS),UNIT=SYSSQ,            X00080000
XX               SPACE=(400,(40,20),RLSE),                              *00100014
XX               DCB=(RECFM=FB,BLKSIZE=400,LRECL=80)                     00100020
//FORT.SYSIN DD *                                     SOURCE DECK NEXT
IEF236I ALLOC. FOR GDS2036  FORT      FORTRAN
IEF237I SYSPRINT ON 137
IEF237I SYSLIN    ON 136
IEF237I SYSIN     ON 136
```

```
      C BEGIN
      C*****DIMENSIONS,COMMON,ARITHMETHIC FUNCTIONS AND CONSTANTS
            DIMENSION XSTORE(20),YSTORE(20),ZSTORE(20),ESTORE(20),CAPX(20)
            DIMENSION CAPY(20),CAPZ(20)
            DIMENSION  NUCLST(20)
            DIMENSION  TINT(21)
            DIMENSION SECII(11),SECIJ(9)
            DIMENSION NPIIN(21,100),NPIOUT(21,100),NNOUT(21,100)
            DIMENSION  NSUM(21)
            COMMON W1C2,W2C2,BETA,GAMMA,RN
            COMMON  WAFT
            TTOE(T,W)=(T*T+2.*W*T)**.5
            ETOT(E,W)=(E*E+W*W)**.5-W
            PI=3.141593
            RZERO=1.4
             IPAGE=0
      C*****READ DATA
      C READ 1
            READ (1,13) TINT
         13 FORMAT (7(F6.1,2X))
            READ (1,3)SECII
          3 FORMAT (11(F6.1,1X))
            READ (1,11) SECIJ
         11 FORMAT (9(F6.1,1X))
            READ (1,1) W1,W2,W3
          1 FORMAT (3(E10.3,2X))
            READ (1,17) KCHAR
         17 FORMAT (I2)
      C READ 2
        100 READ (1,2) IRN,IN
          2 FORMAT (I10,I6)
            IF(IRN)1191,118,119
        118 IRN=JRN
        119 CONTINUE
            READ(1,3)TINIT
            READ (1,6) TCOUL,TMIN,TPAULP,TPAULN,AA,AN,AP
          6 FORMAT (4(E10.3,2X),3(F4.0,2X))
            WRITE (3,20)
         20 FORMAT('* P MASS * N MASS*PION MASS*   A    *    N     *    Z     *COUL
           1. E.*MIN. E. *PAULI P *PAULI N *RANDOM NO*NO OF PART.*INC. CHAR.*'
           2)
            WRITE (3,19)W1,W2,W3,AA,AN,AP,TCOUL,TMIN,TPAULP,TPAULN,IRN,IN,
           1KCHAR
```

```
0036          19  FORMAT (1H0,10F9.2,3I10)
           C*****SET CONSTANTS FROM DATA
0037              ISKIP=50
0038              W2C2=W2
0039              EMINPI=TTOE(TMIN,W3)
0040              EMIN=TTOE(TMIN,W1)
0041              EPAULP=TTOE(TPAULP,W1)
0042              EPAULN=TTOE(TPAULN,W2)
           C*****SET INITIAL CONDITIONS
0043              DO 43 I=1,21
0044              DO 43 J=1,100
0045              NPIOUT(I,J)=0
0046              NPIIN(I,J)=0
0047          43  NNOUT(I,J)=0
0048              DO 40 L=1,IN
0049              TOTEN=0.0
0050         103  IF(ISKIP-40) 301,302,302
0051         302  WRITE (3,303)
0052         303  FORMAT(98H1*PART.* INC  *INC. PION* OUT  *OUT  PION* ISOBAR  *  IS
                 1OBAR  * PROTON  * NEUTRON * NO *   OUT   */1H ,97H*  NO *CHARGE*
                 2ENERGY *CHARGE*  ENERGY *MASS%MEV<* PC %MEV< *  ENERGY *  ENERGY *
                 3COL.*DIRECTION*)
0053              IPAGE=IPAGE+1
0054              WRITE (3,304) IPAGE
0055         304  FORMAT(T120,'PAGE  ',I4)
0056              ISKIP=0
           C START
0057         301  ICOL=0
0058              NO=0
0059              TINI =TINIT-TCOUL+TMIN
0060              EINIT=TTOE(TINI ,W3)
0061              E=EINIT
0062              W1C2=W3
0063              WAFT=W1C2
0064              NUCL=-1
0065              ICHAR=KCHAR
0066              I=1
0067              K=1
           C
           C      SELECT IMPACT POSITION
0068              XDIR=0.
0069              YDIR=0.
0070              ZDIR=-1.
```

```
  400 CALL RANDU(IRN,JRN,RN)
       IRN=JRN
      XPOS=1.-2.*RN
      CALL RANDU(IRN,JRN,RN)
       IRN=JRN
      YPOS=1.-2.*RN
      ZPOS=1.-XPOS*XPOS-YPOS*YPOS
      IF (ZPOS) 400,401,401
  401 ZPOS=ZPOS**.5
C*****FOLLOW PARTICLE TILL IT STRIKES AND FIND NEW CONDITIONS
C FOLLOW
      INT=.1*TINIT+1.
      IMT=10.*(ZDIR+1.)+1.
      NPIIN(IMT,INT)=NPIIN(IMT,INT)+1
C
C PION OR NUCLEON
  116 IF (NUCL) 28,106,106
C     CALCULATE X-SECTION FOR PIONS
   28 T=ETOT(E,W3)
      IF (T-720.) 130,131,131
  131 SIGIJ=50.
      GO TO 132
  130 INT=T/90.+1.
      AINT=INT-1
      SIGIJ=SECIJ(INT)+((T-AINT*90.)/90.)*(SECIJ(INT+1)-SECIJ(INT))
  132 IF (T-580.) 133,134,134
  134 SIGII=20.
      GO TO 135
  133 INT=T/58.+1.
      AINT=INT-1
      SIGII=SECII(INT)+((T-AINT*58.)/58.)*(SECII(INT+1)-SECII(INT))
  135 IF (ICHAR) 136,137,138
  136 PS=AP*SIGIJ
      SN=AN*SIGII
      GO TO 38
  137 PS=AP*(SIGII+SIGIJ)*.5
      SN=AN*(SIGII+SIGIJ)*.5
      GO TO 38
  138 PS=AP*SIGII
      SN=AN*SIGIJ
      GO TO 38
C     CALCULATE X-SECTION FOR NUCLEONS
  106 ESQ=E*E
```

```
0108            BETSQ=ESQ/(ESQ+WI*WI)
0109            BET=BETSQ**.5
0110            SIGII=(10.63-29.92*BET+42.9*BETSQ)/BETSQ
0111            SIGIJ=(34.10-82.2*BET+82.2*BETSQ)/BETSQ
0112            IF (NUCL) 34,34,33
0113         33 PS=AP*SIGII
0114            SN=AN*SIGIJ
0115            GO TO 38
0116         34 PS=AP*SIGIJ
0117            SN=AN*SIGII
0118         38 SIGMA=(PS+SN)/AA
0119        37  AMBDA=41.888*RZERO*RZERO/(SIGMA*AA**.3333333)
0120            PROBP=PS/(PS+SN)
0121       101  CALL RANDU(IRN,JRN,RN)
0122             IRN=JRN
          C     DETERMINE IF COLLISION IS WITH A PROTON OR A NEUTRON
0123            IF (PROBP-RN) 36,35,35
0124         35 NUCL2=1
0125            GO TO 102
0126         36 NUCL2=0
0127       102  CALL RANDU(IRN,JRN,RN)
0128             IRN=JRN
          C     NOW CALCULATE THE PENETRATION
0129            DIST=-AMBDA*ALOG(RN)
          C PION OR NUCLEON
0130            IF (NUCL) 320,321,321
0131        320 IF (E-EMINPI) 322,321,321
0132        322 DIST=0.
          C     CALCULATE THE NEW POSITION
0133        321 XPOS=XPOS+XDIR*DIST
0134            YPOS=YPOS+YDIR*DIST
0135            ZPOS=ZPOS+ZDIR*DIST
          C
          C     CHECK IF STILL INSIDE THE NUCLEUS
0136            Q=XPOS*XPOS+YPOS*YPOS+ZPOS*ZPOS
0137            IF(1.0000001-Q)  21,152,152
          C GO TO OUTPUT 1 IF OUTSIDE OF NUCLEUS
          C
          C PION OR NUCLEON
          C     DECIDE IF CHARGE EXCHANGE OCCURS
0138        152 IF (NUCL) 140,22,22
0139       140  CALL RANDU(IRN,JRN,RN)
0140             IRN=JRN
```

```
0141            RNG=RN-.3333333
0142            NN=ICHAR+NUCL2
0143            NNU=NN+2
0144            GO TO (22,144,146,22),NNU
0145        144 IF(RNG) 145,147,147
0146        145 ICHAR=-1
0147            GO TO 154
0148        147 ICHAR=0
0149            GO TO 154
0150        146 IF(RNG) 148,147,147
0151        148 ICHAR=+1
0152        154 NUCL2=NN-ICHAR
          C
          C     SELECT ANGLES IN CM
0153         22 CALL RANDU(IRN,JRN,RN)
0154             IRN=JRN
0155            QDIR=1.-2.*RN
0156            CALL RANDU(IRN,JRN,RN)
0157             IRN=JRN
0158            PHICM=2.*PI*RN
0159        171 ICOL=ICOL+1
0160            X1=XDIR
0161            Y1=YDIR
0162            Z1=ZDIR
0163            E1=E
          C
          C     FIND THE ENERGY AND DIRECTION OF STRUCK NUCLEON
0164            IF (NUCL2) 123,123,122
0165        122 EPAULI=EPAULP
0166            GO TO 124
0167        123 EPAULI=EPAULN
0168       124  CALL RANDU(IRN,JRN,RN)
0169             IRN=JRN
0170            EFERMI=EPAULI*RN**.3333333
0171            CALL RANDU(IRN,JRN,RN)
0172             IRN=JRN
0173            ZRST=1.-2.*RN
0174            QRST=SOMXSB(ZRST)
0175            CALL RANDU(IRN,JRN,RN)
0176             IRN=JRN
0177            TETA=2.*PI*RN
0178            XIQ=COS(TETA)
0179            YIQ=SIN(TETA)
```

```
          IF (W2C2) 169,169,170
      C
      C   NOW FIND THE ENERGY AND DIRECTION IN LAB SYSTEM
    190   CALL RANDU(IRN,JRN,RN)
           IRN=JRN
          QDIR=1.-2.*RN
          CALL RANDU(IRN,JRN,RN)
           IRN=JRN
          PHICM=2.*PI*RN
          NO=NO+1
          IF (50-NO) 162,170,170
      C PION OR NUCLEON
    170   IF (NUCL) 160,161,161
    160   CALL RANDU(IRN,JRN,RN)
           IRN=JRN
      C   CALCULATE THE ABSORPTION FRACTION  %ABFRCT<
           ABFRCT=1./EXP(T/200.)
      C   DETERMINE IF PION IS ABSORBED OR IF ISOBAR DECAYS
    308   IF (RN-ABFRCT) 162,161,161
      C   PION ABSORBED
    162   CALL RANDU(IRN,JRN,RN)
           IRN=JRN
      C   DETERMINE IF THIRD PARTICLE IS A PROTON OR A NEUTRON
          IF (RN-AP/AA) 163,164,164
    163   NNO=NN+3
          GO TO 173
    164   NNO=NN+2
    173   GO TO (160,165,166,166,160),NNO
    165   NUCL2=0
          GO TO 168
    166   NUCL2=1
    168   CALL LBRSTB (QRST,XIQ,YIQ,ZRST,EFERMI,X1,Y1,Z1,E1)
          NUCL3=NNO-NUCL2-2
      C   CALCULATE THE MASS AND THE VELOCITY OF THE ISOBAR
          UPRIM=W2C2+SSTSQB(E1,W1C2)
          BCM1=E1/UPRIM
          W4=(UPRIM-BCM1*E1)/SOMXSB(BCM1)
          W1C2=W4
          W2C2=0.
          CALL RSTLAB (QRST,XIQ,YIQ,ZRST,X1,Y1,Z1,E1)
      C OUTPUT 2
          WRITE (3,4) L,KCHAR,TINIT,NN,W4,E1,ICOL
      4   FORMAT(1H0,2X,I4,3X,I2,3X,F9.2,2X,1H*,I2,13X,F9.2,1X,F10.2,21X,I3)
```

```
          ISKIP=ISKIP+2
          ICOL=0
          IF (NUCL3) 123,123,122
      169 CONTINUE
      172 W2C2=W2
C         CALCULATE THE ENERGY AND DIRECTION OF THE OUTCOMING NUCLEONS
          CALL LBRSTB (QRST,XIQ,YIQ,ZRST,EFERMI,X1,Y1,Z1,E1)
          WAFT=W2C2
          CALL CMSLOB (X1,Y1,Z1,E1,QDIR,PHICM,X2,Y2,Z2,E2)
          W1C2=W2C2
          CALL RSTLAB (QRST,XIQ,YIQ,ZRST,X1,Y1,Z1,E1)
          CALL RSTLAB (QRST,XIQ,YIQ,ZRST,X2,Y2,Z2,E2)
          NUCL=NUCL3
C GO TO STORE
          GO TO 32
C         ELASTIC COLLISIONS
      161 CALL LBRSTB (QRST,XIQ,YIQ,ZRST,EFERMI,X1,Y1,Z1,E1)
          CALL CMSLOB (X1,Y1,Z1,E1,QDIR,PHICM,X2,Y2,Z2,E2)
          CALL RSTLAB (QRST,XIQ,YIQ,ZRST,X1,Y1,Z1,E1)
          W5=W1C2
          W1C2=W2C2
          CALL RSTLAB (QRST,XIQ,YIQ,ZRST,X2,Y2,Z2,E2)
          W1C2=W5
C*****AND CHECK IF PARTICLES ARE WORTHWHILE TO FOLLOW
C
C         CHECK IF ENERGY OF SECONDARY IS GREATER THAN EPAULY AND EMIN
          IF (NUCL2) 109,109,108
      108 EPAULI=EPAULP
          GO TO 110
      109 EPAULI=EPAULN
      110 IF (E2-EPAULI) 180,23,23
      180 IF (NUCL) 190,102,102
       23 IF (NUCL) 32,112,111
      111 EPAULI=EPAULP
          GO TO 113
      112 EPAULI=EPAULN
      113 IF(E1-EPAULI) 102,32,32
       32 IF(E2-EMIN) 117,25,25
C
C         CHECK IF WITHIN DIMENSION
C STORE
       25 IF(I-20) 31,31,30
C
```

```
      C      AND STORE THE SECONDARY
0247      31 XSTORE(I)=X2
0248         YSTORE(I)=Y2
0249         ZSTORE(I)=Z2
0250         ESTORE(I)=E2
0251         CAPX(I)=XPOS
0252         CAPY(I)=YPOS
0253         CAPZ(I)=ZPOS
0254         NUCLST(I)=NUCL2
0255         I=I+1
      C
      C      FOLLOW  INCIDENT PARTICLE
      C PION OR NUCLEON
0256     117 IF (NUCL)  27,104,104
0257     104 IF(E1-EMIN) 26,27,27
0258      26 ICOL=0
0259         GO TO 105
0260      27 E=E1
0261         XDIR=X1
0262         YDIR=Y1
0263         ZDIR=Z1
      C GO TO FOLLOW
0264         GO TO 116
      C*****OUTPUT AND FOLLOW NEXT PARTICLE
      C
      C      CUT ROUTINE
0265      21 TFIN=ETOT(E,W1C2)
0266         TFIN=TFIN+TCOUL-TMIN
      C OUTPUT 1
0267     115 IF (NUCL) 150,120,39
0268     150 WRITE (3,16) L,KCHAR,TINIT,ICHAR,TFIN,ICOL,XDIR,YDIR,ZDIR
0269      16 FORMAT(1H0,I6,I5,F12.2,I5,F12.2,42X,I3,F10.4,F10.4,F10.4)
0270         IMT=10.*(ZDIR+1.)+1.
0271         INT=.1*TFIN+1.
0272         IF(ICHAR)141,142,143
0273     141 NPIOUT(IMT,INT)=NPIOUT(IMT,INT)+1
0274         GO TO 139
0275     142 NPIOUT(IMT,INT)=NPIOUT(IMT,INT)+1000
0276         GO TO 139
0277     143 NPIIN(IMT,INT)=NPIIN(IMT,INT)+1000
0278     139 CONTINUE
0279         ISKIP=ISKIP+1
0280         GO TO 300
```

```
FORTRAN IV G LEVEL 1, MOD 3          MAIN          DATE = 69007          12/44/34

0281        39 WRITE (3,14) TFIN,ICOL,XDIR,YDIR,ZDIR
0282        14 FORMAT(1H ,62X,F9.2,11X,I3,F10.4,F10.4,F10.4)
0283           IF(TFIN-0.) 300,311,311
0284       311 INT=.1*TFIN+1.
0285           IMT=10.*(ZDIR+1.)+1.
0286           NNOUT(IMT,INT)=NNOUT(IMT,INT)+1
0287           GO TO 300
0288       120 WRITE (3,15) TFIN,ICOL,XDIR,YDIR,ZDIR
0289        15 FORMAT(1H ,72X,F9.2,I4,F10.4,F10.4,F10.4)
0290           IF(TFIN-0.) 300,312,312
0291       312 INT=.1*TFIN+1.
0292           IMT=10.*(ZDIR+1.)+1.
0293           NNOUT(IMT,INT)=NNOUT(IMT,INT)+1000
0294       300 ISKIP=ISKIP+1
0295           TOTEN=TOTEN+TFIN
0296           ICOL=0
         C     CHECK IF ANY PARTICLES ARE LEFT IN STORAGE
0297       105 IF (I-K)40,40,29
0298        29 E=ESTORE(K)
0299           XDIR=XSTORE(K)
0300           YDIR=YSTORE(K)
0301           ZDIR=ZSTORE(K)
0302           XPOS=CAPX(K)
0303           YPOS=CAPY(K)
0304           ZPOS=CAPZ(K)
0305           NUCL=NUCLST(K)
0306           W1C2=W2
0307           WAFT=W1C2
0308           K=K+1
         C GO TO FOLLOW
0309           GO TO 106
         C
         C     REJECTION  ROUTINE
0310        30 WRITE (3,10)
0311        10 FORMAT (1H0,19HTOO MANY COLLISIONS)
         C GO TO START
0312       305 FORMAT(120X,F9.2)
0313        40 WRITE(3,305)TOTEN
         C OUTPUT 3
0314        18 FORMAT(1X,I4,20I6,I7)
0315        62 FORMAT('OTOT ',21I6)
0316         9 FORMAT('0 -1.0  -0.9  -0.8  -0.7  -0.6  -0.5  -0.4  -0.3  -0.2  -0
            1.1   0.0   0.1   0.2   0.3   0.4   0.5   0.6   0.7   0.8   0.9   1
```

```
                 2.0   TOT'//)
 0317        12    FORMAT('1')
 0318              WRITE (3,8)
 0319              WRITE(3,9)
 0320         8    FORMAT(74H1INPUT PION E-A DIST.(UNITS) AND POSITIVE OUTPUT PION E-
                 1A DIST.(THOUSANDS))
 0321              DO 50 I=1,21
 0322        50    NSOM(I)=0
 0323              DO 47 J=1,100
 0324              JEN=J*10-10
 0325              NSUM=0
 0326              DO 53 I=1,21
 0327              NSOM(I)=NSOM(I)+NPIIN(I,J)
 0328        53    NSUM=NSUM+NPIIN(I,J)
 0329              IF(J-51) 47,45,47
 0330        45    WRITE(3,12)
 0331              WRITE(3,9)
 0332        47    WRITE (3,18) JEN,(NPIIN(I,J),I=1,20),NSUM
 0333              WRITE (3,62) (NSOM(I),I=1,21)
 0334              WRITE (3,5)
 0335              WRITE(3,9)
 0336         5    FORMAT(60H1OUTPUT PION E-A DIST.NEGATIVE(UNITS) AND NEUTRAL(THOUSA
                 1NDS))
 0337              DO 51 I=1,21
 0338        51    NSOM(I)=0
 0339              DO 48 J=1,100
 0340              JEN=J*10-10
 0341              NSUM=0
 0342              DO 54 I=1,21
 0343              NSOM(I)=NSOM(I)+NPIOUT(I,J)
 0344        54    NSUM=NSUM+NPIOUT(I,J)
 0345              IF(J-51)48,44,48
 0346        44    WRITE (3,12)
 0347              WRITE(3,9)
 0348        48    WRITE (3,18) JEN,(NPIOUT(I,J),I=1,20),NSUM
 0349              WRITE (3,62) (NSOM(I),I=1,21)
 0350              WRITE (3,7)
 0351         7    FORMAT(56H1OUTPUT PROTONS(UNITS) AND NEUTRONS(THOUSANDS) E-A DIST.
                 1)
 0352              WRITE(3,9)
 0353              DO 52 I=1,21
 0354        52    NSOM(I)=0
 0355              DO 49 J=1,100
```

```
              JEN=J*10-10
              NSUM=0
              DO 55 I=1,21
              NSOM(I)=NSOM(I)+NNOUT(I,J)
          55  NSUM=NSUM+NNOUT(I,J)
              IF (J-51) 49,46,49
          46  WRITE (3,12)
              WRITE(3,9)
          49  WRITE (3,18) JEN,(NNOUT(I,J),I=1,20),NSUM
              WRITE (3,62) (NSOM(I),I=1,21)
        C GO TO READ 2
              GO TO 100
        1191  IN=IN-L+1
              WRITE (2,2) IRN,IN
              STOP
              END
```

```
LEVEL0 1OCT67                            IBM OS/360 BASIC FORTRAN IV (E) COMPILATION

 S.0001          SUBROUTINE LBRSTB (O,XIO,YIO,Z2,ES,X,Y,Z,E)
 S.0002          COMMON W1,W2,BETA,GAMMA
          C
          C      ROTATE AXIS INTO DIRECTION OF MOTION
 S.0003          XP=O*(XIO*X&YIO*Y)&Z2*Z
 S.0004          YP=XIO*Y-YIO*X
 S.0005          ZP=O*Z-Z2*(XIO*X&YIO*Y)
          C      FIND THE MOMENTA
          C      FIND RELATIVISTIC CONSTANTS BETA ,GAMMA AND U
 S.0006          BETA=ES/SSTSQR(ES,W2)
 S.0007          GAMMA=1./SQMXSB(BETA)
 S.0008          U=SSTSQR(E,W1)
          C      DO RELATIVISTIC TRANSFORMATION ON MOMENTA
 S.0009          XP=GAMMA*(XP-BETA*U/E)
          C      CALCULATE NEW E,X,Y,Z
 S.0010          SUM=SUMSQR(XP,YP,ZP)
 S.0011          E=SUM*E
 S.0012          SINV=1./SUM
 S.0013          X=XP*SINV
 S.0014          Y=YP*SINV
 S.0015          Z=ZP*SINV
 S.0016          RETURN
 S.0017          END

                   SIZE OF COMMON  000016   PROGRAM  000756

                                    END OF COMPILATION  LBRSTB

LEVEL0 1OCT67                            IBM OS/360 BASIC FORTRAN IV (E) COMPILATION

 S.0001          SUBROUTINE RSTLAB (O,XIO,YIO,Z2,X,Y,Z,E)
 S.0002          COMMON W1,W2,B,G
 S.0003          U=SSTSQR(E,W1)
 S.0004          X=G*(X&B*U/E)
 S.0005          SUM=SUMSQR(X,Y,Z)
 S.0006          E=SUM*E
 S.0007          SUMINV=1./SUM
 S.0008          X=X*SUMINV
 S.0009          Y=Y*SUMINV
 S.0010          Z=Z*SUMINV
 S.0011          COM=O*X-Z2*Z
 S.0012          Z=Z2*X&O*Z
 S.0013          X=XIO*COM-YIO*Y
 S.0014          Y=YIO*COM&XIO*Y
 S.0015          RETURN
 S.0016          END

                   SIZE OF COMMON  000016   PROGRAM  000652

                                    END OF COMPILATION  RSTLAB
```

```
LEVEL0 1OCT67                       IBM OS/360 BASIC FORTRAN IV (E) COMPILATION

S.0001                SUBROUTINE CMSLOB (X,Y,Z,E,QDIR,PHICM,X2,Y2,Z2,E2)
                C     THIS SUBROUTINE IS DESIGNED TO CALCULATE THE EXIT ENERGY AND       HM000011
                C     DIRECTION OF A PARTICLE OF GIVEN INCIDENT ENERGY AND DIRECTION     HM000011
                C     WHICH IS SCATTERED THROUGH ANGLES TETA AND PHI IN THE CM SYSTEM.   HM000011
                C     THE RECOIL ENERGY AND DIRECTION OF THE TARGET ARE ALSO CALCULATED.HM000011
S.0002                COMMON W1C2,W2C2,ABC,ABD,RN,W
                C     CALCULATE THE MOMENTUM OF THE PARTICLE IN THE CM BEFORE COLLISION.HM000011
S.0003                U=SSTSQB(E,W1C2)
S.0004                BETACM=E/(U&W2C2)                                                  HM000011
S.0005                GAMACM=1./SQMXSB(BETACM)
S.0006                PCMBEF=BETACM*W2C2*GAMACM
S.0007                UCM1=SSTSQB(PCMBEF,W1C2)
S.0008                UCM2=SSTSQB(PCMBEF,W2C2)
S.0009                IF (W1C2-W) 32,33,32
S.0010           32   UCM1=(UCM1&UCM2)*.5
S.0011                UCM2=UCM1
S.0012                PCMBEF=(UCM1*UCM1-W*W)**.5
                C     CALCULATE THE MOMENTUM IN CM AFTER COLLISION.                      HM000011
S.0013           33   PCMAFX=PCMBEF*QDIR
S.0014                PCMAYZ=PCMBEF*SQMXSB(QDIR)
S.0015                PAFY=PCMAYZ*SIN(PHICM)
S.0016                PAFZ=PCMAYZ*COS(PHICM)
                C     TRANSFORM TO LAB PRIMED SYSTEM.                                    HM000011
S.0017                PAFX=GAMACM*(BETACM*UCM1&PCMAFX)
                C     NOW CALCULATE E,X,Y,Z                                              HM000011
S.0018                I=0                                                                HM000011
S.0019                Q=SSTSQB(X,Y)
S.0020           21   IF (Q) 31,31,30
S.0021           30   PX=PAFX*X-(PAFY*Y&PAFZ*Z*X)/Q
S.0022                PY=PAFX*Y&(PAFY*X-PAFZ*Z*Y)/Q                                      HM000011
S.0023                PZ=PAFX*Z&PAFZ*Q                                                   HM000011
S.0024                GO TO 20                                                           HM000011
S.0025           31   PX=-PAFZ*Z                                                         HM000011
S.0026                PY=PAFY                                                            HM000011
S.0027                PZ=PAFX*Z                                                          HM000011
S.0028           20   PSQR=SUMSQB(PX,PY,PZ)                                              HM000011
S.0029                I=I&1
S.0030                GO TO (22,23),I                                                    HM000011
S.0031           22   E1=PSQR                                                            HM000011
S.0032                X1=PX/PSQR
S.0033                Y1=PY/PSQR
S.0034                Z1=PZ/PSQR
                C     AND CALCULATE E2,X2,Y2,Z2
S.0035                PAFY=-PAFY                                                         HM000011
S.0036                PAFZ=-PAFZ                                                         HM000011
S.0037                PAFX=GAMACM*(BETACM*UCM2-PCMAFX)                                   HM000011
S.0038                GO TO 21
S.0039           23   E2=PSQR                                                            HM000011
S.0040                X2=PX/PSQR
S.0041                Y2=PY/PSQR                                                         HM000011
S.0042                Z2=PZ/PSQR                                                         HM000011
S.0043                E=E1                                                               HM000011
S.0044                X=X1
```

```
S.0045          Y=Y1
S.0046          Z=Z1
S.0047          RETURN
S.0048          END                                                    HM000011
                                                                       HM000011

           SIZE OF COMMON  000024   PROGRAM  001356

                      END OF COMPILATION  CMSLQB


LEVEL0 1OCT67                  IBM OS/360 BASIC FORTRAN IV (E) COMPILATION

S.0001          SUBROUTINE RANDU(IX,IY,YFL)
S.0002          IY=IX*65539                                            RANDU040
S.0003          IF(IY)5,6,6                                            RANDU041
S.0004        5 IY=IY&2147483647&1                                     RANDU042
S.0005        6 YFL=IY                                                 RANDU043
S.0006          YFL=YFL*.4656613E-9                                    RANDU044
S.0007          RETURN                                                 RANDU045
S.0008          END                                                    RANDU046
                                                                       RANDU047
           SIZE OF COMMON  000000   PROGRAM  000400

                      END OF COMPILATION  RANDU


LEVEL0 1OCT67                  IBM OS/360 BASIC FORTRAN IV (E) COMPILATION

S.0001          FUNCTION SOMXSB(X)
S.0002          DOUBLE PRECISION SOM
S.0003          SOM=(0.1D+01-X*X)**.5
S.0004          SOMXSB=SOM
S.0005          RETURN
S.0006          END

           SIZE OF COMMON  000000   PROGRAM  000344

                      END OF COMPILATION  SOMXSB


LEVEL0 1OCT67                  IBM OS/360 BASIC FORTRAN IV (E) COMPILATION

S.0001          FUNCTION SUMSQB(X,Y,Z)
S.0002          SUMSQB=(X*X&Y*Y&Z*Z)**.5
S.0003          RETURN
S.0004          END

           SIZE OF COMMON  000000   PROGRAM  000356

                      END OF COMPILATION  SUMSQB
```

PART. NO	INC *CHARGE*	*INC. PION* ENERGY	OUT *CHARGE*	*OUT PION* ENERGY	ISOBAR *MASS%MEV<*	* ISOBAR PC %MEV< *	* PROTON ENERGY *	* NEUTRON ENERGY *	* NO *COL.*
1	1	50.00	* 2		1137.53	352.21			1
							130.60		0
								42.51	1
2	1	50.00	* 2		1115.25	231.75			2
							24.71		2
							20.91		0
							74.42		1
3	1	50.00	* 2		1139.59	210.07			1
							44.26		0
							126.43		0
4	1	50.00	* 2		1169.41	214.06			1
							32.87		1
							4.28		5
							34.05		1
							37.63		4
								18.32	2
5	1	50.00	1	50.00					0
6	1	50.00	* 2		1143.71	340.46			1
							83.54		3
							18.26		2
							83.48		0
7	1	50.00	* 2		1185.83	134.60			1
							83.04		1
								82.23	2
8	1	50.00	* 1		1134.12	328.47			1
								93.79	0
9	1	50.00	1	50.00					0

Continued on page 178

* OUT * *DIRECTION*			TOTAL ENERGY OUT
0.7403	-0.4186	-0.5132	
0.1226	-0.2834	-0.9511	
			173.11
0.4023	-0.7706	0.4943	
-0.3209	-0.9056	0.2774	
-0.5596	0.8263	0.0637	
			120.03
-0.3859	0.1015	0.9169	
-0.2411	0.0011	-0.9705	
			170.69
0.6264	0.3232	0.7093	
-0.3310	0.7588	-0.5609	
-0.0507	0.7457	-0.6644	
-0.5755	-0.2091	0.7906	
-0.8973	-0.4200	-0.1360	
			127.15
0.0	0.0	-1.0000	
			50.00
0.3404	-0.8741	-0.3466	
0.5105	0.8455	0.1566	
-0.3045	-0.1571	0.9395	
			185.28
0.9743	-0.0728	-0.2132	
-0.8578	0.3742	-0.3524	
			165.27
-0.0202	-0.9626	-0.2703	
			93.79
0.0	0.0	-1.0000	
			50.00

Appendix 4 Kinematics Used in Subroutines

In the Monte Carlo calculations shown in appendix 3, the important kinematical calculations were carried out by using the subroutines LBRSTB, CMSLOB and RSTLAB. With the help of these subroutines, the final momenta of the two particles involved in a collision were calculated. In this appendix, the explicit rotations and relativistic transformation matrices used in these subroutines are described.

The first subroutine, LBRSTB, transforms the incident particle to the rest frame of the target nucleon: This consists of 1) a rotation, R_1, of the laboratory frame so that the target particle moves along the x-axis and 2) a relativistic transformation T_1.

In fig. A-2, $\vec{p}$ denotes the momentum of the target nucleon. Hence, the total rotation R_1 consists of a rotation about the z-axis through an angle φ, followed by a rotation about the new y-axis through an angle $(^{\pi}/2 - \theta)$. Thus

$$R_1 = \begin{pmatrix} \sin\theta & 0 & \cos\theta \\ 0 & 1 & 0 \\ -\cos\theta & 0 & \sin\theta \end{pmatrix} \begin{pmatrix} \cos\varphi & \sin\varphi & 0 \\ -\sin\varphi & \cos\varphi & 0 \\ 0 & 0 & 1 \end{pmatrix}$$

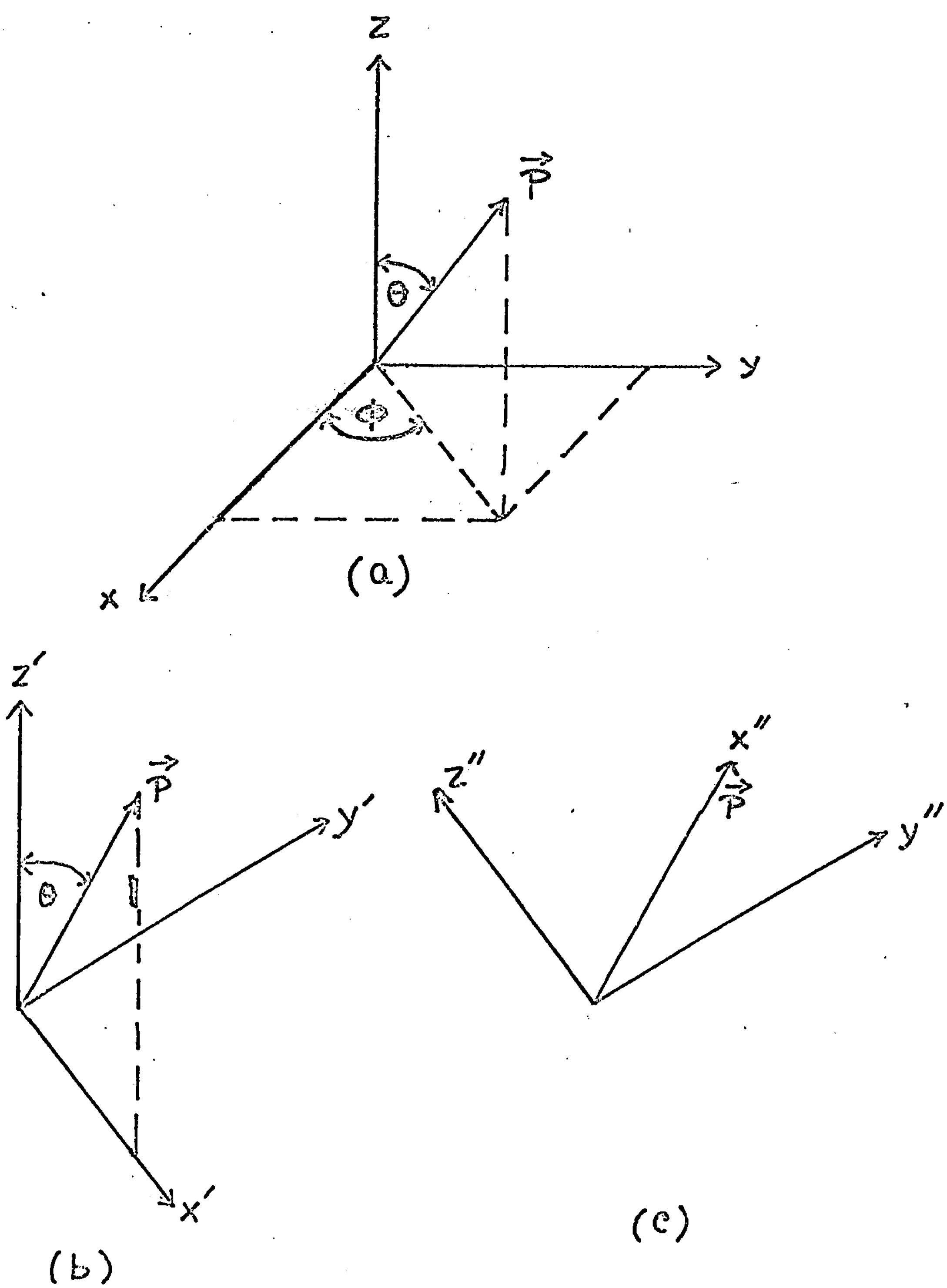

Fig. A.2 Geometry used in kinematics subroutine

a) Momentum vector $\vec{p}$ of the particle in the lab. system.

b) Momentum vector $\vec{p}$ after the frame has been rotated through an angle ϕ about the z axis

c) Momentum vector coincides with the new x axis (x") after the frame is rotated through $\Pi/2 - \theta$ about Y'

$$= \begin{pmatrix} \sin\theta\cos\varphi & \sin\theta\sin\varphi & \cos\theta \\ -\sin\varphi & \cos\varphi & 0 \\ -\cos\theta\cos\varphi & -\cos\theta\sin\varphi & \sin\theta \end{pmatrix}$$

This transformation is only applied to the incident momentum $\vec{p}_1$, since the target particle will be along the x-axis. The quantities $\sin\theta$, $\cos\theta$, $\sin\varphi$ and $\cos\varphi$ are obtained from the main programme using random numbers.

The relativistic transformation, T_1, is then applied to the momentum four-vector, P_1, of the incident particle:

$$P_1 = \begin{pmatrix} P_{x1} \\ P_{y1} \\ P_{z1} \\ iU_1 \end{pmatrix}$$

where U_1 is the total energy of the particle. The transformation, T_1, is given by:

$$\begin{pmatrix} \gamma_1 & 0 & 0 & i\gamma_1\beta_1 \\ 0 & 1 & 0 & 0 \\ 0 & 0 & 1 & 0 \\ -i\gamma_1\beta_1 & 0 & 0 & \gamma_1 \end{pmatrix}$$

where β_1 is the velocity of the moving frame:

$$\beta_1 = \frac{|\vec{P}_2|}{\sqrt{\vec{P}_2^{\,2} + M_2^{\,2}}}$$

and γ_1 is the Lorentz factor:

$$\gamma_1 = \frac{1}{\sqrt{1 - \beta_1^{\,2}}}$$

These two transformations complete the subroutine LBRSTB and transforms the incident particle to the appropriate rest frame of the target nucleon. This information is supplied to the next subroutine CMSLOB.

The subroutine CMSLOB transforms both particles to their center of mass and determines their new directions and momenta in the center of mass after collision and finally transforms back to the original rest frame of the target nucleon.

First, a rotation similar to R_1 is again performed. In this case the frame is rotated so that the incident particle moves along the x-axis. The value of

$\sin\theta$, $\cos\theta$, $\sin\varphi$ and $\cos\varphi$ are calculated from the direction cosines (x, y, z) of the incident particle in the rest frame of the target nucleon. The expressions are:

$$\cos\theta = z$$
$$\sin\theta = \sqrt{1 - z^2} = Q$$
$$\cos\varphi = {}^{x}/Q$$
$$\sin\varphi = {}^{y}/Q$$

The rotation, R_2, is then given by:

$$R_2 = \begin{pmatrix} x & y & z \\ -{}^{y}/Q & {}^{x}/Q & 0 \\ -{}^{zx}/Q & -{}^{zy}/Q & Q \end{pmatrix}$$

The rotation is not actually applied to either particle, since it is known that the incident particle will be moving along the x-axis. However, R_2 will be used later, to obtain the inverse transformation, R_2^{-1}.

A relativistic transformation, T_2, is then performed to the center of mass frame of the two particles. The velocity of the center of mass, β_2, and the Lorentz factor, γ_2, are obtained from

$$\beta_2 = \frac{\vec{P}_1}{U_1' + M_2}$$

and

$$\gamma_2 = \frac{1}{\sqrt{1 - \beta_2{}^2}}$$

where U_1' is the total energy of the incident particle in the rest frame of the target particle and M_2 is the mass of the target particle.

In the center of mass system, the momenta, $\vec{p}*$, are equal and opposite, and are given by:

$$|\vec{p}*| = \beta_2\gamma_2 M_2$$

Hence the total energy, U*, in the center of mass system is given by:

$$U* = \sqrt{(\vec{p}*^2 + M_1{}^2)} + \sqrt{(\vec{p}*^2 + M_2{}^2)}$$

This quantity is conserved and can, therefore, be equated with the total energy after the collision. This enables to determine the momenta of the two particles. The main programme determines (by using random numbers) the new directions in the center of mass system. If $\vec{p}_f*$ is the center of mass momentum of each of the particles after the collision and M_3 and M_4 are their masses, then the total energy

$$U^* = \sqrt{(\vec{P}_f^{*2} + M_3^2)} + \sqrt{(\vec{P}_f^{*2} + M_4^2)}$$

i.e.

$$|\vec{P}_f^*| = \left\{ \left(\frac{U^{*2} + M_4^2 - M_3^2}{2U^*} \right)^2 - M_4^2 \right\}^{\frac{1}{2}}$$

In our case $M_3 = M_4$. Hence;

$$|\vec{P}_f^*| = \{ (\frac{U^*}{2})^2 - M_4^2 \}^{\frac{1}{2}}$$

This portion essentially describes the collision and can be represented by a transformation C. This transformation rotates and transforms the momenta of the particles, whereas all other transformations rotate and transform the frame of reference.

The new momentum four-vectors are transformed back to the original rest frame of the target nucleon by T_2^{-1}:

$$T_2^{-1} = \begin{pmatrix} \gamma_2 & 0 & 0 & -i\beta_2\gamma_2 \\ 0 & 1 & 0 & 0 \\ 0 & 0 & 1 & 0 \\ i\beta_2\gamma_2 & 0 & 0 & \gamma_2 \end{pmatrix}$$

and rotated back by using R_2^{-1}; where R_2^{-1} is given by:

$$R_2^{-1} = \begin{pmatrix} x & -y/Q & -zx/Q \\ y & x/Q & -zy/Q \\ z & 0 & Q \end{pmatrix}$$

These transformations are applied to both the outgoing particles and the data are supplied to the next subroutine RSTLAB.

The subroutine RSTLAB transforms both particles back to the original laboratory frame. This is accomplished by the inverse transformation T_1^{-1} followed by the inverse rotation R_1^{-1}. These transformations are applied to both particles and the resultant momenta and directions are supplied to the main programme.

REFERENCES

1. Ancsin, J., and Hébert, J. 1964. Photographie Corpusculair.III, p.393. Edited by P. Demers.
   Anderson, H.L., Davidon, W.C., Kruse, U.E. 1955. Phys. Rev. 100, 339

2. Adelman, F.L. 1952. Phys. Rev. 85, 249

3. Auerbach, E.H., Fleming, D.M., and Sternheim, M.M. 1967. Phys. Rev. 162, 1683

4. Baltay, C. et al. 1966. Phys. Rev. 145, 1103

5. Barkas, W.H. et al. 1957. Phys. Rev. 105, 1037

6. Bernardini, G., and Levy, F. 1951. Phys. Rev. 84, 1063

7. Bethe, H.A. 1932. Zeits. f. Physik 76, 293

8. Bethe, H.A. 1940. Phys. Rev. 57, 1125

9. Blau, M., Oliver, R. and Smith, J. 1953. Phys. Rev 91, 949

10. Blinov, G.A. et al. 1959. Sov. Phy. JETP 35(8), 609

11. Brueckner, K.A. Serber, R., and Watson, K.M. 1951. Phys. Rev. 84, 258

12. Burcham, W.E. 1962. Nuclear Physics, Longmans publication.

13. Byfield, H., Kessler, J., and Lederman, L.M. 1952. Phys. Rev. 86, 17

14. CERN Conference on High-Energy Physics and Nuclear Structure, 1963

15. Chamberlain, O. et al. 1959. Phys. Rev. 113, 1615

16. Chew, G.F. and Low, F.E. 1956. Phys. Rev. 101, 1570

17. Cresti, M. et al. 1963. Proceeding of the Vienna Conference on High Energy Physics, P.263

18. Ericson, T.E.O. 1965. Invited talk at the topical conference "Use of Elementary Particles in Nuclear Structure Research", Brussels.

19. Fay, H., Gottstein, K. and Hain, K. 1954. Suppl. Nuovo Cim. 11, 234

20. Fernbach, S., Serber, R., and Taylor, T.B. 1949. Phys. Rev. 75, 1352

21. Focacci, M.N. and Giacomelli, G. 1966. CERN report No.: 66-18

22. Fowler, P.H. 1950. Phil. Mag. 41, 169

23. Fraenkel, Z. 1963. Phys. Rev. 130, 2407

24. Frank, R.M., Gammel, J., and Watson, K. 1956. Phys. Rev. 101, 891

25. Fuji, T.A. 1959. Phys. Rev. 113, 695

26. Gell-Mann, M. and Watson, K. 1954. Ann. Rev. Nucl. Science

27. Genève conference, on High Energy Physics, Proceedings of 1958

28. Hébert, J. and Mes, H. 1968. Nucl. Phys. B4, 244

29. Hirt, W. et al. 1968. CERN Preprint. Richard-Serre, C. 1969. These de Doctorat, Grenoble University.

30. Jean, M. 1964. Suppl. Nuovo Cim. 2, 400

31. Kimura, Y., and Nagashima, Y. 1965. Progr. Theor. Phys. 33, 43

32. Kopaleishvili, T.I. 1967. Sov. J. of Nucl. Phys. 4, 382

33. Letourneux, J., and Eisenberg, J.M. 1966. Nucl. Phys. 87, 331

34. Menon, M.G.K., Muirhead, H. and Rochat, O. 1950. Phil. Mag. 41, 583

35. Mes, H., Ahmad, I., and Hébert, J. 1966. Progr. Theor. Phys. 35, 566

36. Mes, H. 1968. Ph.D. Thesis, Univ. of Ottawa

37. Metropolis, N. et al. 1958. Phys. Rev. 110, 185

38. Metropolis, N. et al. (2). 1958. Phys. Rev. 110, 204

39. Miyazawa, H. 1964. J. of the Phys. Soc. of Japan 19, 1764

40. Muirhead, H. 1965. The Physics of the Elementary Particles; Pergamon Press.

41. Nikol'skii, B.A., Kudrin, L.P. and Ali-Zade, S.A. 1957. Sov. Phy: JETP 5, 93

42. Nishijima, K. 1964. Fundamental Particles. W.A. Benjamin Inc.

43. Ozaki, S. et al. 1960. Phys. Rev. Letters 4, 533

44. Powell, C.F., Fowler, P.H., and Perkins, D.H. 1959. The study of Elementary Particles by the Photographic method; Pergamon Press.

45. Rainwater, J. 1959. Proc. of the Int. Conf. on the Nuclear Optical Model, p. 228

46. Rankin, B. and Bradner, H. 1952. Phys. Rev. 87, 553

47. Rossi, B. 1956. High-Energy Particles; Prentice-Hall, Inc.

48. Sakamoto, Y. 1966. Nucl. Phy. 87, 414

49. Saphir, G. 1956. Phys. Rev. 104, 535

50. Shapiro, A.M. 1951, Phys. Rev. 84, 1063

51. Schewber, S.S. 1962. An Introduction to Relativistic Quantum Field Theory. Harper and Row, publishers.

52. Serber, R. 1947. Phys. Rev. 72, 1008

53. Stork, D.H. 1954. Phys. Rev. 93, 868

54. Tracy, J.F. 1953. Phys. Rev. 91, 960

55. UCRL Reports. 1964. Vols I-IV

56. Werbrouck, A. 1964. Proceedings of the 1964 Easter School for Physicists (Vol. 1). Herceg Novi, CERN 64-13 (1964)

57. Williams, R.E., Baker, W.F., and Rainwater, J. 1956. Phys. Rev. 104, 1695

Curriculum Vitae

Name: Subhas Chandra Chakravartty.

Born: Dumka, Bihar, India.

Education:

Secondary: Dumka Zila School, Dumka, India, 1947-1955.

University: St. Xavier's College, Ranchi, India, 1955-1957.
Ranchi College, Ranchi, 1957-1961.
University of Windsor, Windsor, Canada, 1963-1965.

Degree: M.Sc. in Experimental Physics.

Position Held: Lecturer in Physics, Ranchi College, Ranchi, 1961-1963.